Surface Effects in Plane Deformations of Micropolar Elastic Solids

by

Alireza Gharahi

A thesis submitted in partial fulfillment of the requirements for the degree of

Doctor of Philosophy

Department of Mechanical Engineering

University of Alberta

Abstract

The predictive modelling of the mechanics of materials at small scales has attracted increasing attention in the recent literature mainly due to the scientific and technological demand for models which accommodate the influence of both material internal structure and surface effects from micro- to nano-scales. Materials whose deformation is significantly influenced by their internal structure and surface effects include the class of micro/nano composites as well as polycrystalline, granular and fibrous materials used increasingly in a wide variety of advanced technological applications. Micropolar theory and surface mechanics are developed to bestow upon the continuum-based mathematical models the capability of analyzing such advanced materials. Notwithstanding the fact that the internal micro/nano-constituents and the surface effects are incorporated into the model as two different enhancing strategies, the simultaneous use of them remains rare in the literature. In particular, a systematic design and examination of such a model which describes plane deformations in micro/nano-materials is missing.

In this thesis we present two new linear micropolar surface mechanics models coupled with the plane deformations of a micropolar elastic bulk. The surface models are proposed as elastic micropolar shells capable of incorporating flexural resistance. In that sense, the adopted surfaces are the micropolar counterpart of the classical linear Steigmann-Ogden surface model. In conjunction with the micropolar bulk, the proposed surface models capture

both the effects of surface and the effects of internal structures which are known to be dominant in most of the materials from micro- to nano-meter scale.

Among the two, we apply and demonstrate the feasibility of the higher order model using three popular micro/nano-mechanics problems. In addition, we discuss the improvements that follow from such a comprehensive mathematical model. We evaluate the problems of stress concentration around a cavity, effective elastic properties of nano-composites and a dislocation near a surface. In each case, we obtain meaningful results which are in corroboration with the existing literature.

In the next step, we perform a rigorous mathematical analysis to investigate "well-posedness" of the models. First, we establish the general fundamental boundary value problems associated with the models and discuss the uniqueness of solutions. We then proceed with the analysis by applying the boundary integral equation method to examine the existence of solutions of the corresponding boundary value problems. The incorporation of surface effects as a separate micropolar structure gives rise to a set of highly nonstandard boundary conditions that require special treatments. The boundary integral equations method allows us to reduce the boundary value problems to systems of singular integro-differential equations. However, a series of carefully chosen transforms are required to rearrange the system of singular integro-differential equations in a form accommodated by the well-established theory of singular integral equations. Consequently, we establish the solvability of the boundary value problems and validate the corresponding mathematical models.

Preface

Our research was motivated by evaluating first the importance of bending resistance in any surface model without reference to micropolar elasticity. This resulted in the following two publications which confirmed a significant contribution of bending rigidity to any surface model:

1. M. Dai *, A. Gharahi and P. Schiavone, Analytic solution for a circular nano-inhomogeneity with interface stretching and bending resistance in plane strain deformations, *Appl. Math. Model.* 55 (2018) 160-170.

2. M. Dai *, A. Gharahi and P. Schiavone, Note on the Deformation-induced Change in the Curvature of a Material Surface in Plane Deformations, *Mech. Res. Commun.* 94 (2018) 88-90.

The present thesis is composed of the following five published papers: Chapter 2 is published as a part of the article:

- Gharahi, A. and Schiavone, P. Uniqueness of solution for plane deformations of a micropolar elastic solid with surface effects *Continuum Mech. Thermodyn.*, 2019

Chapter 3 is published with slight differences as:

- Gharahi, A. and Schiavone, P. Plane micropolar elasticity with surface flexural resistance. *Continuum Mech. Thermodyn.*, 2018, 30, 675-688

*M. Dai was a visiting doctoral student from Nanjing University of Aeronautics and Astronautics, China, 2016-2017

Chapter 4 is published with slight differences as:

- Gharahi, A. and Schiavone, P. Effective elastic properties of plane micropolar nanocomposites with interface flexural effects. *Int. J. Mech. Sci.*, 2018, 149, 84-92

Chapter 5 is published with slight differences as:

- Gharahi, A. and Schiavone, P. Edge dislocation with surface flexural resistance in micropolar materials *Acta Mechanica*, 2019, 230, 1513-1527

Chapter 6, Section 6.2 is published as the article:

- Gharahi, A. and Schiavone, P. Uniqueness of solution for plane deformations of a micropolar elastic solid with surface effects *Continuum Mech. Thermodyn.*, 2019

Chapter 6, Section 6.3 is published as the article:

- Gharahi, A. and Schiavone, P. Existence and integral representation of solutions for plane deformations of a micropolar elastic solid with surface elasticity *ZAMM - Journal of Applied Mathematics and Mechanics / Zeitschrift für Angewandte Mathematik und Mechanik*, 2020

A continuation of Chapter 6 is published as the article:

- Gharahi, A. and Schiavone, P. The Neumann problem in plane deformations of a micropolar elastic solid with micropolar surface effects *Mathematics and Mechanics of Solids* , 2020

Content of the latter publication is excluded from the thesis.

To my father, my mother, and my brother

The beauty of mathematics only shows itself to more patient followers.

— Maryam Mirzakhani

Acknowledgements

First and Foremost, I would like to express my highest gratitude and appreciation to my advisor and mentor, Professor Peter Schiavone, whose unstinting help and support, and continuous encouragement made this thesis possible. From our first meeting when he set our objective as to "educate" me, he inspired me by his insightful vision, expertise, confidence, and noble generosity. He has truly created in me a lifelong impression, and I feel, from my heart, most fortunate to have been advised by such an excellent scholar and scientist, a wonderful educator, and an outstanding role-model, both professionally and personally.

I would like to thank my supervisory committee Dr. Chong-Qing Ru and Dr. Chun Il Kim and the members of my examination committee for taking their time to evaluate this research.

I extend my heartfelt gratitude to Professor Rahimian and Dr. Eskandari-Ghadi who instilled in me the confidence and enthusiasm for science, academia, and research. I cannot thank them enough for introducing me to the beauties of mathematics and mechanics.

I am profoundly in debt to my family for their ceaseless emotional support, constant patience, and inspiring energy. I am deeply thankful to my father for being my strong reinforcement in difficult times. I am deeply in debt to my mother for her emotional support and her motivating spirit. I would like to thank my wonderful only brother who lightened the way for me to pursue my dreams, no matter how long it takes, no matter how far they are.

Finally, I wish to thank my colleagues and friends, all who have left incredible memories for me during my studies and career at the University of Alberta.

Table of Contents

1 Introduction **1**

2 Mathematical Modelling of Surface Elasticity **17**

2.1 Preliminaries 18

2.1.1 Fundamentals of the Theory of Micropolar Elasticity 19

2.1.2 Function Spaces 23

2.2 Proposition 23

2.3 Governing Equations of Plane Micropolar Elasticity 24

2.4 Micropolar surface effects: boundary conditions of fourth order 28

2.5 Micropolar surface effects: boundary conditions of the second order via three dimensional micropolar theory (Eremeyev-Lebedev-Altenbach) 35

2.6 Boundary value problems 38

2.6.1 (a) Interior problem 38

2.6.2 (b) Exterior problem 39

3 Stress Distribution Around a Circular Hole in a Micropolar Material with Micropolar Surface Effects **40**

3.1 Preliminaries 41

3.2 Statement of the problem 43

3.3 Boundary value problem 47

3.4 Numerical Evaluation 51

4 Effective Elastic Properties of Nano-Composites with Interface Effects 55

4.1 Preliminary Concepts . . . 58

4.1.1 Mori-Tanaka Procedure . . . 59

4.2 Circular inhomogeneity in an infinite medium . . . 63

4.3 Effective bulk and shear moduli of plane micropolar nano-composite wth circular nano-inhomogeneities . . . 67

4.3.1 Effective bulk modulus . . . 68

4.3.2 Effective shear modulus . . . 69

4.4 Numerical Evaluation . . . 72

5 Plane Problem of an Edge Dislocation in the Presence of Micropolar Surface Effects 76

5.1 Preliminaries . . . 78

5.1.1 Theory of Dislocations: edge dislocation . . . 78

5.1.2 Helmholtz Theorem in Plane Micropolar Elasticity . . . 79

5.2 An Edge Dislocation in a Half-plane Medium with Surface Effects . . . 82

5.2.1 Special Case of Classical Elasticity . . . 86

5.3 Numerical Illustrations . . . 87

6 Wellposedness Analysis of the Micropolar Surface Model 92

6.1 Preliminaries . . . 93

6.1.1 Integral Equations . . . 94

6.1.2 Analysis Background . . . 94

6.1.3 Singular Integral Equations . . . 104

6.1.4 Singular Integro-differential Equation . . . 105

6.2 Uniqueness of the Solution . . . 107

6.2.1 (a) Interior boundary value problem . . . 107

6.2.2 (b) Exterior boundary value problem . . . 108

6.2.3 Uniqueness of Solutions of Interior and Exterior Problems . . . 109

6.3 Existence of Solutions 112
6.3.1 Reduction to singular integral equations 112
6.3.2 Singular Integro-differential Equation in the Standard Form 118
6.3.3 Existence Theorems 122
6.3.4 Existence Theorem for the Case of Second Order Boundary Conditions 124

7 Conclusions **128**
7.1 Future Work 130

References **132**

List of Figures

2.1 Configuration of the model 24
2.2 Configuration of reinforcement shell 30
2.3 Interior and exterior problems 39

3.1 Circular hole in an infinite plane 43
3.2 Hoop-stress concentration on the circumference of a hole of radius $R = 1$nm under uniaxial remote loading 52
3.3 Variation of hoop-stress concentration with radius of circular hole 53

4.1 Circular inhomogeneity in an infinite plane matrix. 63
4.2 Variation of the effective shear modulus ratio with radius of the void for different degrees of micropolarity ($\delta = c_2/c_s$) using Case 1 boundary condition 74
4.3 Variation of the effective shear modulus ratio with radius of the void for different degrees of micropolarity ($\delta = c_2/c_s$) using Case 2 boundary condition 75

5.1 Screw and edge dislocations 77
5.2 Edge dislocation in a depth h of a half-plane with slip plane parallel to the surface 82
5.3 Variation of the normalized stress component σ_{11} at relative depth $\bar{x}_1 = 0.1$ and $\bar{x}_1 = 1$, for an edge dislocation at $\bar{h} = 1$. 89
5.4 Variation of the normalized stress component σ_{12} at relative depth $\bar{x}_1 = 0.1$ and $\bar{x}_1 = 1$, for an edge dislocation at $\bar{h} = 1$. 90

5.5 Variation of the normalized stress component σ_{22} at relative depth $\bar{x}_1 = 0.1$ and $\bar{x}_1 = 1$, for an edge dislocation at $\bar{h} = 1$. 91

6.1 Interior and exterior problems 108

Chapter 1

Introduction

Mathematical models are vastly used in various disciplines of applied sciences and engineering. The use of mathematical models is not limited to natural sciences but also social sciences, computer, and economics extensively benefit from the those models. A mathematical model is an abstract description of the behavior of a system in the language of mathematics.

Classical mechanics originated in the seventeenth century from Newton's laws of motion and developed further to Eulerian, Lagrangian and Hamiltonian mechanics in the eighteenth and nineteenth century, provides extensive mathematical tools to model the physics of motion of macroscopic objects. From the macroscopic view stems a branch of classical models that idealize materials as a continuous mass rather than discrete particles. The viewpoint of materials as bodies continuously occupying a region in the space due to A.L. Cauchy (1789-1857) allows for differentiation with respect to space in addition to time in the mathematical model. Such mathematical apparatus provides the model with analytical advantages barely offered by any other methods. Determinism and rationality of the model, excellent agreement with observations and a myriad numerical methods for analysis are only a few of the advantages achieved from the continuum perspective. It is the mathematical and computational benefits that promote the continuum mechanics to an elegant hypothesis to describe physics of force and motion of material bodies. Again the same desirable advantages prompted the attempts to extend the idea of continua to physics of deformation and motion of materials in microscopic scales of time and space. However, in the microscopic scales the behavior of

materials are significantly influenced by the heterogeneity, distinguishable constituents and discrete particle structures, the properties that in the first glance appear to be inconsistent with the premises of continuum mechanics.

The question posed by Eringen [45] arises here as "how to reconcile" the concept of discrete particles and constituents of a body with continuum hypothesis? Obviously, the equations constructed within the framework of modeling particles as physical points suitable for the microscopic view, stand outside the classical definitions and principles of the continuum mechanics. The answer was sought in the successive releasing of certain assumptions built in the Cauchy classical continuum models, what Maugin calls working hypotheses [99], to obtain a "generalized" continuum model. The first working hypotheses of the Cauchy's classical continuum to be released is that there are no couples transferred between two surfaces dividing a volume. The second working hypothesis is that there are no internal degrees of freedom to describe any internal micro-structures. Relaxing these assumptions, gives rise to non-symmetric stress tensors, surface couples and body couples, couple stress tensors, and internal degrees of freedom. These emerging quantities constitute the components of the theory of asymmetric continua [138] named after Cosserat brothers [24] as the Cosserat continua. In its most general case, a Cosserat continuum consists of deformable point elements with three global translational degrees of freedom as well as six internal micro-structural degrees of freedom including independent translations and rotations representing micro-deformations of each element. This is known as a micromorphic continuum [45, 48]. What Eringen [46] calls "micropolar theory" emerges as a special case of the micromorphic deformation theory when the state of micro-deformations is described by independent local rigid rotation of material point elements, also known as micro-rotations [46]. Based on the latter assumption, a point element of material has total six degrees of freedom, including three translational and three independent rigid rotational degrees of freedom. Kinetically, such independently rotating rigid elements transfer not only force per unit area, but also moment(couple) per unit area or namely "couple-stress". A Cosserat continuum with such simplifying assumptions work suitably for a large class of solid materials, particularly those with significant

micro/nano-structures (e.g. polymeric composites, granular and fibrous materials).

The generalized continuum theories with independent internal degrees of freedom carry length scales into the model. In particular, a micropolar material incorporates an intrinsic characteristic length in the mechanical behavior of the corresponding body; a quantity which is absent from the materials in the classical continuum. It is observed that the mechanical behavior of a body modeled as a micropolar material is dramatically influenced by the characteristic length of the material when the length scale of the external stimuli (such as wavelength), or the geometrical dimensions of the body are comparable to the intrinsic characteristic length of the material. This effect is commonly named "size-dependency" of the material's behavior and is not captured via the classical theory.

The mid-twentieth century marks the rebirth of the Cosserat continuum theories after half a century of dormancy, mainly because of the growing use of the materials whose micro/nano-structures significantly affect their mechanical behavior. In a period of years in 1960s-1970s, researchers attempted to overcome the inadequacy of the classical models by refurbishing the Cosserat theories to achieve more comprehensive models capable of including the micro/nano-mechanical effects. From these years forward, solid mechanics in particular, was enhanced with generalized theories such as micropolar elasticity [49, 112], couple stress elasticity [104, 141, 142], strain-gradient elasticity [103], and non-local elasticity [50, 84]. The couple stress theory of elasticity results as a special case of the micropolar elasticity where the micro-rotations coincide with the global rotation of point elements in the way defined in the classical elasticity. The strain-gradients are generated where the constitutive theories depend on the higher derivatives of strain tensors. Further, the non-local theories abandon the locality hypothesis in the classical elasticity meaning that the constitutive law depends on the strain in a certain range of space about a point and the history of strain in time rather than the strain at that point in a fixed time. For a comprehensive account of the continuum theories, we refer to Truesdell and Noll [143].

The micropolar theory of elastic materials was surmised ahead of its experimental validations. The earliest efforts were conducted by Schijve [127, 41] in search of couple stress

effects in real materials. The objective was to detect the effects of thickness on the flexural rigidity of metallic plates. These tests, however, reported no departure from the classical predictions of stress fields in small scale metals due to the insufficient smallness of specimens which were still far from the intrinsic characteristic length of the metals [11]. The first evidence of the presence of micropolar and couple stress effects was observed in 1970s due to Askar [5], and Perkins and Thompson [115]. More successful investigations of the size dependence in micropolar theory began in 1980s with a series experiments by Lakes and co-workers [152, 87, 88, 89]. For example, Lakes-co-worker's team showed that certain porous solids [88] and metallic foams [13] are describable as micropolar materials for which they found six corresponding elastic constants. Since the observation of the micropolar elastic effects in advanced materials, a great deal of effort was put to determine the elastic constants corresponding to the micropolar model. A method of detecting size dependence is to test and identify the changes in the stiffness of material samples made with similar geometries and varying sizes. These methods of size-effect identification were adopted in experiments by Lakes and co-workers, also popularly by others [12] to determine the micropolar elastic parameters. In a later effort, Mora and Waas [106] calculated the micropolar characteristic lengths for a polycarbonate circular-cell honeycomb using uniaxial compression tests and direct measurement of strain and displacement. More recently, the mechanical properties of heterogeneous materials with periodic circular voids were interpreted in the sense of the constitutive laws of micropolar elasticity [10, 149]. In most cases, the experimental studies conclude that the characteristic length defined in micropolar models is equivalent to the average size of internal microstructures of the corresponding materials. Even though the generalized continuum theories, and particularly the micropolar theory, are still ahead of the experiments because of the technical challenges that arise in small scale testing, the experimental studies remain an open and ongoing area. A comprehensive review of the experimental studies is given by Hassanpour and Heppler [68].

Supported and validated by numerous experimental studies, micropolar continua have proved to be a promising tool in modeling and studying advanced materials. For instance,

using graph theory and energy based homogenization of granular media Goddard [61] demonstrated that micropolar theories represent plausible models for such materials. Subsequently, the micropolar descriptions of granular materials were used to elaborate the theory of porous materials which otherwise suffered from classical disadvantages in their views of microscopic phenomena such as shear band localization [40, 39]. De Borst [29] showed that micropolar models as higher order continua can eliminate the numerical anomalies that occur in finite element simulation of failure modes and elastoplastic localization. Consequently, the micropolar theories are more amenable for use in numerical analysis of granular materials. For example, Mori et al. [107] formulated a finite element method using Cosserat continuum constitutive properties which made the model capable of considering the microrotations of powder grains and lead to an extension of finite element analysis to applications for microscopic behavior of granular materials. Two other examples of modifying finite element method to accommodate Cosserat continuum properties of granular materials can be found in [145, 160]. These generalizations of continuum mechanics contributed successfully to developing models of porous, foamy and multi-phase materials [31, 32, 30]. The micropolar theory was also adopted for an adequate representation of plastic behavior of poly-crystals [133]. The application of micropolar theory is not limited to granular and poly-crystalline materials. At the nano-scale level, Xie and Long [52] employed micropolar theory to model the nanostructure of carbon nanotubes. They considered elements having kinematic properties of micropolar point elements and assigned couple stress interaction between the carbon bonds of two neighboring elements. Before them, Ivanova et al. [76, 75] had applied the idea of including moment components to the inter-atomic interactions. They, as well, included rigid rotational degrees of freedom for a group of atoms taken as a single point element. Hence, they interpreted the atomic group nano-structures in the framework of a micropolar model. Furthermore, the micropolar mechanics was use in developing enhanced theories of beams, plates, and shells [72, 116, 47, 1, 42, 122]. For a comprehensive review on various applications of Cosserat continua and the development of theories of micropolar plates and shell we refer to Altenbach et al. [2].

Micropolar theory offers many advantages over classical elasticity where a small-scale phenomenon is involved. First, the micropolar models provide a more adequate account of stress distribution around cracks, notches and defects where the stress/train gradients are large [79]. The application of micropolar theory alters the stress fields and mainly abates the stress distribution about a crack, however, it does not affect the singularity order of the stress at the crack tip [154]. The stress concentration in small-scale mechanics is important because usually the classical theories fail to provide a sufficient prediction of stress in the regions of high stress and strain gradient intensity. The stress concentration regions commonly appear in the problems of defects, notches, cracks and contact. The numerical finite element analysis of notches and contact problems by Eremeyev et al [44] demonstrates that the micropolar elasticity results in an ameliorated stress concentration compared to the classical approach and it captures the experimentally observed size dependence of such problems [121]. The couple stresses, in particular, appear near high stress gradient regions and singularities. Shmoylova et al [130] presented similar results for the stress concentration about a crack in bone and and proved that their results agree well with the experimental data in [90]. In addition, the micropolar theory generally predicts higher measures of stiffness for a material where the size of micro-structures are comparable with the configurational measures. The accurate estimation of such properties become particularly important in design and prediction of behavior of micro/nano-scale devices. While the effect of size is absent from the classical elasticity, a substantial increase in the apparent elastic moduli is predicted by the micropolar model where the size of specimen is smaller. Rueger and Lakes [119] observed such effects in accordance with the micropolar predictions, while those effects are missing from classical models.

Despite mostly aiming micro/nano-mechanics of materials, the concept of micropolar elasticity found use even beyond the small-scale problems. For example, Pau and Trovalusci [114] employed micropolar theory to study the behavior masonry walls. They demonstrated that any material with even macroscopic internal features requires higher order continuum models, as long as their internal kinematics effectively alters their mechanical behavior. In

particular, they concluded that the micropolar effects are more intense when the microrotation of elements depart further from the classical (macro)rotations. Traditionally, discrete element methods are the common approach to the problems involving materials with distinct features, yet Pau and Trovalusci [114] demonstrated that the micropolar model can successfully replicate the discrete models for such materials.

Refining the classical models based on internal degrees of freedom and presence of couple stress is not the only approach for generalization of continuum models. Observations indicate yet another phenomenon which becomes significantly dominant at the nano-scale level. It is well-known that the material particles (atoms or molecules) experience a different local balancing formation than the particles deep inside the materials. As a result, the particles on the surface assume a different structure than that of the bulk. The reconstruction of the surface usually occurs in a form of relaxation or general reconstruction. Relaxation happens when the surface atoms change position with respect to the bulk arrangement. General reconstruction refers to relaxation plus rearrangement of surface atoms with respect to each other. These different arrangements of atoms on the surface lead to different energy states of the surface compared to that of the bulk. The difference between the energy states of the surface and the bulk is referred to as Gibbs free surface energy [62]. The surface stress appears as the variation of the surface free energy to the variation of strain on the surface; a ratio that obviously assumes a different measure on the surface than the bulk. Consequently, the constitutive properties of the surface of solids are different than the entire body. Such different mechanical properties of material surface generally extend to a few atomic layers, therefore their effects are usually neglected in classical continuum models. However, these surface effects are significant in materials with non-negligible nano-structures. Such materials often have configurations of nano-meter dimensions with a large surface area to volume ratio. Consequently, the incorporation of surface effects in continuum models become vital in modeling nano-structured solids, such as nano-composites, nano-porous, multi-layer nano-film superlattices, nano-beams, nano-shells and nano-tubes.

The first rational continuum based model of surface mechanics was introduced by Gurtin

and Murdoch [64]. In their model Gurtin and Murdoch regarded the surface of a solid as a membrane of separate elasticity adhering to the underlying solid. Gurtin and Murdoch developed their theory based on a concurrent use of linear elasticity for the bulk and finite deformation formulation for the surface. Due to coupling a two dimensional surface structure with a three dimensional bulk, a quantity of the length dimension arises from the equations which introduces size-dependence into the model. Some implications of Gurtin and Murdoch (G-M) model were presented by Ru [118]. Since its first appearance in the literature, G-M model has been widely used in the area of nanomechanics [93].

Among the myriad of research that model size dependence of nano-scale materials using the G-M model of surface effects, Sharma et al. [129] incorporated surface effects into the model of nano-inhomogeneities with eigenstrains. They illustrated the surface effects on the size dependence of stress concentration about spherical inhomogeneities. A more general version of the account of stress concentration about a spherical void was given in [69]. Tian and Rajapakse conducted similar studies [139, 140] for circular and elliptical inhomogeneities under plane deformations. In most cases, reduced stress concentrations were obtained about voids and inhomogeneities of nano-scale size due to the positive surface elastic stiffness. As mentioned earlier, however, because of their size-independent nature, the classical continuum models generally overestimate the stress concentration near nano-scale structures such as nano-inhomogeneities. Another interesting problem of nano-mechanics is to determine homogeneous mechanical properties of heterogeneous materials containing nano-structures. In that regard, Yang [151] investigated the size-dependence generated from the surface effects on the equivalent homogenized elastic properties of a heterogeneous nano-composite. The surface effects on the elastic properties of other nano-sized materials have also been of great interest. For example, Gua and Zhao [63] and Wang and Feng [146] considered the size-dependence of nano-beams due to surface effects. Wang and Feng [146] demonstrated that the positive surface elastic constants increase the predicted natural frequency of nano-beams regardless of the corresponding modes of vibration. Gua and Zhao [63] concluded that with positive surface constants the bending modulus of nano-beams increases due to

the significant surface effects at nano-scale level. Notably, experimental observations back up their conclusion [14]. Surface mechanics also dominates the response of materials to the nano-size phenomena such as inclusions, dislocations, cracks, and nano-scale defects. Dai et al.[27] analyzed the effects of G-M surfaces of a thin film on the stress distribution and image forces generated due to a screw dislocation in the film. They observed that the stress concentration about the surface is lower for a positive surface elastic constant. In addition, the positive surface elastic constant reduces the magnitude of image force and the tendency of the dislocation toward escaping form the crystal. Wang and Schiavone [147] presented an analytical solution of plane deformations induced by dislocations and inclusions in the presence of surface effects and demonstrated the significant size-dependence of these interacting nano-size defects.

The G-M surface model provides a more realistic account of nano-scale phenomena where the classical continuum models fail. Antipov and Schiavone [4] using G-M model reduced the order of singularities of the crack tip and showed that the surface effects can predict a more physically plausible strain at the crack tip. Kim et al. [81, 82], as well, obtained reduced stress singularities at the crack tip for different crack modes and interface cracks. We refer the reader to [80] for a comprehensive account of the role of crack tip conditions in the reduction of stress singularities at a crack tip in classical linear elasticity with surface effects. Consequently, in all the aforementioned examples, the G-M surface mechanics serves as a powerful tool to provide a more adequate description of mechanics of solids at the nano-scale level.

The neutrality of stress fields is another interesting problem of nano-mechanics that was tackled using G-M surface model. The problem arose with the following questions: under what conditions the presence of surface effects retains a uniform stress field around nano-sized inhomogeneities in nano-composites? In other words, researchers tried to find the condition under which the inhomogeneities are neutral or "invisible". This problem is particularly important for exploiting surface mechanics in design of nano-materials with desirable properties. Benveniste and Miloh [9] addressed this question by modifying the con-

tact mechanisms of inhomogeneities to achieve a undisturbed stress field or neutrality. They employed a membrane-type interface to neutralize the stress disturbance about elliptical and spheroidal inhomogeneities. Using G-M surface model, Dai et al. [26] proved that only the circular elastic inhomogeneities can achieve neutrality under uniform external loads creating plane or anti-plane deformations.

Surface effects at the nano-scale level can be so substantial that they dramatically increase the elastic constants of a nano-structured material. This fact encouraged design of nano-materials whose stiffness is higher than their regular homogeneous counterpart. Duan et al. [37] showed that a nano-porous material can be made stiffer than their parent material out of which they are manufactured. This is outstanding for optimization of design where a more desirable elastic properties can be acquired by using less material.

Despite being successful in investigating the size dependent mechanical behavior of nano-materials, the G-M model suffers an inconsistency with the fundamental Gibbsian principles of thermodynamics [113]. Atomistic simulations [101] show that the elastic parameters of surface may be negative. However, the physical nature of G-M surface as an elastic membrane does not comply with this possibility, since having a negative elastic modulus is physically implausible for the two dimensional elastic body of a membrane. Furthermore, Steigmann and Ogden [136, 137] argued that an energy-minimizing configuration of surface/bulk combination is impossible to achieve under compressive surface stresses with the G-M model. To address these issues, they generalized the G-M model to incorporate the effects of flexural resistance into the model.

The modified surface model of Steignann and Ogden form (hereafter referred to as S-O model) has recently attracted numerous applications in analyses of nano-materials. Chhapadia et al. [17] in their work verified the important aspects of S-O model by comparison with atomistic simulation results. They argued that, depending on the desired accuracy, the use of S-O model becomes necessary for problems involving surface wrinkling and bending modes. Among other attempts to enhance the analysis of nano-materials with more elegant surface models, Zemlyanova and Mogilevskaya [158, 159] presented a comprehensive account

of circular and spherical inhomogeneities with S-O interfaces. They determined stress fields, effective elastic properties and the neutrality conditions in the presence of S-O model of surface effects. Han et al. [67] generalized their work to calculate the effective elastic properties of nano-composites with multiple interacting nano-inhomogeneities of circular cylindrical shape. The S-O surface mechanics also found use in the models of fracture, contact and defect mechanics. Zemlyanova [156] revisited mechanics of mixed mode cracks in the presence of S-O surface model. Modeling fracture with the S-O surface predicted bounded stress and strain fields at the crack tips of the fracture while satisfying the material symmetry conditions. As a result, the S-O surface proved advantageous over the G-M surface model. Zemlyanova, Li and Mi [157, 94] reconstructed the contact and nano-indentation models to incorporate S-O surface effects. Comparison between responses of the curvature-independent G-M model and curvature-dependent S-O model indicates that the curvature-dependency incorporated by the S-O model surface is increasingly important at the very small scales. Li and Mi [94] showed that in most cases the S-O model result in higher nano-indentation hardness. Finally, a recent analysis of an edge dislocation as an elastic defect near a S-O planar interface by Dai and Schiavone [28] demonstrated that the bending resistance of the interface characterizes the equilibrium state of the dislocation and diminishes the residual interface tension as the dislocation approaches the interface. They also showed that the use of S-O interface model with bending resistance dramatically affects the image forces between the dislocation and the interface. It may indeed lead to a physically acceptable stable equilibrium position for the dislocation in the vicinity of the interface.

So far, we introduced two main approaches in enhancing the continuum models to become well-suited for micro/nano-mechanical analysis: elastic surface mechanics and higher order continuum theory of micropolar elasticity. The main idea of this thesis is to include both theories simultaneously into a model of mechanical behavior of micro/nano-scale materials. Each of these theories improve some aspects of the mechanical models, therefore, we expect that the combination of these theories provides a more comprehensive account of mechanics of materials with micro/nano-structures. As a result, the present thesis provides a basis

where surface elasticity and micropolar theory meet. The objective is to develop a model that captures the micro/nano-mechanical behavior of the bulk as well as the contribution of surface effects both of which have manifested significance in certain classes of real materials wherein the effects of both surface and internal micro/nano-structures are substantial.

The idea of incorporating both internal micro/nano-constituents and surface effects was considered by only a handful of researchers, probably due to the mathematical complexities associated with these models. Perhaps Zhang and Sharma [161] were among the first to include the surface effects in the framework of generalized nonlocal theory for the internal structures to analyze quantum dots. A similar idea was adopted in the context of couple-stress theory to develop new modified models of nano-beams and nano-plates [128, 53]. As one of the few attempts to develop such comprehensive models, Chen et al. [15, 16] proposed a micropolar elastic model of nano-composites in the presence of surface effects. However, they employed the G-M type surface in which the classical flexural resistance of the surface is absent. In a more recent work, Sigaeva and Schiavone [131] proposed a micropolar surface mechanics to develop a comprehensive model of anti-plane deformations in solids. They presented a meticulous analysis to ensure their mathematical model is well-posed. We, as well, believe that the two aforementioned approaches individually open separate gateways to improving the accuracy of predictive modelling in solids at smaller length scales. We expect that coupling both approaches would lead to a more comprehensive representation of size-dependence in solids.

As stated earlier, our objective in this research is to devise a mathematical model which brings together both surface elastic effects and microstructural aspects of a solid body subjected to plane deformations. Such a mathematical model requires rigorous analysis to investigate the proper establishment of the corresponding boundary value problem. As a result, any such mathematical model must be designed in such a way that it will be 'well-posed'. In the sense of Hadamard, being well-posed means that the model puts forward a mathematical construction which is solvable, the solution to this construction is unique, and the solution is stable with respect to the prescribed data. Any attempt to implement

a mathematical model without meeting the Hadamard's "well-posedness" criteria may lead to ineffective numerical analysis or physically incorrect solutions. We intend to develop a well-posed mathematical model and carry out a comprehensive evaluation in terms of the foregoing factors.

Boundary integral equation methods (BIEM) are the classical strategy for analyzing well-posedness of the boundary value problem corresponding to a mathematical model [23, 22, 21]. A comprehensive account of well-posedness analysis of different forms of elasticity and thermoelasticity theories using the boundary integral equation methods can be found in the seminal book by Kupradze [85]. These methods (BIEM) commonly involve presenting solutions of the boundary value problems (BVP)s in the form of potentials and reducing the BVPs to some integral equations over the boundaries. This is beneficial because the boundary value problems can be handled more efficiently in their corresponding form of integral equations. The integral equations theory consists of well-established statements that facilitate the well-posedness analysis [109, 144]. Consequently, the BIEMs have been the key to the analysis of boundary value problems of classical elasticity [22, 23] and even micropolar theory [123, 71]. However, since the BIEMs convert the BVPs to their integral representation over the boundaries, the states of boundary conditions become extremely important in the analysis. As a matter of fact, the incorporation of surface mechanics into the model will further complicate the description of the boundaries and give rise to highly-nonstandard boundary conditions. Therefore, we need to modify the BIEM technique to be applicable to our proposed complex mathematical model.

Despite the complicated nature of the analysis, Sigaeva [132] discussed the micropolar surface mechanics of anti-plane shear deformations. In that proposed model, however, the micropolar surface effects were of the G-M nature with only stretching resistance assigned to the surface. This was mainly due to the mechanism of the anti-plane deformation model that excludes the possibility of bending across the surface. Whereas, the present thesis proposes a micropolar model plane deformation that incorporates surface effects. As such, the surface deformations entail the classical stretching and bending modes as well as the independent

micro-rotations of the micropolar theory. Consequently, we aim to provide a more general S-O type surface description capable of accounting for curvature dependence and flexural resistance of the surface.

In Chapter 2 of this thesis, we formulate two mathematical models of linear elastic plane deformations incorporating micropolar surface mechanics. We model the surface as a micropolar shell perfectly bonded to the surface (or interface) of a micropolar elastic material. We establish the corresponding boundary value problems for a simply connected domain occupied with a micropolar linear elastic material partially bounded by closed curves having separate micropolar surface elastic properties. We use two different micropolar shell theories to describe the surface effects, each of which having particular advantages in terms of application and elegance. The derivation of the two mathematical model is a detailed version of the first five sections of the paper by Gharahi and Schiavone [59] published in *Journal of Continuum Mechanics and Thermodynamics*.

Chapters 3, 4 and 5 proceed with some interesting applications of the proposed model. In Chapter 3, we evaluate the stress concentration around a circular hole in an infinite planar medium using our proposed model. In this chapter, we illustrate that our enhanced model contributes to the adequacy and accuracy of the stress fields around imperfections such as holes by introducing more variables into the problem. In addition, based on our results we discuss the class of problems for which the use of such advanced models become substantial. The main course of this chapter with a slightly different surface modeling is published in *Journal of Continuum Mechanics and Thermodynamics* [57].

Chapter 4 is dedicated to yet another interesting problem that we mentioned earlier in this Introduction. Evaluating the effective elastic properties of a material is a very important application of micro/nano-mechanics because it provides a better insight into the mechanics of micro/nano-materials which are increasingly used in several areas of advanced technology. Finding global material properties based on the size-dependent nano-mechanical behavior has always been one of the objectives pursued in nano-mechanics. In this chapter, we demonstrate that our model yields a successful account of size-dependent deformations of materials

with nano-inhomogeneities. As such, our proposed model can predict the overall mechanical properties of materials for which the internal structure as well as surface effects are significant. Having more data involved in the advanced mathematical model proposed in the thesis a higher precision of calculations of mechanical properties can be achieved. However, the more variables involved in the model the more they complicate the formulations. The entire Chapter 4 is summarized in a publication in *International Journal of Mechanical Sciences* [56] with a slight difference in the formulation of the surface effects.

We continue our evaluation of the model in Chapter 5, with a very common nano-scale phenomenon. The presence of dislocations in the arrangement of material particles is the key to many mechanical behavioral properties. Appearing only at the nano-scale level, dislocations are commonly treated in the framework of micro and nano-mechanics. Although, the deformation theory of dislocations as a nano-scale defect is usually formulated in the classical elasticity. Thus, the dislocation problems require further investigation in the context of generalized continuum models. In that respect, in Chapter 4, we try our model on the problem of interaction of an edge dislocation with the surface of a half-plane micropolar medium. Knowing that our model is constructed in a way that takes into account both the effects of nano-constituents and the micropolar surface with bending resistance, we presume that it provides a more adequate account of the problem. In particular, we study the deviations made from the existing literature by the use of our model. This chapter is published in *Acta Mechanica* [58].

Chapter 6 contains the climax of the thesis. After demonstrating the merits of the proposed model in its successful application to many practical nano-mechanics problems, we proceed to analyze the model in terms of mathematical well-posedness. We reformulate the boundary value problems corresponding to the mathematical model of plane deformations with micropolar surface effects to investigate the existence and uniqueness of the solutions. We establish the existence and uniqueness theorems and the conditions under which they hold true. As a result, the main components of well-posedness in the sense of Hadamard are obtained for the two micropolar surface models. A summary of Chapter 6 is contained in

two publications by Gharahi and Schiavone [59, 60] in *Journal of Continuum Mechanics and Thermodynamics* and *Journal of Applied Mathematics and Mechanics (ZAMM)*, respectively.

Chapter 2

Mathematical Modelling of Surface Elasticity

We aim to present an enhanced mathematical model of the deformation of a solid body whose mechanical properties incorporate both surface and microstructural effects. The two effects become particularly important when dealing with materials with significant internal micro-/nano-structure and materials considered at the nano-scale. Generalized continuum mechanics furnishes well-established theories that attempt to release mechanics of materials from their underlying classical assumptions as a continuum and incorporate the effects of material constitution into the description of their mechanical behavior. For instance, under less restrictive assumptions, the generalized theories allow stress vector on a cut surface of a solid to be nonlinear in its unit normal; there may appear applied couples on the surface and inside the volume of a solid body; and additional degrees of freedom account for the internal motion of micro-/nano constituents [98]. Surface mechanics enhances continuum-based approaches to nanostructured solids by recognizing that material surfaces behave rather differently than the bulk and subsequently incorporating these differences in an enhanced mathematical model of deformation. It is customary to model the surface as a thin elastic membrane capable only of extension (with no flexural resistance) [64, 65]. However, among other deficiencies, these membrane type models are incapable of predicting an energy minimizing configuration in certain compressive states of stress. To obtain a more comprehensive

account of the contribution of surface to deformations, it is therefore necessary to improve the surface model and include the effects of curvature and flexural resistance of the surface [137, 136].

Another important consideration is that a large majority of research involving surface elasticity is conducted in the framework of classical elasticity, while the extension of surface theories to higher order continua involves inevitable mathematical challenges. In this chapter we present plane deformations of a micropolar elastic solid coupled with a micropolar surface model that allows for bending and twisting effects of the surface. First we present the surface as a Kirchhoff-Love thin micropolar elastic shell bonded to the bulk micropolar material. Two types of derivations of micropolar shell theory give rise to two types of boundary conditions reflecting the surface effects. Finally in this chapter we formulate fundamental interior and exterior mixed boundary value problems describing plane deformations of a micropolar elastic solid with surface elasticity. These problems serve to describe fundamental scenarios in which a combination of stress and displacement are prescribed on parts of the boundaries of a multiply connected domain.

2.1 Preliminaries

Before we begin to formalize the model, it is necessary to set up the notations used in the thesis. Also in this section we summarize the theory of linear micropolar elasticity and demonstrate its relation to the usual classical elasticity. We, as well, define the function spaces wherein the mathematical model is designed and further analyses take place later on in the thesis.

In what follows, Greek and Latin indices take the values 1, 2, and 1, 2, 3, respectively, and we sum over repeated indices, unless otherwise stated. In a Cartesian system of coordinates $\{x_i\}_{i=1}^3$, the partial derivative with respect to the position component x_i is indicated by the notation $(...)_{,i} \equiv \partial(...)/\partial x_i$.

We consider the Cartesian coordinates $\{x_1, x_2, x_3\}$ oriented in such a way that the $\{x_1, x_2\}$-plane coincides with the plane of deformation and x_3, with the antiplane (out-

of-plane) direction. A vector $\mathbf{a}$ in the Cartesian coordinates is indicated by its components $\mathbf{a} = \{a_1, a_2, a_3\}$, the inner product of two vectors $\mathbf{a}$ and $\mathbf{b}$, by $\mathbf{a} \cdot \mathbf{b} = a_1 b_1 + a_2 b_2 + a_3 b_3$, and the cross product (or the vector product) is denoted by $\mathbf{a} \times \mathbf{b}$. In addition, the tensor product of the two vectors is denoted by $\mathbf{a} \otimes \mathbf{b}$ and the inner product of two tensors, $\mathbf{M}$ and $\mathbf{N}$ is denoted by $\mathbf{M} : \mathbf{N} = M_{ij} N_{ij}$. A superscript "$T$" indicates transposition of a tensor or a vector. If a generic point of a body in Cartesian coordinates is regarded as $\mathbf{x} = (x_1, x_2, x_3)$, then the gradient operator in Cartesian coordinates is defined as $\nabla \equiv \left(\frac{\partial}{\partial x_1}, \frac{\partial}{\partial x_2}, \frac{\partial}{\partial x_3} \right)$, and the Laplacian operator as $\Delta \equiv \frac{\partial^2}{\partial x_1^2} + \frac{\partial^2}{\partial x_2^2} + \frac{\partial^2}{\partial x_3^2}$.

2.1.1 Fundamentals of the Theory of Micropolar Elasticity

Classical elasticity models solids as ideal elastic continua in which load transfer on an arbitrary surface element dA in the body occurs only through the stress vectors. This assumption results in describing the kinematics and kinetics of the body by symmetric expressions for stress and strain tensors. We denote the stress and strain tensors in terms of their Cartesian components as σ_{ij} and ϵ_{ij} respectively. According to classical elasticity theory, for a material occupying a region $\mathfrak{B}$ of volume V bounded by surface A, the components of the stress vector, p_j, acting on an element of the surface dA are expressed by $p_j = \sigma_{ij} n_i$, where n_i are the Cartesian components of the outward unit normal vector to the surface element dA. In the static case and in the absence of body forces Euler's postulates for this piece of material leads to the following descriptions for the balance of forces:

$$\oint_A p_j dA = \oint_A \sigma_{ij} n_i dA = \int_V \sigma_{ij,i} dV = 0, \tag{2.1}$$

and the balance of moments:

$$\oint_A \varepsilon_{ijk} x_i p_j dA = \oint_A \varepsilon_{ijk} x_i \sigma_{lj} n_l dA = \int_V \left(\varepsilon_{ijk} x_i \sigma_{lj} \right)_{,l} dV = 0, \tag{2.2}$$

where ε_{ijk} is the Levi-Civita symbol of permutation and the divergence theorem is used to convert the surface integrals to the volume integrals. The integrals vanish for every arbitrary

piece of material, therefore, by the localization theorem the integrands must vanish. The balance equations become,

$$\sigma_{ij,i} = 0, \quad \sigma_{ij} = \sigma_{ji}. \tag{2.3}$$

Kinematics of a classical elastic body is identified by infinitesimal deformations including infinitesimal displacements, u_i and infinitesimal displacement gradients $u_{i,j}$. Consistent with this assumption and the symmetry of the stress tensor, the strain tensor, ϵ_{ij}, is defined as the symmetric part of the displacement gradient, i.e.

$$\epsilon_{ij} = \frac{1}{2}(u_{i,j} + u_{j,i}). \tag{2.4}$$

For an isotropic elastic material with infinitesimal deformations the constitutive law that characterizes the strain and stress relation is given by

$$\sigma_{ij} = 2\mu\epsilon_{ij} + \lambda\delta_{ij}\epsilon_{kk}, \tag{2.5}$$

where μ and λ are the two material parameters known as Lamé constants which determine a homogeneous isotropic elastic material. The stress field σ_{ij}, inducing a strain field ϵ_{ij} causes an internal strain energy whose density is expressed by $E = \frac{1}{2}\sigma_{ij}\epsilon_{ij}$. The strain energy density in terms of the strain field in components can be written as

$$E = \mu\epsilon_{ij}\epsilon_{ij} + \frac{\lambda}{2}\left(\epsilon_{kk}\right)^2, \tag{2.6}$$

Positive definiteness of the strain energy restricts the Lamé constants to $\mu > 0$ and $\mu + \lambda > 0$. The classical theory of elasticity, briefly described here, is in good agreement with experimental results for many structures within the linear elastic deformation range. In several cases, however, the discrepancy between the experimental results and the classical theory is noticeable. These cases include the presence of large stress gradient, large frequency elastic vibrations and bodies with significant granular structures, microstructures or large polymeric molecules [112].

The theory of micropolar elasticity, also known as Cosserat elasticity due to the seminal work of the Cosserat brothers [24], describes the static deformation of each point by a

displacement vector $\mathbf{u}(\mathbf{x})$ and an independent rotation vector $\boldsymbol{\varphi}(\mathbf{x})$. This assumption endows each element of the material body with six degrees of freedom, three of displacement, u_i and three of microrotation, φ_i, and the possibility of non-symmetric strains and stresses. Consistent with this assumption, two arbitrary body parts interact on their dividing surface element, dA, in the body through forces, $p_j dA = \sigma_{ij} n_i dA$, and moments, $m_j dA = \mu_{ij} n_i dA$ acting on the surface element. Thus, we define a quantity, μ_{ij}, analogous to the stress tensor, known as couple stress tensor. Now, consider a material body in equilibrium occupying a region $\mathfrak{B}$ of the volume V and enclosed by the surface A. In the absence of body forces, the statement of balance of forces for this piece of material remains as given in (2.1), whereas the balance of moments take the form

$$\oint_A (\varepsilon_{ijk} x_i p_j + m_k)\, dA = \oint_A (\varepsilon_{ijk} x_i \sigma_{lj} n_l + \mu_{lk} n_l)\, dA = \int_V (\varepsilon_{ijk} x_i \sigma_{lj} + \mu_{lk})_{,l}\, dV = 0,$$

in Cartesian coordinates. Again the local description of the balance equations become,

$$\sigma_{ij,i} = 0, \quad \varepsilon_{ijk}\sigma_{ij} + \mu_{ik,i} = 0. \tag{2.7}$$

For the micropolar body, under deformations due to the external force stress $\mathbf{p}$ and the couple stress $\mathbf{m}$, and with the assumption of absence of body forces, body moments, heat conduction, time dependence and dynamic effects, we can write the total potential energy as,

$$\Pi = \mathcal{U} - \mathcal{W}. \tag{2.8}$$

Here, $\mathcal{U}$ is the internal energy and $\mathcal{W}$ is the work of external forces, $\mathbf{p}$ and moments $\mathbf{m}$. Based on the principle of least action for a balanced system, variation of the total potential energy vanishes, i.e. $\delta\Pi = \delta\mathcal{U} - \delta\mathcal{W} = 0$.

$$\begin{aligned}\delta\mathcal{U} = \delta\mathcal{W} &= \int_A (p_i \delta u_i + m_i \delta\varphi_i) dA = \int_A (\sigma_{ji} n_j \delta u_i + \mu_{ji} n_j \delta\varphi_i) dA \\ &= \int_V (\sigma_{ji,j}\delta u_i + \sigma_{ji}\delta u_{i,j} + \mu_{ji,j}\delta\varphi_i + \mu_{ji}\delta\varphi_{i,j}) dV.\end{aligned}$$

We use the balance equations (2.7) and rearrange the equation to obtain,

$$\delta\mathcal{U} = \int_V \delta E dV = \int_V (\sigma_{ji}\delta(u_{i,j} + \varepsilon_{ijk}\varphi_k) + \mu_{ji}\delta\varphi_{i,j})dV, \tag{2.9}$$

where E, indicates the internal energy (strain energy) per unit volume. The equation (2.9) holds for every part of the body, therefore the localization theorem yields the internal energy per unit volume as,

$$\delta E = \sigma_{ji}\delta(u_{i,j} + \varepsilon_{ijk}\varphi_k) + \mu_{ji}\delta\varphi_{i,j}, \tag{2.10}$$

The expression for the variation of strain energy density leads us to the definition of microstrain tensor, $\epsilon_{ji}^{(mi)}$ and microrotation tensor, $\varkappa_{ji}$ as follows:

$$\epsilon_{ji}^{(mi)} = u_{i,j} + \varepsilon_{ijk}\varphi_k, \quad \varkappa_{ji} = \varphi_{i,j}, \tag{2.11}$$

We regard $\delta()$ as total differential in (2.10), to obtain the relations,

$$\sigma_{ji} = \frac{\partial E}{\partial \epsilon_{ji}^{(mi)}}, \quad \mu_{ji} = \frac{\partial E}{\partial \varkappa_{ji}}, \tag{2.12}$$

which for a linear isotropic elastic solid imply that E must be a quadratic function of $\epsilon_{ji}^{(mi)}$ and $\varkappa_{ji}$ in the following form

$$\begin{aligned} E = \frac{\mu+\alpha}{2}\epsilon_{ji}^{(mi)}\epsilon_{ji}^{(mi)} + \frac{\mu-\alpha}{2}\epsilon_{ji}^{(mi)}\epsilon_{ij}^{(mi)} + \frac{\lambda}{2}\epsilon_{jj}^{(mi)}\epsilon_{ii}^{(mi)} \\ + \frac{\gamma+\varsigma}{2}\varkappa_{ji}\varkappa_{ji} + \frac{\gamma-\varsigma}{2}\varkappa_{ji}\varkappa_{ij} + \frac{\beta}{2}\varkappa_{jj}\varkappa_{ii}, \end{aligned} \tag{2.13}$$

Thus, the constitutive equations of the linear isotropic micropolar solid become,

$$\begin{aligned} \sigma_{ji} &= (\mu+\alpha)\epsilon_{ji}^{(mi)} + (\mu-\alpha)\epsilon_{ij}^{(mi)} + \lambda\epsilon_{kk}^{(mi)}\delta_{ji}, \\ \mu_{ji} &= (\gamma+\varsigma)\varkappa_{ji} + (\gamma-\varsigma)\varkappa_{ij} + \beta\varkappa_{kk}\delta_{ji}. \end{aligned} \tag{2.14}$$

It is not difficult to see that a linear isotropic micropolar material is identified by six material parameters μ, λ, α, γ, β, and ς, instead of the two Lamé parameters in classical elasticity. Using the equations (2.11) in (2.14) and substituting the results for the stress and couple

stress tensors in the balance equations (2.7), we obtain the deformation field equations in the body,

$$\begin{aligned}(\mu+\alpha)u_{i,jj}+(\mu+\lambda-\alpha)u_{j,ij}+2\alpha\varepsilon_{ijk}\varphi_{k,j}=0,\\ (\gamma+\varsigma)\varphi_{i,jj}+(\gamma+\beta-\varsigma)\varphi_{j,ij}+2\alpha\varepsilon_{ijk}u_{k,j}-4\alpha\varphi_i=0.\end{aligned} \tag{2.15}$$

2.1.2 Function Spaces

In this section, we define the function spaces that are considered throughout the thesis. In the sections that follow, we use these function spaces to specify the boundary curves. In the upcoming chapters, as well, we highlight the function space in which the solutions are to be sought.

We define the class of Hölder continuous functions with index $a \in (0,1]$ as the space of functions, $\mathbf{f}(\mathbf{x})$, on a subset $\bar{S}$ of a Euclidean space satisfying Hölder's condition. The Hölder's condition states that for all $\mathbf{x},\mathbf{y} \in \bar{S}$ there is a real non-negative constant C for which, $|\mathbf{f}(\mathbf{x})-\mathbf{f}(\mathbf{y})| \leq C\,|\mathbf{x}-\mathbf{y}|^a$. Note that a bar indicates the closure of a set, i.e. $\overline{S} = S \cup \partial S$, and $|\mathbf{x}-\mathbf{y}|$ denotes the Euclidean distance between the two points $\mathbf{x}$ and $\mathbf{y}$. The functions satisfying Hölder's condition formally belong to the space of Hölder continuous functions on $\bar{S}$ denoted by $C^{0,a}(\bar{S})$. Similarly, the functions whose nth partial derivative satisfy the Hölder's condition belong to the space $C^{n,a}(\bar{S})$. Moreover, we denote the space of functions whose nth partial derivative is continuous on the domain $\bar{S}$ by $C^n(\bar{S})$. Accordingly, we call $C(\bar{S})$ and $C^1(\bar{S})$, respectively, the spaces of continuous and continuously differentiable functions on $\bar{S}$.

2.2 Proposition

Having the preliminary conventions and definitions in mind we now begin to introduce the model. Let S be a multiply-connected domain in $\mathbb{R}^2$ whose boundary is denoted by ∂S composed of the union of a finite number of sufficiently smooth closed curves. Let S be occupied by a linear, homogeneous and isotropic micropolar elastic material with Lamé-type

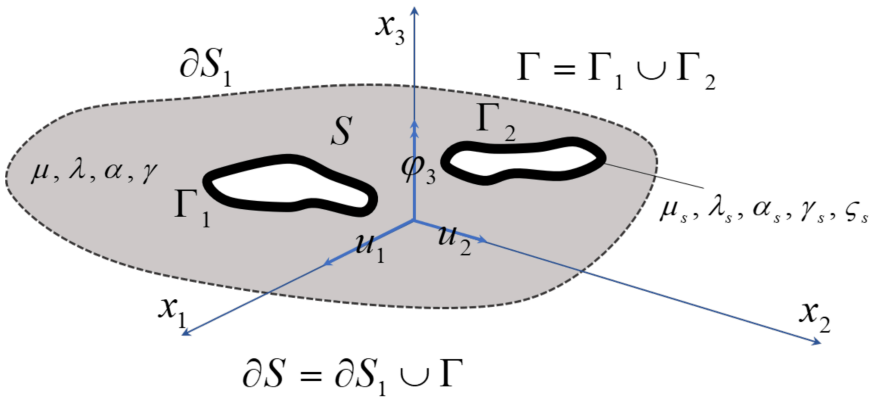

Figure 2.1: Configuration of the model

constants μ, λ, α, and γ. Without loss of generality, we consider a subset Γ of the boundary ∂S, comprised of a finite number of sufficiently smooth, closed curves made of thin elastic micropolar material with separate elastic constants, μ_s, λ_s, α_s, ς_s, and γ_s. The subset, Γ will therefore represent the part of the surface which incorporates additional surface effects (see Figure 2.1).

2.3 Governing Equations of Plane Micropolar Elasticity

Deformations of a plane micropolar bulk occupying the domain S are identified by displacement and microrotation fields described by [112],

$$\mathbf{u} = (u_1, u_2, 0), \ \boldsymbol{\varphi} = (0, 0, \varphi_3), \tag{2.16}$$

where the non-vanishing components u_1, u_2 and φ_3 are functions of the generic point $\mathbf{x} = (x_1, x_2)$ in the plane of deformation which is considered a subspace of the Euclidean space $\mathbb{R}^3$ with an orthonormal basis $\{\mathbf{e}_1, \mathbf{e}_2, \mathbf{e}_3\}$, represented by a Cartesian system of coordinates $\{x_1, x_2, x_3\}$. We neglect body forces and body couples for simplicity. In the absence of body forces and body moments, we use (2.15) to obtain the following system of equilibrium

equations [123],

$$\mathbf{L}(\partial\mathbf{x})\mathbf{w}(\mathbf{x}) = 0, \tag{2.17}$$

where, $\mathbf{w} = (u_1, u_2, \varphi_3)^T$, and $\mathbf{L}(\partial\mathbf{x}) = \mathbf{L}(\partial/\partial x_1, \partial/\partial x_2)$ is the matrix of partial differential operators defined by,

$$\mathbf{L}(\partial\mathbf{x}) = \begin{bmatrix} (\mu+\alpha)\Delta + (\mu-\alpha+\lambda)\frac{\partial^2}{\partial x_1^2} & (\mu-\alpha+\lambda)\frac{\partial^2}{\partial x_1 \partial x_2} & 2\alpha\frac{\partial}{\partial x_2} \\ (\mu-\alpha+\lambda)\frac{\partial^2}{\partial x_1 \partial x_2} & (\mu+\alpha)\Delta + (\mu-\alpha+\lambda)\frac{\partial^2}{\partial x_2^2} & -2\alpha\frac{\partial}{\partial x_1} \\ -2\alpha\frac{\partial}{\partial x_2} & 2\alpha\frac{\partial}{\partial x_1} & \gamma\Delta - 4\alpha \end{bmatrix}, \tag{2.18}$$

and $\Delta = \partial^2/\partial x_1^2 + \partial^2/\partial x_2^2$ is the usual two-dimensional Laplacian. We define the boundary stress operator $\mathbf{T}(\partial\mathbf{x}) = \mathbf{T}(\partial/\partial x_1, \partial/\partial x_2)$ as [123]

$$\mathbf{T}(\partial\mathbf{x}) = \begin{bmatrix} (2\mu+\lambda)n_1\frac{\partial}{\partial x_1} + (\mu+\alpha)n_2\frac{\partial}{\partial x_2} & (\mu-\alpha)n_2\frac{\partial}{\partial x_1} + \lambda n_1\frac{\partial}{\partial x_2} & 2\alpha n_2 \\ (\mu-\alpha)n_1\frac{\partial}{\partial x_2} + \lambda n_2\frac{\partial}{\partial x_1} & (2\mu+\lambda)n_2\frac{\partial}{\partial x_2} + (\mu+\alpha)n_1\frac{\partial}{\partial x_1} & -2\alpha n_1 \\ 0 & 0 & \gamma\left(n_1\frac{\partial}{\partial x_1} + n_2\frac{\partial}{\partial x_2}\right) \end{bmatrix}, \tag{2.19}$$

where $\mathbf{n} = (n_1, n_2)^T$ is the unit outward normal to ∂S. Upon determining the inner product of $\mathbf{T}(\partial\mathbf{x})\mathbf{w}(\mathbf{x})$, with an arbitrary vector $\mathbf{v} = (v_1, v_2, v_3)$ belonging to the real coordinate space $\mathbb{R}^3$, integrating over the boundary ∂S, and using the divergence theorem, we obtain

$$\begin{aligned} \int_{\partial S} \mathbf{v}\cdot\mathbf{T}(\partial\mathbf{x})\mathbf{w}(\mathbf{x})ds \;=\; & \int_S \operatorname{div}\{(2\mu+\lambda)(v_1u_{1,1}, v_2u_{2,2}) \\ & +\lambda(v_1u_{2,2}, v_2u_{1,1}) + (\mu+\alpha)(v_2u_{2,1}, v_1u_{1,2}) \\ & +(\mu-\alpha)(v_2u_{1,2}, v_1u_{2,1}) + 2\alpha(-v_2\varphi_3, v_1\varphi_3) \\ & +\gamma(v_3\varphi_{3,1}, v_3\varphi_{3,2})\}\,dv, \end{aligned} \tag{2.20}$$

where (a, b) is an ordered pair corresponding to the vector expression in the Cartesian coordinates $\{x_1, x_2\}$. After some straightforward yet tedious calculations, we can show that,

$$\int_{\partial S} \mathbf{v}\cdot\mathbf{T}(\partial\mathbf{x})\mathbf{w}(\mathbf{x})ds = 2\int_S E(\mathbf{v},\mathbf{w})dv + \int_S \mathbf{v}\cdot L(\partial\mathbf{x})\mathbf{w}(\mathbf{x})dv, \tag{2.21}$$

where,

$$\begin{aligned} E(\mathbf{v},\mathbf{w}) &= (2\mu+\lambda)\left(v_{1,1}u_{1,1}+v_{2,2}u_{2,2}\right)+\lambda\left(v_{1,1}u_{2,2}+v_{2,2}u_{1,1}\right) \\ &\quad +(\mu+\alpha)\left(v_{2,1}u_{2,1}+v_{1,2}u_{1,2}\right)+(\mu-\alpha)\left(v_{2,1}u_{1,2}+v_{1,2}u_{2,1}\right) \\ &\quad +2\alpha\left(-v_{2,1}\varphi_3+v_{1,2}\varphi_3\right)+\gamma\left(v_{3,1}\varphi_{3,1}+v_{3,2}\varphi_{3,2}\right) \\ &\quad +2\alpha\left(u_{1,2}-u_{2,1}+2\varphi_3\right)v_3. \end{aligned} \tag{2.22}$$

Denote by S^+ the bounded domain enclosed by ∂S and $S^- = \mathbb{R}^2\backslash(S^+ \cup \partial S)$. Assume also that the expression $\mathbf{a} \in X$ means that every component of $\mathbf{a}$ belongs to X. If we let $\mathbf{w} \in C^2(S^+)\cap C^1(\overline{S}^+)$ be a solution of (2.17) and take $\mathbf{v} = \mathbf{w}$, we obtain the first Betti formula in the (interior) domain $S^+ \cup \partial S$:

$$\int\limits_{\partial S} \mathbf{w}\cdot\mathbf{T}(\partial\mathbf{x})\mathbf{w}(\mathbf{x})ds = 2\int\limits_{S^+} E(\mathbf{w},\mathbf{w})dv, \tag{2.23}$$

where now $E(\mathbf{w},\mathbf{w})$ expresses the internal energy density of a micropolar bulk given by [123]

$$\begin{aligned} E(\mathbf{w},\mathbf{w}) &= \frac{\lambda}{2}u_{\alpha,\alpha}u_{\beta,\beta}+\frac{\mu}{4}(u_{\alpha,\beta}+u_{\beta,\alpha})(u_{\alpha,\beta}+u_{\beta,\alpha}) \\ &\quad +\frac{\alpha}{2}\left(u_{1,2}-u_{2,1}+2\varphi_3\right)^2+\frac{\gamma}{2}\left(\varphi_{3,1}^2+\varphi_{3,2}^2\right). \end{aligned} \tag{2.24}$$

The strain energy density is a positive quadratic form under the assumptions [47]

$$\mu+\lambda>0,\ \mu,\gamma,\alpha>0,$$

and hence the differential operator $\mathbf{L}(\partial\mathbf{x})$ is elliptic. Additionally, $E(\mathbf{w},\mathbf{w}) = 0$ if and only if $\mathbf{w}$ represents a rigid displacement-microrotation vector compatible with the theory of plane deformation; that is,

$$\mathbf{w} = (c_1 - c_3x_2, c_2 + c_3x_1, c_3), \tag{2.25}$$

where c_1, c_2, and c_3 are arbitrary constants. Clearly, the vector $\mathbf{w}$ of the form (2.25) satisfies $\mathbf{L}(\partial\mathbf{x})\mathbf{w}(\mathbf{x}) = \mathbf{0}$, and $\mathbf{T}(\partial\mathbf{x})\mathbf{w}(\mathbf{x}) = \mathbf{0}$.

Next, for the exterior domain, let (2.17) be satisfied in S^-. Any solution $\mathbf{w}$ of (2.17) may involve an arbitrary rigid displacement/microrotation of the form given in (2.25). The

non-rigid motion part of the solution $\mathbf{w}$ which is accountable for the non-zero strain-energy in the domain is assumed to satisfy the following restrictions at infinity ($r = |\mathbf{x}| \to \infty$) written here in polar coordinates (r, θ), [123], referred to henceforth as the class $\mathcal{A}$:

$$\begin{aligned} u_1(r,\theta) &= r^{-1}(\beta m_0 \sin\theta + m_1 \cos\theta + m_0 \sin 3\theta + m_2 \cos 3\theta) + O(r^{-2}), \\ u_2(r,\theta) &= r^{-1}(m_3 \sin\theta + \beta m_0 \cos\theta + m_4 \sin 3\theta - m_0 \cos 3\theta) + O(r^{-2}), \\ \varphi_3(r,\theta) &= r^{-2}(m_5 \sin 2\theta + m_6 \cos 2\theta) + O(r^{-3}), \end{aligned} \tag{2.26}$$

where

$$\beta = \frac{3\mu + \lambda}{\mu + \lambda},$$

and m_i $(i = 0, ..., 6)$ are arbitrary constants. Define further the class $\mathcal{A}^*$ by

$$\mathcal{A}^* = \{\mathbf{v} : \mathbf{v} = (c_1 - c_3 x_2, c_2 + c_3 x_1, c_3) + \mathbf{v}^{\mathcal{A}}\}, \tag{2.27}$$

where $\mathbf{v}^{\mathcal{A}} \in \mathcal{A}$. Also let $\mathbf{w} \in C^2(S^-) \cap C^1(\overline{S}^-) \cap \mathcal{A}^*$ satisfy $\mathbf{L}(\partial\mathbf{x})\mathbf{w} = \mathbf{0}$ in the multiply-connected domain S^- and consider a disk K_R of radius R which encloses ∂S. Then, we can write the first Betti formula in the domain $S^- \cap K_R$ as:

$$\int_{\partial K_R} \mathbf{w} \cdot \mathbf{T}(\partial\mathbf{x})\mathbf{w}(\mathbf{x}) ds - \int_{\partial S} \mathbf{w} \cdot \mathbf{T}(\partial\mathbf{x})\mathbf{w}(\mathbf{x}) ds = 2 \int_{S^- \cap K_R} E(\mathbf{w}, \mathbf{w}) dv. \tag{2.28}$$

Using (2.26) we can show that,

$$\int_{\partial K_R} \mathbf{w} \cdot \mathbf{T}(\partial\mathbf{x})\mathbf{w}(\mathbf{x}) ds \to 0 \text{ as } R \to \infty.$$

Thus, letting $R \longrightarrow \infty$, the first Betti formula in the exterior domain S^- is given by:

$$-\int_{\partial S} \mathbf{w} \cdot \mathbf{T}(\partial\mathbf{x})\mathbf{w}(\mathbf{x}) ds = 2 \int_{S^-} E(\mathbf{w}, \mathbf{w}) dv. \tag{2.29}$$

If we write

$$\mathbf{F} = \begin{pmatrix} 1 & 0 & x_2 \\ 0 & 1 & -x_1 \\ 0 & 0 & 1 \end{pmatrix},$$

then the column matrices

$$\mathbf{F}^{(1)}=\begin{pmatrix}1\\0\\0\end{pmatrix},\mathbf{F}^{(2)}=\begin{pmatrix}0\\1\\0\end{pmatrix},\mathbf{F}^{(3)}=\begin{pmatrix}x_2\\-x_1\\1\end{pmatrix}$$

form a basis for (2.25) and $\mathbf{Fk}$, with $\mathbf{k}=(c_1,c_2,c_3)^T$ representing any vector of the form (2.25).

The matrix of fundamental solutions for the operator $\mathbf{L}$ is given by [123]

$$\mathbf{D}(\mathbf{x},\mathbf{y})=\mathbf{L}^*t(\mathbf{x},\mathbf{y}), \tag{2.30}$$

where $\mathbf{L}^*$ is the operator adjoint to $\mathbf{L}$ and whose components are given by

$$\begin{aligned}
L^*_{11} &= (\mu+\alpha)\gamma\Delta^2+(\mu-\alpha+\lambda)\gamma\Delta\frac{\partial^2}{\partial x_2^2}-4\alpha\mu\Delta-4\alpha(\mu+\alpha)\frac{\partial^2}{\partial x_2^2},\\
L^*_{22} &= (\mu+\alpha)\gamma\Delta^2+(\mu-\alpha+\lambda)\gamma\Delta\frac{\partial^2}{\partial x_1^2}-4\alpha\mu\Delta-4\alpha(\mu+\alpha)\frac{\partial^2}{\partial x_1^2},\\
L^*_{33} &= (\mu+\alpha)(2\mu+\lambda)\Delta^2,\\
L^*_{12} &= L^*_{21}=(\mu-\alpha+\lambda)\gamma\Delta\frac{\partial^2}{\partial x_1\partial x_2}-4\alpha(\mu+\lambda)\frac{\partial^2}{\partial x_1\partial x_2},\\
L^*_{13} &= -L^*_{31}=2\alpha(2\mu+\lambda)\Delta\frac{\partial}{\partial x_2}.
\end{aligned}$$

Here, the scalar function t is defined by

$$t(\mathbf{x},\mathbf{y})=\frac{a}{8\pi k^4}\left(k^2\left|\mathbf{x}-\mathbf{y}\right|^2\ln\left|\mathbf{x}-\mathbf{y}\right|+4\ln\left|\mathbf{x}-\mathbf{y}\right|+4K_0(k\left|\mathbf{x}-\mathbf{y}\right|)\right),$$

with

$$a=\frac{1}{\gamma(2\mu+\lambda)(\mu+\alpha)},\ k^2=\frac{4\mu\alpha}{\gamma(\mu+\alpha)}.$$

It is not difficult to show that the columns $\mathbf{D}^{(i)}(\mathbf{x},\mathbf{y})$ satisfy $\mathbf{L}(\partial\mathbf{x})\mathbf{D}^{(i)}(\mathbf{x},\mathbf{y})=\mathbf{0}$ for all $\mathbf{x}\in\mathbb{R}^2$, where $\mathbf{x}\neq\mathbf{y}$.

2.4 Micropolar surface effects: boundary conditions of fourth order

We describe the boundary conditions on the reinforced subset Γ of the boundary ∂S by a surface model that incorporates classical and micropolar bending and twisting effects. To

this end, we consider a micropolar shell whose mid-surface coincides with Γ and is perfectly bonded to the reinforced subset of the surface of the plane micropolar region S. Let us assume that $\mathbf{x}^{\Gamma}(s)$ denotes a generic point on Γ indicating the position of the curve Γ that is the mid-surface of the shell (see Figure 2.2). We also assume that the function $\mathbf{x}^{\Gamma}(s)$ is injective and continuously differentiable with respect to the arclength s. We recall the Cartesian basis $\{\mathbf{e}_1, \mathbf{e}_2, \mathbf{e}_3\}$ and adopt normal-tangential $(n-t)$ coordinates with orthonormal basis $\{\mathbf{e}_0, \mathbf{e}_3, \mathbf{n}\}$ for which,

$$\mathbf{e}_0 \equiv \frac{d\mathbf{x}^{\Gamma}(s)}{ds}, \ \mathbf{n} \equiv \mathbf{e}_0 \times \mathbf{e}_3. \tag{2.31}$$

The two systems of coordinates are related by

$$\begin{aligned} \mathbf{e}_0 &= \cos\theta(s)\mathbf{e}_1 + \sin\theta(s)\mathbf{e}_2, \\ \mathbf{n} &= \sin\theta(s)\mathbf{e}_1 - \cos\theta(s)\mathbf{e}_2, \end{aligned}$$

where $\theta(s)$ is the angle between $\mathbf{e}_0$ and $\mathbf{e}_1$. The set of points $\mathbf{r}$, satisfying the relation,

$$\mathbf{r}(s) = \mathbf{x}(s) + z\mathbf{n}(s), \quad -\frac{t}{2} \leq z \leq \frac{t}{2}, \tag{2.32}$$

identify the micropolar shell region of thickness t reinforcing the boundary (see Figure 2.2). The micropolar shell is endowed with the material properties, μ_s, α_s, λ_s, ς_s, and γ_s separate from that of the adjoining bulk. Under the general Timoshenko kinematic assumption, the tangential displacements are linearly distributed within the shell's thickness while the normal displacement as well as the only non-vanishing component of microrotation remain independent of the transverse coordinate, z. Formally,

$$\mathbf{u} = \mathbf{u}_0(s) - z\mathbf{v}_0(s) + u_n(s)\mathbf{n}, \tag{2.33}$$

$$\boldsymbol{\varphi} = \varphi_3(s)\mathbf{e}_3, \tag{2.34}$$

where $\mathbf{u}_0$ is the tangential displacement of the median surface of the shell at Γ, and u_n is the normal component of the displacement. We carry (2.33) and (2.34) into the relation for the microstrain tensor in the reinforcing shell,

$$\boldsymbol{\epsilon} = (\nabla\mathbf{u})^T - \boldsymbol{\varphi}_{\times}. \tag{2.35}$$

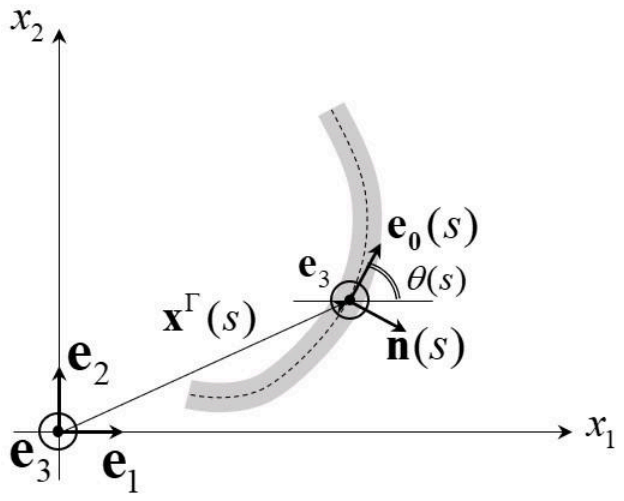

Figure 2.2: Configuration of reinforcement shell

where $\nabla(.)$ is the gradient operator, $\boldsymbol{\varphi}_\times$ is the permutation of the vector $\boldsymbol{\varphi}$ and T indicates the transpose of a tensor. After substituting (2.33) and (2.34) into (2.35) and making use of the curvature tensor defined by $\mathbf{B} \equiv -\frac{\partial \mathbf{n}}{\partial s} \otimes \mathbf{e}_0 = b_0 \mathbf{e}_0 \otimes \mathbf{e}_0$ ($\otimes$ denoting the tensor product), we obtain,

$$\begin{aligned} \boldsymbol{\epsilon} &= \left(\frac{du_0}{ds} - z\frac{dv_0}{ds} - u_n b_0 \right) (\mathbf{e}_0 \otimes \mathbf{e}_0) \\ &\quad + \left(b_0 u_0 + \frac{du_n}{ds} + \varphi_3 \right) (\mathbf{e}_0 \otimes \mathbf{n}) \\ &\quad + (-v_0 - \varphi_3) (\mathbf{n} \otimes \mathbf{e}_0) . \end{aligned} \tag{2.36}$$

where u_0 and v_0 are the tangential components of $\mathbf{u}_0$ and $\mathbf{v}_0$, respectively. Note that in deriving (2.36), we make use of the assumption of a sufficiently thin and smooth shell such that terms $t \|\mathbf{B}\| \ll 1$ ($\|\cdot\|$ denotes the norm of the tensor defined as usual by $\|\mathbf{M}\| = (\mathbf{M} : \mathbf{M})^{1/2}$) so that any term of the form $z\mathbf{B}$ becomes negligible. Through the constitutive relations of the reinforcement on the surface, i.e.

$$\boldsymbol{\sigma} = (\mu_s + \alpha_s)\boldsymbol{\epsilon} + (\mu_s - \alpha_s)\boldsymbol{\epsilon}^T + \lambda_s(\mathrm{tr}\epsilon)\mathbf{I}_s, \tag{2.37}$$

$$\boldsymbol{\mu} = (\gamma_s + \varsigma_s)(\nabla\boldsymbol{\varphi})^T + (\gamma_s - \varsigma_s)\nabla\boldsymbol{\varphi}, \tag{2.38}$$

where $\mathbf{I}_s = \mathbf{I} - \mathbf{n} \otimes \mathbf{n}$ is the unit tensor of the surface since we assume $\sigma_{nn} = 0$ (not summed over n). We may write the stress and couple stress tensors of the shell in the $(n-t)$ coordinates as,

$$\begin{aligned}
\boldsymbol{\sigma} &= (2\mu_s + \lambda_s)\left(\frac{du_0}{ds} - z\frac{dv_0}{ds} - u_n b_0\right)(\mathbf{e}_0 \otimes \mathbf{e}_0) \\
&+ \left[\mu_s\left(\frac{du_n}{ds} + b_0 u_0 - v_0\right) + \alpha_s\left(\frac{du_n}{ds} + b_0 u_0 + v_0 + 2\varphi_3\right)\right](\mathbf{e}_0 \otimes \mathbf{n}) \\
&+ \left[\mu_s\left(\frac{du_n}{ds} + b_0 u_0 - v_0\right) - \alpha_s\left(\frac{du_n}{ds} + b_0 u_0 + v_0 + 2\varphi_3\right)\right](\mathbf{n} \otimes \mathbf{e}_0) \\
&+ \lambda_s\left(\frac{du_0}{ds} - z\frac{dv_0}{ds} - u_n b_0\right)(\mathbf{e}_3 \otimes \mathbf{e}_3), \qquad (2.39)
\end{aligned}$$

$$\boldsymbol{\mu} = (\gamma_s + \varsigma_s)\frac{d\varphi_3}{ds}(\mathbf{e}_0 \otimes \mathbf{e}_3) + (\gamma_s - \varsigma_s)\frac{d\varphi_3}{ds}(\mathbf{e}_3 \otimes \mathbf{e}_0). \qquad (2.40)$$

The surface equilibrium equations for the reinforcing shell can be written in the form [43]

$$\frac{d\sigma^s_{00}}{ds} - \sigma^s_{0n} b_0 = 0. \qquad (2.41)$$

$$\frac{d\sigma^s_{0n}}{ds} + \sigma^s_{00} b_0 = 0. \qquad (2.42)$$

$$\frac{d\mu^s_{03}}{ds} - \sigma^s_{0n} = 0, \qquad (2.43)$$

where σ^s_{00}, σ^s_{0n}, and μ^s_{03} are, respectively, the components of the surface stress and surface couple-stress tensors, $\boldsymbol{\sigma}^s = \mathbf{I}_s\boldsymbol{\sigma}$ and $\boldsymbol{\mu}^s = \mathbf{I}_s\boldsymbol{\mu}$, in the $\{\mathbf{e}_0, \mathbf{e}_3, \mathbf{n}\}$ system. We integrate both sides of the equilibrium equations (2.41) to (2.43) over the thickness, $z \in \left[-\frac{t}{2}, \frac{t}{2}\right]$, while considering the traction on both faces of the shell and exchanging the components by their expressions from the equations (2.32) and (2.33). This leads us to the three equilibrium equations,

$$\begin{aligned}
&(2\mu_s + \lambda_s)t\frac{d}{ds}\left(\frac{du_0}{ds} - u_n b_0\right) \\
&- \left[\mu_s t\left(\frac{du_n}{ds} + b_0 u_0 - v_0\right) b_0\right. \\
&\left.+ \alpha_s t\left(\frac{du_n}{ds} + b_0 u_0 + v_0 + 2\varphi_3\right) b_0\right] + f_0^+ - f_0^- = 0, \qquad (2.44)
\end{aligned}$$

$$
\begin{aligned}
&(2\mu_s+\lambda_s)t\left(\frac{du_0}{ds}-u_n b_0\right)b_0\\
&+\left[\mu_s t\left(\frac{d^2u_n}{ds^2}+\frac{d(b_0u_0)}{ds}-\frac{dv_0}{ds}\right)\right.\\
&\left.+\alpha_s t\left(\frac{d^2u_n}{ds^2}+\frac{d(b_0u_0)}{ds}+\frac{dv_0}{ds}+2\frac{d\varphi_3}{ds}\right)\right]+f_n^+-f_n^-=0, \qquad (2.45)
\end{aligned}
$$

$$
(\gamma_s+\varsigma_s)t\frac{d^2\varphi_3}{ds^2}-\alpha_s t\left(\frac{du_n}{ds}+b_0u_0+v_0+2\varphi_3\right)+\frac{t}{2}(f_0^++f_0^-)+m_3^+-m_3^-=0, \qquad (2.46)
$$

where f_0^+, f_n^+ and m_3^+ are respectively, the prescribed stress and couple stress traction components in the tangential, normal and the antiplane direction on the outer surface of the shell. On the other hand, the stress and couple stress traction components generated from the substrate on the inner surface of the shell are respectively, f_0^-, f_n^- and m_3^-, in the tangential, normal and the antiplane directions (see Figure 2.3).

We introduce the classical bending resistance of the shell by taking the vector product ($\times$) of the terms of the equilibrium equation with $z\mathbf{n}$ to construct the stress couples equilibrium around the median surface of the shell [47],

$$
z\mathbf{n}\times\frac{d\boldsymbol{\sigma}_0}{ds}+z\mathbf{n}\times\frac{d\boldsymbol{\sigma}_n}{dz}=\mathbf{0}, \qquad (2.47)
$$

where, $\boldsymbol{\sigma}_0$ and $\boldsymbol{\sigma}_n$ are the stress vectors acting on the surfaces with unit outward normals, $\mathbf{e}_0$ and $\mathbf{n}$, respectively. We use the equation (2.43) in (2.47) and then integrate (2.47) over the thickness to achieve the fourth equation of stress couples,

$$
\begin{aligned}
&\left[\mu_s t\left(\frac{du_n}{ds}+b_0u_0-v_0\right)+\alpha_s t\left(\frac{du_n}{ds}+b_0u_0+v_0+2\varphi_3\right)\right]=\\
&-(2\mu_s+\lambda_s)I\frac{d^2v_0}{ds^2}+(\gamma_s+\varsigma_s)t\frac{d^2\varphi_3}{ds^2}+\frac{t}{2}(f_1^++f_1^-),\quad I=t^3/12. \qquad (2.48)
\end{aligned}
$$

We carry (2.48) into (2.44) and (2.45), and implement the Kirchhoff-Love kinematic assumption that the classical shear strain vanishes, i.e. $\epsilon_{0n}^c=0$, where $\epsilon_{0n}^c=0$ is a component of $\boldsymbol{\epsilon}^c=\frac{1}{2}(\boldsymbol{\epsilon}+\boldsymbol{\epsilon}^T)$. This assumption leads to

$$
\mathbf{v}_0=\mathbf{B}\mathbf{u}_0+\nabla_s u_n,
$$

to remove the possibility of shear deformations from the shell model. Consequently, we arrive at the following set of boundary conditions on the reinforced subset Γ of the boundary ∂S,

$$\begin{aligned}
&A_s\left(\frac{d^2u_0}{ds^2}-\frac{d(u_nb_0)}{ds}\right)\\
&+B_sb_0\left(\frac{d^2(b_0u_0)}{ds^2}+\frac{d^3u_n}{ds^3}\right)-H_sb_0\frac{d^2\varphi_3}{ds^2}\\
&-\frac{tb_0}{2}(f_0^+ + f_0^-)+f_0^+ - f_0^- = 0
\end{aligned} \tag{2.49}$$

$$\begin{aligned}
&A_s\left(\frac{du_0}{ds}-u_nb_0\right)b_0-B_s\left(\frac{d^3(b_0u_0)}{ds^3}+\frac{d^4u_n}{ds^4}\right)\\
&+H_s\frac{d^3\varphi_3}{ds^3}+\frac{t}{2}(\frac{df_0^+}{ds}+\frac{df_0^-}{ds})+f_n^+-f_n^-=0
\end{aligned} \tag{2.50}$$

$$H_s\frac{d^2\varphi_3}{ds^2}-2G_s\left(\frac{du_n}{ds}+b_0u_0+\varphi_3\right)+\frac{t}{2}(f_0^+ + f_0^-)+m_3^+-m_3^-=0. \tag{2.51}$$

In the foregoing equations (2.49-2.51), $A_s=(2\mu_s+\lambda_s)t$, $B_s=(2\mu_s+\lambda_s)I$, $H_s=(\gamma_s+\varsigma_s)t$ and $G_s=\alpha_st$ are the stretching, classical bending and first and second micropolar twisting rigidities, respectively. The boundary conditions (2.49-2.51) are written in $(n-t)$ coordinates and for a solution of $\mathbf{L}(\partial\mathbf{x})\mathbf{w}(\mathbf{x})=\mathbf{0}$, the substrate tractions, f_0^-, f_n^- and m_3^- can be written as boundary stress operators in component form,

$$\begin{aligned}
f_0^- &= T_0^{(1)^{nt}}(\partial\mathbf{x})\mathbf{w},\\
f_n^- &= T_n^{(1)^{nt}}(\partial\mathbf{x})\mathbf{w},\\
m_3^- &= T_3^{(1)^{nt}}(\partial\mathbf{x})\mathbf{w},
\end{aligned} \tag{2.52}$$

where, $T_0^{(1)^{nt}}$, $T_n^{(1)^{nt}}$ and $T_3^{(1)^{nt}}$ are the components of $\mathbf{T}^{(1)}(\partial\mathbf{x})$ from the equation (2.19) in the $(n-t)$ coordinate system. Using this fact, the boundary conditions on the reinforcement Γ can be written in the original Cartesian coordinates as,

$$\mathbf{T}^{(1)}(\partial\mathbf{x})\mathbf{w}(\mathbf{x})=\mathbf{A}(\mathbf{x})\mathbf{R}^{(1)}(d/ds)\mathbf{A}^{-1}(\mathbf{x})\mathbf{w}+\mathbf{A}(\mathbf{x})\mathbf{t}^{(1)}(\mathbf{x}). \tag{2.53}$$

Here, $\mathbf{A}(\mathbf{x})$ is the transformation operator from normal-tangential coordinates to Cartesian coordinates defined by,

$$\mathbf{A}(\mathbf{x}) = \begin{bmatrix} \cos\theta(s) & \sin\theta(s) & 0 \\ \sin\theta(s) & -\cos\theta(s) & 0 \\ 0 & 0 & 1 \end{bmatrix}. \tag{2.54}$$

The prescribed data $\mathbf{t}^{(1)}(\mathbf{x})$ on the reinforced boundary Γ has the expression,

$$\mathbf{t}^{(1)}(\mathbf{x}) = \begin{bmatrix} f_0^+ - \frac{tb_0}{2} f_0^+ \\ f_n^+ + \frac{t}{2}\frac{df_0^+}{ds} \\ m_3^+ + \frac{t}{2} f_0^+ \end{bmatrix}, \tag{2.55}$$

in the $(n-t)$ coordinates. The fourth order boundary differential operator $\mathbf{R}^{(1)}(d/ds)$ is given by

$$\begin{aligned} \mathbf{R}^{(1)}(d/ds) &= \mathbf{R}_4^{(1)}(d^4/ds^4) + \mathbf{R}_3^{(1)}(d^3/ds^3) + \mathbf{R}_2^{(1)}(d^2/ds^2) \\ &\quad + \mathbf{R}_1^{(1)}(d/ds) + \mathbf{R}_0^{(1)}. \end{aligned} \tag{2.56}$$

The operators $\mathbf{R}_i^{(1)}$, $i = 0, 1, 2, 3, 4$ are defined by

$$\mathbf{R}_0^{(1)} = \begin{bmatrix} B_s b_0 \frac{d^2 b_0}{ds^2} - G_s b_0^2 & -A_s \frac{db_0}{ds} & -G_s b_0 \\ -B_s \frac{d^3 b_0}{ds^3} + G_s \frac{db_0}{ds} & -A_s b_0^2 & 0 \\ -G_s b_0 & 0 & -G_s \end{bmatrix},$$

$$\mathbf{R}_1^{(1)} = \begin{bmatrix} 2B_s b_0 \frac{db_0}{ds} & -A_s b_0 - b_0 G_s & 0 \\ A_s b_0 - 3B_s \frac{d^2 b_0}{ds^2} + G_s b_0 & 0 & G_s \\ 0 & -G_s & 0 \end{bmatrix},$$

$$\mathbf{R}_2^{(1)} = \begin{bmatrix} A_s + B_s b_0^2 & 0 & -H_s b_0 \\ -3B_s \frac{db_0}{ds} & G_s & 0 \\ 0 & 0 & H_s \end{bmatrix},$$

$$\mathbf{R}_3^{(1)} = \begin{bmatrix} 0 & B_s b_0 & 0 \\ -B_s b_0 & 0 & H_s \\ 0 & 0 & 0 \end{bmatrix},$$

$$\mathbf{R}_4^{(1)} = \begin{bmatrix} 0 & 0 & 0 \\ 0 & -B_s & 0 \\ 0 & 0 & 0 \end{bmatrix},$$

In deriving (2.56) we use the fact that the reinforcement and the bulk are perfectly bonded and the reactive shearing stress from the bulk (substrate) is given by

$$f_0^- = -\sigma_{n0}|_{z=-\frac{t}{2}} = T_0^{(1)^{nt}}(\partial\mathbf{x})\mathbf{w} = 2\alpha_s\left(\frac{du_n}{ds} + b_0 u_0 + \varphi_3\right)$$

in the boundary conditions (2.49-2.51). Clearly, we must assume that b_0 is sufficiently smooth so that the third derivative of the curvature b_0 with respect to the arc-length s exists on Γ. As we see, the boundary condition described in (2.53) is highly non-standard. On the left hand side of equation (2.53), $\mathbf{T}^{(1)}(\partial\mathbf{x})$, the so called first-order stress operator, is applied to the deformation vector to indicate the stress generated by the bulk's deformation. The right hand side of the equation, however, consists of a fourth order tangential differential operator $\mathbf{R}^{(1)}(d/ds)$, applied to the deformation vector to represent the reactive stresses in the micropolar surface. This kind of boundary condition is particularly interesting in that it is of order higher than that of the governing field (2.17). In the next part, we introduce a second order representation of the micropolar surface effects.

2.5 Micropolar surface effects: boundary conditions of the second order via three dimensional micropolar theory (Eremeyev-Lebedev-Altenbach)

We employ an alternative form of the Kirchhoff-Love kinematic assumption for which the shear "microstrain" component vanishes instead of the classical shear strain, i.e. $\epsilon_{0n} = 0$. From (2.36), this assumption implies that,

$$\varphi_3 = -v_0. \tag{2.57}$$

This Kirchhoff-Love model was adopted for linear micropolar plates by Altenbach and Eremeyev [1]. The shell equations for this model are derived using the same kinematic assumptions (equations 2.32-2.36) and the same surface equilibrium equations (2.41-2.43). Unlike the previous case, however, we consider the coupling of surface force-stresses upon integration of the moment equation (2.43) over the thickness. Accordingly, the surface equilibrium

equations of the reinforcing shell are written as,

$$\begin{aligned}
\frac{dP_{00}}{ds} - P_{0n}b_0 + f_0^+ - f_0^- &= 0, && (2.58)\\
\frac{dP_{0n}}{ds} + P_{00}b_0 + f_n^+ - f_n^- &= 0, && (2.59)\\
\frac{dM_{03}}{ds} - P_{0n} + m_3^+ - m_3^- &= 0, && (2.60)
\end{aligned}$$

where,

$$P_{00} = A_s\left(\frac{du_0}{ds} - u_n b_0\right),$$

$$\begin{aligned}
P_{0n} &= M_s\left(\frac{du_n}{ds} + b_0u_0 - v_0\right)\\
&\quad + G_s\left(\frac{du_n}{ds} + b_0u_0 + v_0 + 2\varphi_3\right),
\end{aligned}$$

$$M_{03} = H_s\frac{d\varphi_3}{ds} - B_s\frac{dv_0}{ds},$$

are the components of the surface stress and couple stress tensors, respectively,

$$\mathbf{P} = \int_{-\frac{t}{2}}^{\frac{t}{2}} \mathbf{I}_s\boldsymbol{\sigma}\,dz, \quad \mathbf{M} = \int_{-\frac{t}{2}}^{\frac{t}{2}} \mathbf{I}_s\left(\boldsymbol{\mu} - z(\boldsymbol{\sigma}_0 + \boldsymbol{\sigma}_n)\otimes\mathbf{e}_3\right)dz, \tag{2.61}$$

Here again, $A_s = (2\mu_s + \lambda_s)t$, $B_s = (2\mu_s + \lambda_s)I$, $H_s = (\gamma_s + \varsigma_s)t$, $G_s = \alpha_s t$ and $M_s = \mu_s t$. In fact, the kinematic assumption (2.57) renders the in-surface microrotations equal to the classical rotations of the midsurface. For the displacement form under consideration (2.33 and 2.34), that is,

$$\boldsymbol{\varphi} = \frac{1}{2}\nabla\times\mathbf{u} = -v_0\mathbf{e}_3. \tag{2.62}$$

For this case, we ignore the coupling effects of shear tractions on the surfaces of the reinforcement assuming their contribution to the deformation of the surface is insignificant. Using the foregoing assumptions in the equilibrium conditions, we obtain the following conditions

for the reinforced boundary,

$$A_s\left(\frac{d^2u_0}{ds^2}-\frac{d(u_nb_0)}{ds}\right)-(M_s+G_s)b_0\left(\frac{du_n}{ds}+b_0u_0+\varphi_3\right)+f_0^+-f_0^- = 0, \quad (2.63)$$

$$A_s\left(\frac{du_0}{ds}-u_nb_0\right)b_0+(M_s+G_s)\left(\frac{d^2u_n}{ds^2}+\frac{d(b_0u_0)}{ds}+\frac{d\varphi_3}{ds}\right)+f_n^+-f_n^- = 0, \quad (2.64)$$

$$(H_s+B_s)\frac{d^2\varphi_3}{ds^2}-(M_s+G_s)\left(\frac{du_n}{ds}+b_0u_0+\varphi_3\right)+m_3^+-m_3^- = 0. \quad (2.65)$$

The boundary condition in the original Cartesian coordinates is given by

$$\mathbf{T}^{(2)}(\partial\mathbf{x})\mathbf{w}(\mathbf{x})=\mathbf{A}(\mathbf{x})\mathbf{R}^{(2)}(d/ds)\mathbf{A}^{-1}(\mathbf{x})\mathbf{w}+\mathbf{A}(\mathbf{x})\mathbf{t}^{(2)}(\mathbf{x}). \quad (2.66)$$

where the second order boundary differential operator, $\mathbf{R}^{(2)}(d/ds)$, takes the form,

$$\mathbf{R}^{(2)}(d/ds)=\mathbf{R}_2^{(2)}(d^2/ds^2)+\mathbf{R}_1^{(2)}(d/ds)+\mathbf{R}_0^{(2)}. \quad (2.67)$$

The operators $\mathbf{R}_i^{(2)}$, $i=0,1,2$ are expressed as

$$\mathbf{R}_0^{(2)}=\begin{bmatrix} -(M_s+G_s)b_0^2 & -A_s\frac{db_0}{ds} & -(M_s+G_s)b_0 \\ (M_s+G_s)\frac{db_0}{ds} & -A_sb_0^2 & 0 \\ -(M_s+G_s)b_0 & 0 & -(M_s+G_s) \end{bmatrix},$$

$$\mathbf{R}_1^{(2)}=\begin{bmatrix} 0 & -A_sb_0-(M_s+G_s)b_0 & 0 \\ A_s+(M_s+G_s)b_0 & 0 & (M_s+G_s) \\ 0 & -(M_s+G_s) & 0 \end{bmatrix},$$

$$\mathbf{R}_2^{(2)}=\begin{bmatrix} A_s & 0 & 0 \\ 0 & (M_s+G_s) & 0 \\ 0 & 0 & H_s+B_s \end{bmatrix}.$$

Again, the prescribed boundary tractions on the reinforced surface take the values

$$\mathbf{t}^{(2)}(\mathbf{x})=\begin{bmatrix} f_0^+ \\ f_n^+ \\ m_3^+ \end{bmatrix}.$$

Similarly to the previous section, the second order equation (2.66) represents a highly non-standard boundary condition and involves the first order boundary stress operator $\mathbf{T}^{(2)}(\partial\mathbf{x})$ on the left-hand side and the second order tangential differential operator $\mathbf{R}^{(2)}(d/ds)$, on the

right-hand side. We observe, in the same way as in the previous section, that the boundary conditions are of the same order as the governing equations. The types of second order and fourth order boundary conditions introduced in the boundary value problems of plane micropolar elasticity, though posing more mathematical complexities, includes more details corresponding to the physical problem. Consequently, the proposed mathematical model can more accurately describe the behavior of materials at small scaled level. In the next section we introduce the mathematical models in the forms of boundary value problems in interior and exterior domains.

2.6 Boundary value problems

2.6.1 (a) Interior problem

Recall that S is a bounded multiply-connected domain enclosed by ∂S which, for simplicity, here consists of two sufficiently smooth closed curves Γ and ∂S_1 ($\partial S = \Gamma \cup \partial S_1$), representing reinforced and non-reinforced boundaries, respectively (see Figure 2.3). The non-reinforced boundary is divided into two open curves $\partial S_{\mathbf{w}}$ and $\partial S_{\mathbf{t}}$ ($\partial S_1 = \partial S_{\mathbf{t}} \cup \partial S_{\mathbf{w}}$) with common end points a and b, on which the boundary values for displacement/microrotations $\mathbf{w}^{(0)}$, and stress/couple-stress tractions, $\mathbf{t}^{(0)}$ are prescribed, respectively. We note that in the special case when a and b coincide, $\partial S_{\mathbf{t}}$ and $\partial S_{\mathbf{w}}$ are closed curves. A simple example of an interior problem is shown in Figure 2.3.

We pose the interior mixed-boundary value problem of micropolar plane elasticity with surface reinforcement as follows: find a vector $\mathbf{w}$ belonging to an admissible function space $C^2(S) \cap C^1(\overline{S} \backslash \{a, b\})$, such that,

$$\mathbf{L}(\partial \mathbf{x})\mathbf{w}(\mathbf{x}) = \mathbf{0}, \quad \mathbf{x} \in S,$$

$$\mathbf{T}(\partial \mathbf{x})\mathbf{w}(\mathbf{x}) = \mathbf{t}^0(\mathbf{x}), \quad \mathbf{x} \in \partial S_{\mathbf{t}},$$

$$\mathbf{w}(\mathbf{x}) = \mathbf{w}^0(\mathbf{x}), \quad \mathbf{x} \in \partial S_{\mathbf{w}},$$

$$\mathbf{T}^{(i)}(\partial \mathbf{x})\mathbf{w}(\mathbf{x}) = \mathbf{A}(\mathbf{x})\mathbf{R}^{(i)}(d/ds)\mathbf{A}^{-1}(\mathbf{x})\mathbf{w} + \mathbf{A}(\mathbf{x})\mathbf{t}^{(i)}(\mathbf{x}), \quad \mathbf{x} \in \Gamma, \ i = 1, 2. \tag{2.68}$$

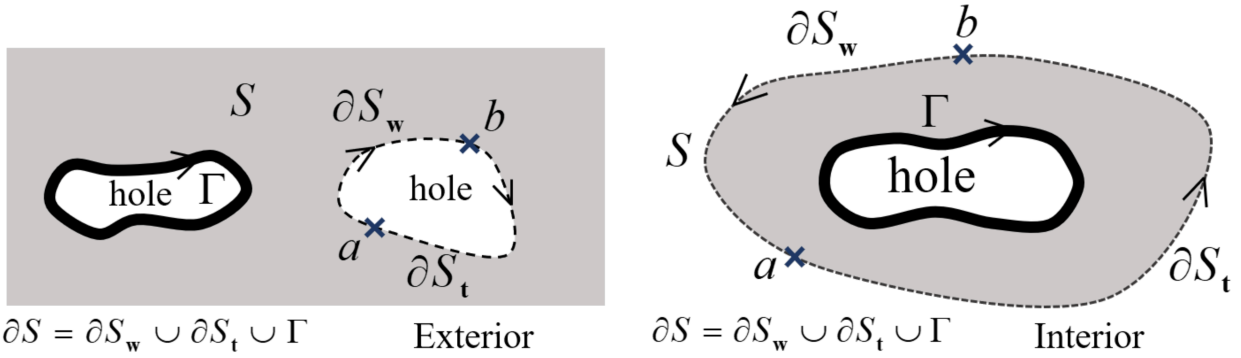

Figure 2.3: Interior and exterior problems

2.6.2 (b) Exterior problem

The exterior problem is defined similarly to the interior problem except that S is now an unbounded domain with ∂S described by $\partial S = \Gamma \cup \partial S_1$. Here, again each one of the non-reinforced ($\partial S_1 = \partial S_{\mathbf{t}} \cup \partial S_{\mathbf{w}}$) and the reinforced ($\Gamma$) parts of ∂S consist of closed curves. The exterior mixed-boundary value problem of plane micropolar elasticity with surface reinforcement is as to find a vector $\mathbf{w} \in C^2(S) \cap C^1(\overline{S} \backslash \{a, b\}) \cap \mathcal{A}^*$ such that,

$$\mathbf{L}(\partial \mathbf{x})\mathbf{w}(\mathbf{x}) = \mathbf{0}, \quad \mathbf{x} \in S,$$

$$\mathbf{T}(\partial \mathbf{x})\mathbf{w}(\mathbf{x}) = \mathbf{t}^0(\mathbf{x}), \quad \mathbf{x} \in \partial S_{\mathbf{t}},$$

$$\mathbf{w}(\mathbf{x}) = \mathbf{w}^0(\mathbf{x}), \quad \mathbf{x} \in \partial S_{\mathbf{w}},$$

$$\mathbf{T}^{(i)}(\partial \mathbf{x})\mathbf{w}(\mathbf{x}) = \mathbf{A}(\mathbf{x})\mathbf{R}^{(i)}(d/ds)\mathbf{A}^{-1}(\mathbf{x})\mathbf{w} + \mathbf{A}(\mathbf{x})\mathbf{t}^{(i)}(\mathbf{x}), \quad \mathbf{x} \in \Gamma, \ i = 1, 2. \tag{2.69}$$

Note that $\mathcal{A}^*$ has been defined in (2.27).

In the following chapters, we present analytical solutions of the boundary value problem for some practical and well-known problems in micro and nanomechanics. Particularly, in the next chapter we focus on the stress distribution around a circular hole and illustrate the effects of micropolar surface model on this classical problem which is of high significance in engineering applications.

Chapter 3

Stress Distribution Around a Circular Hole in a Micropolar Material with Micropolar Surface Effects

In this chapter we consider the problem of an infinite sheet containing a circular hole under uniform remote loading. This problem has a significant meaning in engineering practices. The problem can be regarded as a benchmark for further analysis of stress concentrations around defects and notches. The upcoming analysis also demonstrates the significance of micropolar surface effects with different elastic properties of the surface. Considering the present classical problem from the viewpoint of the introduced surface model illustrates how it can be successfully applied to the analysis of the practical problem of holes in materials with microstructures. The problem of stress concentration around a single circular hole has been subject of study in the development of theory of micropolar elasticity in 1960s. Mindlin [102], among others, investigated the influence of couple stresses around a circular hole using a simplified Cosserat elasticity, known as couple-stress theory. The couple-stress theory, kinematically, follows the classical elasticity, while kinetically complies with the micropolar theory. Mindlin [102] found that the presence of couple stresses which result from non-negligible strain gradients around a hole, decreases the stress concentration factor. Kolani and Ariman argued that the couple stress effects [78] decrease the stress concentration, however, not as significant as Mindlin predicted. On the other hand, the effects of sur-

face mechanics on the stress concentration problems has been a topic of study for many researchers. Among them, Tian and Rajapakse [139, 140] investigated the stress concentration around circular and elliptical inhomogeneities solving the plane elasticity problem in the complex variable format. They used Gurtin–Murdoch interface model for the surface. The more general surface model by Steigmann-Ogden is less considered for solving benchmark problems, particularly the stress concentration problems. The researches presented recently by Zemlyanova and Mogilevskaya [158] and Dai et al [25] are among the rare few which consider problems with Steigmann-Ogden surface effects in classical elasticity.

In what follows, we introduce preliminaries necessary for solving the problem in the cylindrical coordinates system. Next, we formulate the corresponding boundary value problem incorporating the circular surface of a hole in an infinite micropolar plane. Subsequently, we find the analytical solution of the problem using stress functions of plane micropolar elasticity with the corresponding specific boundary conditions on the surface. Lastly, we end the chapter with some numerical examples and concluding remarks.

3.1 Preliminaries

In this section, we introduce the governing equations and relations in a system of cylindrical coordinates. We characterize the cylindrical coordinates $\{r, \theta, x_3\}$ by the Cartesian components of a position vector as,

$$x_1 = r\cos\theta, \quad x_2 = r\sin\theta, \quad r = \sqrt{x_1^2 + x_2^2}. \tag{3.1}$$

The relationship between derivatives in Cartesian and cylindrical coordinates are given by

$$\begin{aligned} \frac{\partial}{\partial x_1} &= \cos\theta\frac{\partial}{\partial r} - \frac{1}{r}\sin\theta\frac{\partial}{\partial\theta}, \\ \frac{\partial}{\partial x_2} &= \sin\theta\frac{\partial}{\partial r} + \frac{1}{r}\cos\theta\frac{\partial}{\partial\theta}, \end{aligned} \tag{3.2}$$

and the orthogonal cylindrical basis vectors $\{\mathbf{e}_r, \mathbf{e}_\theta, \mathbf{e}_3\}$ are expressed in the Cartesian basis $\{\mathbf{e}_1, \mathbf{e}_2, \mathbf{e}_3\}$ as

$$\begin{aligned}\mathbf{e}_r &= (\cos\theta)\mathbf{e}_1 + (\sin\theta)\mathbf{e}_2,\\ \mathbf{e}_\theta &= (-\sin\theta)\mathbf{e}_1 + (\cos\theta)\mathbf{e}_2.\end{aligned} \tag{3.3}$$

For a stress field described in the cylindrical coordinates the balance equations are given by

$$\begin{aligned}\frac{\partial\sigma_{rr}}{\partial r} + \frac{1}{r}\left(\frac{\partial\sigma_{\theta r}}{\partial\theta} + (\sigma_{rr} - \sigma_{\theta\theta})\right) + \frac{\partial\sigma_{3r}}{\partial x_3} &= 0,\\ \frac{\partial\sigma_{r\theta}}{\partial r} + \frac{1}{r}\left(\frac{\partial\sigma_{\theta\theta}}{\partial\theta} + (\sigma_{r\theta} + \sigma_{\theta r})\right) + \frac{\partial\sigma_{3\theta}}{\partial x_3} &= 0,\\ \frac{\partial\sigma_{r3}}{\partial r} + \frac{1}{r}\left(\frac{\partial\sigma_{\theta 3}}{\partial\theta} + \sigma_{r3}\right) + \frac{\partial\sigma_{33}}{\partial x_3} &= 0,\\ \frac{\partial\mu_{rr}}{\partial r} + \frac{1}{r}\left(\frac{\partial\mu_{\theta r}}{\partial\theta} + (\mu_{rr} - \mu_{\theta\theta})\right) + \frac{\partial\mu_{3r}}{\partial x_3} + (\sigma_{\theta 3} - \sigma_{3\theta}) &= 0,\\ \frac{\partial\mu_{r\theta}}{\partial r} + \frac{1}{r}\left(\frac{\partial\mu_{\theta\theta}}{\partial\theta} + (\mu_{r\theta} + \mu_{\theta r})\right) + \frac{\partial\mu_{3\theta}}{\partial x_3} + (\sigma_{3r} - \sigma_{r3}) &= 0,\\ \frac{\partial\mu_{r3}}{\partial r} + \frac{1}{r}\left(\frac{\partial\mu_{\theta 3}}{\partial\theta} + \mu_{r3}\right) + \frac{\partial\mu_{33}}{\partial x_3} + (\sigma_{r\theta} - \sigma_{\theta r}) &= 0.\end{aligned} \tag{3.4}$$

Curl of a tensor in cylindrical coordinates is obtained as

$$\begin{aligned}\nabla\times\mathbf{M} \;=\; &\left(\tfrac{1}{r}\tfrac{\partial M_{r3}}{\partial\theta} - \tfrac{\partial M_{r\theta}}{\partial x_3} - \tfrac{M_{\theta 3}}{r}\right)\mathbf{e}_r\otimes\mathbf{e}_r + \left(\tfrac{1}{r}\tfrac{\partial M_{\theta 3}}{\partial\theta} - \tfrac{\partial M_{\theta\theta}}{\partial x_3} + \tfrac{M_{r3}}{r}\right)\mathbf{e}_r\otimes\mathbf{e}_\theta\\ &+ \left(\tfrac{1}{r}\tfrac{\partial M_{33}}{\partial\theta} - \tfrac{\partial M_{3\theta}}{\partial x_3}\right)\mathbf{e}_r\otimes\mathbf{e}_3 + \left(\tfrac{\partial M_{rr}}{\partial x_3} - \tfrac{\partial M_{r3}}{\partial r}\right)\mathbf{e}_\theta\otimes\mathbf{e}_r\\ &+ \left(\tfrac{\partial M_{\theta r}}{\partial x_3} - \tfrac{\partial M_{\theta 3}}{\partial r}\right)\mathbf{e}_\theta\otimes\mathbf{e}_\theta + \left(\tfrac{\partial M_{3r}}{\partial x_3} - \tfrac{\partial M_{33}}{\partial r}\right)\mathbf{e}_\theta\otimes\mathbf{e}_3\\ &+ \left(\tfrac{M_{r\theta}}{r} + \tfrac{M_{\theta r}}{r} + \tfrac{\partial M_{r\theta}}{\partial r} - \tfrac{1}{r}\tfrac{\partial M_{rr}}{\partial\theta}\right)\mathbf{e}_3\otimes\mathbf{e}_r\\ &+ \left(\tfrac{M_{\theta\theta}}{r} - \tfrac{M_{rr}}{r} + \tfrac{\partial M_{\theta\theta}}{\partial r} - \tfrac{1}{r}\tfrac{\partial M_{\theta r}}{\partial\theta}\right)\mathbf{e}_3\otimes\mathbf{e}_\theta\\ &+ \left(\tfrac{M_{3\theta}}{r} + \tfrac{\partial M_{3\theta}}{\partial r} - \tfrac{1}{r}\tfrac{\partial M_{3r}}{\partial\theta}\right)\mathbf{e}_3\otimes\mathbf{e}_3.\end{aligned} \tag{3.5}$$

The gradient operator in the cylindrical coordinates is defined by $\nabla \equiv \mathbf{e}_r\frac{\partial}{\partial r} + \mathbf{e}_\theta\frac{1}{r}\frac{\partial}{\partial\theta} + \mathbf{e}_3\frac{\partial}{\partial x_3}$.

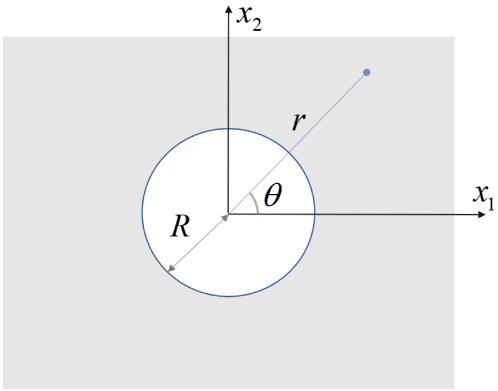

Figure 3.1: Circular hole in an infinite plane

3.2 Statement of the problem

Consider a circular hole of radius R in an infinite micropolar plane subjected to remote uniform loading. We assign to the medium material properties μ, α, λ, γ and ς. We adopt a system of Cartesian coordinates, $\{o : x_1, x_2\}$, such that the positive side of the x_1-axis coincides with the $\theta = 0$ axis of the polar (cylindrical) coordinates $\{o : r, \theta\}$. The plane strain deformations are independent of the antiplane dimension x_3, therefore, they are characterized by the following displacement and microrotation fields:

$$\begin{aligned} \mathbf{u} &= u_r(r,\theta)\mathbf{e}_r(\theta) + u_\theta \mathbf{e}_\theta(\theta), \\ \boldsymbol{\varphi} &= \varphi_3(r,\theta)\mathbf{e}_3. \end{aligned} \tag{3.6}$$

Using the kinematics equations of micropolar theory, (2.11), we write the microstrain and microrotation tensors in cylindrical coordinates as

$$\begin{aligned} \boldsymbol{\epsilon}^{(mi)} = &\frac{\partial u_r}{\partial r}\mathbf{e}_r \otimes \mathbf{e}_r + \left(\frac{\partial u_\theta}{\partial r} - \varphi_3\right)\mathbf{e}_r \otimes \mathbf{e}_\theta \\ &+ \left(\frac{1}{r}\frac{\partial u_r}{\partial \theta} - \frac{u_\theta}{r} + \varphi_3\right)\mathbf{e}_\theta \otimes \mathbf{e}_r + \left(\frac{1}{r}\frac{\partial u_\theta}{\partial \theta} + \frac{u_r}{r}\right)\mathbf{e}_\theta \otimes \mathbf{e}_\theta, \end{aligned} \tag{3.7}$$

$$\boldsymbol{\varkappa} = \frac{\partial \varphi_3}{\partial r}\mathbf{e}_r \otimes \mathbf{e}_3 + \frac{1}{r}\frac{\partial \varphi_3}{\partial \theta}\mathbf{e}_\theta \otimes \mathbf{e}_3. \tag{3.8}$$

Thus, the stress and couple stress tensors are obtained through the constitutive relations (2.14) as

$$\begin{aligned}\boldsymbol{\sigma} &= \left((2\mu+\lambda)\epsilon_{rr}^{(mi)} + \lambda\epsilon_{\theta\theta}^{(mi)}\right)\mathbf{e}_r\otimes\mathbf{e}_r + \left((2\mu+\lambda)\epsilon_{\theta\theta}^{(mi)} + \lambda\epsilon_{rr}^{(mi)}\right)\mathbf{e}_\theta\otimes\mathbf{e}_\theta \\ &\quad + \left(\mu(\epsilon_{\theta r}^{(mi)} + \epsilon_{r\theta}^{(mi)}) + \alpha(\epsilon_{\theta r}^{(mi)} - \epsilon_{r\theta}^{(mi)})\right)\mathbf{e}_\theta\otimes\mathbf{e}_r + \left(\mu(\epsilon_{\theta r}^{(mi)} + \epsilon_{r\theta}^{(mi)}) + \alpha(\epsilon_{r\theta}^{(mi)} - \epsilon_{\theta r}^{(mi)})\right)\mathbf{e}_r\otimes\mathbf{e}_\theta \\ &\quad + \lambda\left(\epsilon_{rr}^{(mi)} + \epsilon_{\theta\theta}^{(mi)}\right)\mathbf{e}_3\otimes\mathbf{e}_3, \qquad (3.9)\end{aligned}$$

$$\boldsymbol{\mu} = (\gamma+\varsigma)\varkappa_{r3}\mathbf{e}_r\otimes\mathbf{e}_3 + (\gamma+\varsigma)\varkappa_{\theta 3}\mathbf{e}_\theta\otimes\mathbf{e}_3 + (\gamma-\varsigma)\varkappa_{r3}\mathbf{e}_3\otimes\mathbf{e}_r + (\gamma-\varsigma)\varkappa_{\theta 3}\mathbf{e}_3\otimes\mathbf{e}_\theta. \quad (3.10)$$

We identify the nonzero components of the stress and couple stress tensors written in (3.9) and (3.10) and, subsequently, we simplify the balance equations (3.4) to obtain,

$$\begin{aligned}\frac{\partial\sigma_{rr}}{\partial r} + \frac{1}{r}\left(\frac{\partial\sigma_{\theta r}}{\partial\theta} + (\sigma_{rr}-\sigma_{\theta\theta})\right) &= 0, \\ \frac{\partial\sigma_{r\theta}}{\partial r} + \frac{1}{r}\left(\frac{\partial\sigma_{\theta\theta}}{\partial\theta} + (\sigma_{r\theta}+\sigma_{\theta r})\right) &= 0, \\ \frac{\partial\mu_{r3}}{\partial r} + \frac{1}{r}\left(\frac{\partial\mu_{\theta 3}}{\partial\theta} + \mu_{r3}\right) + (\sigma_{r\theta}-\sigma_{\theta r}) &= 0. \qquad (3.11)\end{aligned}$$

Finally, compatibility of the displacement and microrotation fields are equivalent to stating that the displacement and microrotation fields can be obtained by integrating the strain and microrotation tensors (or the gradients of displacements and microrotations). This mathematically means that the for an arbitrary curve C between any two points in a simply-connected domain with displacements $\mathbf{u}$ and $\mathbf{u}_0$, and microrotations $\boldsymbol{\varphi}$ and $\boldsymbol{\varphi}_0$, we have

$$\mathbf{u} = \mathbf{u}_0 + \int_C \nabla\mathbf{u}d\mathbf{x}, \quad \boldsymbol{\varphi} = \boldsymbol{\varphi}_0 + \int_C \nabla\boldsymbol{\varphi}d\mathbf{x}, \qquad (3.12)$$

The path independent integrals in the conditions (3.12), imply that the integral terms vanish over any closed circuit in the domain, i.e.

$$\oint_C \nabla\boldsymbol{u}\mathbf{dx} = \mathbf{0}, \ \oint_C \nabla\boldsymbol{\varphi}\mathbf{dx} = \mathbf{0}. \qquad (3.13)$$

We use the Stokes' theorem over a simply-connected (unbroken) domain A enclosed by the circuit C and find the following sufficient conditions:

$$\nabla \times \nabla \mathbf{u} = \mathbf{0}, \tag{3.14a}$$

$$\nabla \times \nabla \boldsymbol{\varphi} = \mathbf{0}. \tag{3.14b}$$

The condition (3.14b) is readily satisfied, while the condition (3.14a) can form the compatibility in terms of the microstrain $\boldsymbol{\epsilon}^{(mi)}$ and the permutation of microrotations $\boldsymbol{\varphi}_{\times}$ through the equation (2.11) as

$$\nabla \times \left(\boldsymbol{\epsilon}^{(mi)} + \boldsymbol{\varphi}_{\times}\right)^{T} = \mathbf{0}. \tag{3.15}$$

We refer to the expression for the curl of a tensor in cylindrical coordinates given in (3.5) and show that the compatibility condition (2.11) becomes

$$\begin{aligned}\nabla \times \left(\boldsymbol{\epsilon}^{(mi)} + \boldsymbol{\varphi}_{\times}\right)^{T} = &\left(\frac{\epsilon^{(mi)}_{r\theta}}{r} + \frac{\partial \epsilon^{(mi)}_{\theta r}}{\partial r} + \frac{\partial \epsilon^{(mi)}_{r\theta}}{\partial r} - \frac{1}{r}\frac{\partial \epsilon^{(mi)}_{rr}}{\partial \theta} - \frac{\partial \varphi_3}{\partial r}\right)\mathbf{e}_3 \otimes \mathbf{e}_r \\ &+ \left(\frac{\epsilon^{(mi)}_{\theta\theta}}{r} - \frac{\epsilon^{(mi)}_{rr}}{r} + \frac{\partial \epsilon^{(mi)}_{\theta\theta}}{\partial r} - \frac{1}{r}\frac{\partial \epsilon^{(mi)}_{\theta r}}{\partial \theta} - \frac{1}{r}\frac{\partial \varphi_3}{\partial \theta}\right)\mathbf{e}_3 \otimes \mathbf{e}_\theta = \mathbf{0}.\end{aligned} \tag{3.16}$$

The foregoing equation holds if and only if,

$$\begin{aligned}&\frac{\epsilon^{(mi)}_{r\theta}}{r} + \frac{\partial \epsilon^{(mi)}_{\theta r}}{\partial r} + \frac{\partial \epsilon^{(mi)}_{r\theta}}{\partial r} - \frac{1}{r}\frac{\partial \epsilon^{(mi)}_{rr}}{\partial \theta} - \frac{\partial \varphi_3}{\partial r} = 0, \\ &\frac{\epsilon^{(mi)}_{\theta\theta}}{r} - \frac{\epsilon^{(mi)}_{rr}}{r} + \frac{\partial \epsilon^{(mi)}_{\theta\theta}}{\partial r} - \frac{1}{r}\frac{\partial \epsilon^{(mi)}_{\theta r}}{\partial \theta} - \frac{1}{r}\frac{\partial \varphi_3}{\partial \theta} = 0.\end{aligned} \tag{3.17}$$

We may express the microstrain and microrotation gradient components in terms of the stress and couple stress components through the inverse form of the constitutive equations

(2.14), that is

$$\begin{aligned}
\epsilon_{r\theta}^{(mi)} &= \frac{1}{4\alpha\mu}\left((\mu+\alpha)\sigma_{r\theta}-(\mu-\alpha)\sigma_{\theta r}\right),\\
\epsilon_{\theta r}^{(mi)} &= \frac{1}{4\alpha\mu}\left((\mu+\alpha)\sigma_{\theta r}-(\mu-\alpha)\sigma_{r\theta}\right),\\
\epsilon_{rr}^{(mi)} &= \frac{1}{4\mu(\mu+\lambda)}\left((2\mu+\lambda)\sigma_{rr}-\lambda\sigma_{\theta\theta}\right),\\
\epsilon_{\theta\theta}^{(mi)} &= \frac{1}{4\mu(\mu+\lambda)}\left((2\mu+\lambda)\sigma_{\theta\theta}-\lambda\sigma_{rr}\right),\\
\varphi_{3,r} &= \frac{1}{\gamma+\varsigma}\mu_{r3},\quad \varphi_{3,\theta}=\frac{r}{\gamma+\varsigma}\mu_{\theta 3},
\end{aligned} \tag{3.18}$$

Next, we employ the following Airy-type stress functions ϕ and ψ introduced in [102] and defined by:

$$\begin{aligned}
\sigma_{rr} &= \frac{1}{r}\frac{\partial\phi}{\partial r}+\frac{1}{r^2}\frac{\partial^2\phi}{\partial\theta^2}-\frac{1}{r}\frac{\partial^2\psi}{\partial r\partial\theta}+\frac{1}{r^2}\frac{\partial\psi}{\partial\theta},\\
\sigma_{\theta\theta} &= \frac{\partial^2\phi}{\partial r^2}+\frac{1}{r}\frac{\partial^2\psi}{\partial r\partial\theta}-\frac{1}{r^2}\frac{\partial\psi}{\partial\theta},\\
\sigma_{r\theta} &= -\frac{1}{r}\frac{\partial^2\phi}{\partial r\partial\theta}+\frac{1}{r^2}\frac{\partial\phi}{\partial\theta}-\frac{1}{r}\frac{\partial\psi}{\partial r}-\frac{1}{r^2}\frac{\partial^2\psi}{\partial\theta^2},\\
\sigma_{\theta r} &= -\frac{1}{r}\frac{\partial^2\phi}{\partial r\partial\theta}+\frac{1}{r^2}\frac{\partial\phi}{\partial\theta}+\frac{\partial^2\psi}{\partial r^2},\\
\mu_{r3} &= \frac{\partial\psi}{\partial r},\quad \mu_{\theta 3}=\frac{1}{r}\frac{\partial\psi}{\partial\theta}.
\end{aligned} \tag{3.19}$$

Obviously, the Airy-type stress functions, ϕ and ψ in (3.19), satisfy the balance equations (3.4). In other words, the balance equations are necessary and sufficient for existence of Airy-type functions in the form (3.19) [102]. Writing (3.18) in terms of (3.19) and inserting the result into the compatibility relations (3.17), we obtain a coupled system of partial differential equations in terms of the stress functions ϕ and ψ :

$$\begin{aligned}
c^2\frac{\partial}{\partial r}\left(\nabla^2-1\right)\psi &= 2b^2(1-\nu)\frac{1}{r}\frac{\partial}{\partial\theta}\nabla^2\phi,\\
c^2\frac{1}{r}\frac{\partial}{\partial\theta}\left(\nabla^2-1\right)\psi &= -2b^2(1-\nu)\frac{\partial}{\partial r}\nabla^2\phi,
\end{aligned} \tag{3.20}$$

where,

$$c^2 = \frac{(\gamma+\varsigma)(\mu+\alpha)}{4\mu\alpha}, \quad b^2 = \frac{(\gamma+\varsigma)}{4\mu}, \quad v = \frac{\lambda}{2(\mu+\lambda)}. \tag{3.21}$$

The parameters c and b defined by (3.21) are commonly referred to as the characteristic lengths corresponding to a micropolar material. Solving the system of equations (3.20) we arrive at two uncoupled fourth order partial differential equations:

$$\nabla^2\nabla^2\phi = 0, \quad \nabla^2(1 - c^2\nabla^2)\psi = 0. \tag{3.22}$$

The stress functions ϕ and ψ of the plane strain problem without body forces must be the solutions of the equations (3.22) and must be related to each other by the equations (3.20).

3.3 Boundary value problem

Based on the remote boundary conditions which are presentable in cylindrical coordinates by

$$\begin{aligned} \sigma_{rr}(r \to \infty) &= \frac{1}{2}p_2(1 - \cos 2\theta) + \frac{1}{2}p_1(1 + \cos 2\theta), \\ \sigma_{r\theta}(r \to \infty) &= \frac{1}{2}(p_2 - p_1)\sin 2\theta, \\ \mu_{r3}(r \to \infty) &= 0, \end{aligned} \tag{3.23}$$

We can express the general solution to the two uncoupled equations (3.22) as

$$\begin{aligned} \phi &= A\ln r + Br^2 + (C + Dr^2 + Er^{-2} + Fr^4)\cos 2\theta, \\ \psi &= \Big(Gr^{-2} + H^2 + L\ K_2(\frac{r}{c}) + J\ I_2(\frac{r}{c})\Big)\sin 2\theta, \end{aligned} \tag{3.24}$$

where $A, B, C, D, E, F, G, H, L, J$ are constants to be determined, and K_2 and I_2 are modified Bessel functions of the second and first kind, respectively. Using the general solution of the stress functions in the form of (3.24) into (3.19), we may write the stress and couple

stress components as

$$\begin{aligned}
\sigma_{rr} &= 2B + Ar^{-2} \\
&\quad + \big[-2(D+H) - 6(E-G)r^{-4} - 4Cr^{-2} \\
&\quad +2r^{-2}J\left(3I_2\left(\frac{r}{c}\right) - \frac{r}{c}I_1\left(\frac{r}{c}\right)\right) \\
&\quad +2r^{-2}L\left(\frac{r}{c}K_1\left(\frac{r}{c}\right) + 3K_2\left(\frac{r}{c}\right)\right)\big]\cos 2\theta,
\end{aligned}$$

$$\begin{aligned}
\sigma_{\theta\theta} &= 2B - Ar^{-2} \\
&\quad + \big[2(D+H) + 6(E-G)r^{-4} + 12Fr^2 \\
&\quad +2r^{-2}J\left(\frac{r}{c}I_1\left(\frac{r}{c}\right) - 3I_2\left(\frac{r}{c}\right)\right) \\
&\quad -2r^{-2}L\left(\frac{r}{c}K_1\left(\frac{r}{c}\right) + 3K_2\left(\frac{r}{c}\right)\right)\big]\cos 2\theta,
\end{aligned}$$

$$\begin{aligned}
\sigma_{r\theta} &= \big[2(D+H) - 6(E-G)r^{-4} - 2Cr^{-2} + 6Fr^2 \\
&\quad -r^{-2}J\left(\frac{r}{c}I_1\left(\frac{r}{c}\right) - 6I_2\left(\frac{r}{c}\right)\right) \\
&\quad +r^{-2}L\left(\frac{r}{c}K_1\left(\frac{r}{c}\right) + 6K_2\left(\frac{r}{c}\right)\right)\big]\sin 2\theta,
\end{aligned}$$

$$\begin{aligned}
\sigma_{\theta r} &= \big[2(D+H) - 6(E-G)r^{-4} - 2Cr^{-2} + 6Fr^2 \\
&\quad +c^{-2}J\left(-\frac{c}{r}I_1\left(\frac{r}{c}\right) + (1+6\frac{c^2}{r^2})I_2\left(\frac{r}{c}\right)\right) \\
&\quad +c^{-2}L\left(\frac{c}{r}K_1\left(\frac{r}{c}\right) + (1+6\frac{c^2}{r^2})K_2\left(\frac{r}{c}\right)\right)\big]\sin 2\theta, \qquad (3.25)
\end{aligned}$$

$$\begin{aligned}
\mu_{r3} &= \big[-2Gr^{-3} + 2Hr \\
&\quad +r^{-1}J\left(\frac{r}{c}I_1\left(\frac{r}{c}\right) - 2I_2\left(\frac{r}{c}\right)\right) \\
&\quad -r^{-1}L\left(\frac{r}{c}K_1\left(\frac{r}{c}\right) + 2K_2\left(\frac{r}{c}\right)\right)\big]\sin 2\theta,
\end{aligned}$$

$$\begin{aligned}
\mu_{\theta 3} &= 2\big[Gr^{-3} + Hr + r^{-1}J\ I_2\left(\frac{r}{c}\right) \\
&\quad +r^{-1}L\ K_2\left(\frac{r}{c}\right)\big]\cos 2\theta. \qquad (3.26)
\end{aligned}$$

We find the microstrains and microrotations using constitutive equations and the stress expressions in terms of the two stress functions. We integrate the resulting components to compute the displacement and microrotation components as

$$\begin{aligned} u_r &= -\frac{1}{2\mu}\left[\frac{\partial\phi}{\partial r}+\frac{1}{r}\frac{\partial\psi}{\partial\theta}-(1-\nu)r\frac{\partial\eta}{\partial\theta}\right], \\ u_\theta &= -\frac{1}{2\mu}\left[\frac{1}{r}\frac{\partial\phi}{\partial\theta}-\frac{\partial\psi}{\partial r}-(1-\nu)r^2\frac{\partial\eta}{\partial r}\right], \\ \varphi_3 &= \frac{1}{(\gamma+\varsigma)}\psi, \end{aligned} \tag{3.27}$$

where η satisfies the conditions

$$\frac{\partial^2(r\eta)}{\partial r\partial\theta}=0, \quad \Delta\eta=0, \tag{3.28}$$

which by integration determine the function η as

$$\eta = 4B\theta+(2Cr^{-2}+2Fr^2)\sin 2\theta. \tag{3.29}$$

From the equations (3.27) we arrive at

$$\begin{aligned} u_r^* &= 2\mu u_r = -\left\{Ar^{-1}-2Br(1-2\nu)\right. \\ &\quad +\left(2(D+H)r+2(G-E)r^{-3}-4(1-\nu)Cr^{-1}\right. \\ &\quad \left.\left.+4\nu Fr^3+2Jr^{-1}I_2\left(\frac{r}{c}\right)+2Lr^{-1}K_2\left(\frac{r}{c}\right)\right)\cos 2\theta\right\}, \end{aligned}$$

$$\begin{aligned} u_\theta^* &= 2\mu u_\theta = -\left\{-2(D+H)r+2(G-E)r^{-3}+2(1-2\nu)Cr^{-1}\right. \\ &\quad -2(3-2\nu)Fr^3-J\left(\frac{1}{c}I_1\left(\frac{r}{c}\right)-\frac{2}{r}I_2\left(\frac{r}{c}\right)\right) \\ &\quad \left.+L\left(\frac{1}{c}K_1\left(\frac{r}{c}\right)+\frac{2}{r}K_2\left(\frac{r}{c}\right)\right)\right\}\sin 2\theta, \end{aligned}$$

$$\begin{aligned} \varphi_3^* &= (\gamma+\varsigma)\varphi_3 = \left\{Gr^{-2}+Hr^2\right. \\ &\quad \left.+L\ K_2(\frac{r}{c})+J\ I_2(\frac{r}{c})\right\}\sin 2\theta, \end{aligned} \tag{3.30}$$

for the normalized displacement and microrotations. We now employ the boundary conditions for a remotely loaded infinite medium containing the circular hole (3.23) to determine the unknown coefficients. Accordingly, the remote loading conditions in cylindrical coordinates as $r \to \infty$ result in

$$\begin{aligned} J &= 0,\ F = 0,\ H = 0, \\ B &= \frac{1}{4}(p_1 + p_2),\ D = \frac{1}{4}(p_2 - p_1). \end{aligned} \tag{3.31}$$

The surface of the circular hole is assumed to be traction-free. We adopt the fourth order elastic surface structure introduced in Section 2.4, with the assumption that $G_s = 0$. By virtue of this latter assumption, we may demonstrate the pure effect of micropolar twisting rigidity of the surface free from the asymmetric shear-type contributions of micro-structures of the surface. In the equations (2.49-2.51), we incorporate the fact that for the circular surface under consideration, $ds = Rd\theta$ and $b_0 = -1/R$. Thus, the boundary conditions incorporating surface effects on the circular hole become,

$$\begin{aligned} &\frac{A_s}{2\mu R}\left(\frac{d^2u_\theta^*}{d\theta^2} + \frac{du_r^*}{d\theta}\right) + \frac{B_s}{2\mu R^3}\left(-\frac{d^3u_r^*}{d\theta^3} + \frac{d^2u_\theta^*}{d\theta^2}\right) \\ &\quad + \frac{H_s}{(\gamma+\varsigma)R^2}\frac{d^2\varphi_3^*}{d\theta^2} + R\sigma_{r\theta}(R,\theta) = 0, \end{aligned} \tag{3.32}$$

$$\begin{aligned} &-\frac{A_s}{2\mu R}\left(\frac{du_\theta^*}{d\theta} + u_r^*\right) + \frac{B_s}{2\mu R^3}\left(-\frac{d^4u_r^*}{d\theta^4} + \frac{d^3u_\theta^*}{d\theta^3}\right) \\ &\quad + \frac{H_s}{(\gamma+\varsigma)R^2}\frac{d^3\varphi_3^*}{d\theta^3} + R\sigma_{rr}(R,\theta) = 0, \end{aligned} \tag{3.33}$$

$$\frac{H_s}{(\gamma+\varsigma)R^2}\left(\frac{d^2\varphi_3^*}{d\theta^2}\right) + \mu_{r3}(R,\theta) = 0. \tag{3.34}$$

With reference to the equations (2.49-2.51) we can express the material properties of the surface in (3.32 to 3.34) by $A_s = (2\mu_s + \lambda_s)t$, $B_s = (2\mu_s + \lambda_s)t^3/12$, and $H_s = (\gamma_s + \varsigma_s)t$ which respectively, represent the stretching, bending and twisting rigidities of the surface. Clearly, the values of the stretching, bending and twisting rigidities depend on the choice

of the effective thickness t which may differ for different modes of deformation (i.e. for stretching and bending) [101] and also on the choice of Lamé coefficients of the surface μ_s and λ_s. Indeed, to obtain realistic values of these surface parameters, more experimental data is required as well as atomistic simulations such those undertaken in [17]. Using the boundary conditions (3.32 to 3.34), we can determine the remaining coefficients A, C, E, G, and L leading to a complete analytic solution of the problem.

3.4 Numerical Evaluation

Here we present some numerical results to illustrate the contribution of micropolar surface elasticity with bending rigidity. We adopt the numerical values of the material constants as per existing studies of surface effects given in the literature [129, 17]. However, the lack of experimental data on the values of micropolar elastic constants and bending rigidities of surfaces and interfaces (see, for example, [54, 3, 86] for ongoing research in this area) means that we cannot relate our chosen values of the bulk and surface moduli via an empirical relation. As a result, for a micropolar material with $\mu_m = 20$ Gpa, $\nu = 0.2$, $(\gamma + \varsigma) = 4\mu_m b^2(\mathrm{N})$, $c = 0.4$ nm and $b = 0.3$ nm, we assume a surface of $A_s = 6$ N/m, and $B_s = H_s = 10^{-18}$ N.m. The plane medium containing the circular hole is subjected to a uniaxial remote loading ($p_1 = 0$ and $p_2 \neq 0$). In Figure 3.2, we illustrate the variation of the normalized stress component $\sigma_{\theta\theta}$ on the circumference of the hole. Accordingly, we observe the contribution of the surface effect in classical and micropolar elasticity. As shown in the figure, incorporating surface effects in both classical and micropolar models leads to quite convergent predictions for the hoop stress. We can identify three types of similar solutions. The classical and micropolar elasticity models without surface effects furnish the first type of solutions which demonstrate a reduction in the stress concentration when the micropolar solution is compared to the classical. This is, indeed, in agreement with the results presented by Kolani and Ariman [78]. We highlight the second type of solution by the classical elasticity with surface effects. The incorporation of bending resistance to the surface decreases the stress concentration even further. However, the two classical solutions for hoop

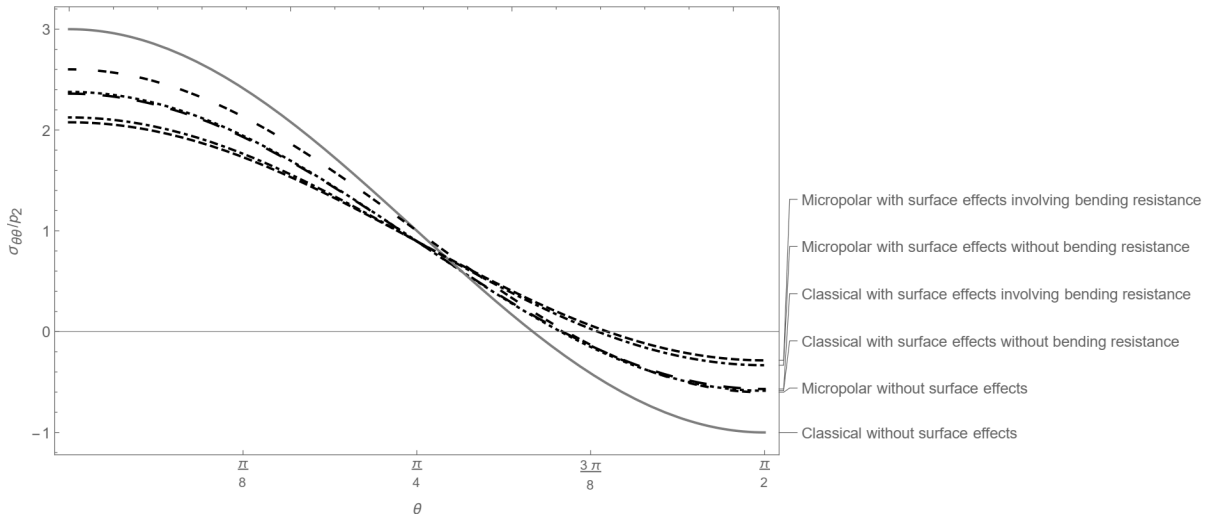

Figure 3.2: Hoop-stress concentration on the circumference of a hole of radius $R = 1$nm under uniaxial remote loading

stress concentration with surface effect are quite close. The micropolar elasticity model of surface effects makes up the third type of solutions which predict the lowest hoop stress concentration. An overall observation of the solutions indicate that the more size-dependent effects incorporated into the model of deformation (including surface effects with bending resistance and microstructure of the material via micropolar elasticity), the more accurate the results become. This is determined from the solutions converging to a minimum prediction of the stress concentration. We have shown further, in [57], that for the components $\sigma_{r\theta}$ and σ_{rr}, the incorporation of the surface bending rigidities of both classical and micropolar case contributes more to the stress solutions.

Figure 3.3 shows variations of the normalized hoop stress with radius of the hole. We observe that including surface effects in both classical and micropolar elasticity leads to significant differences in the results. The difference between the solutions with and without bending rigidity is perceptible when the radius of the hole is small enough. For the presented numerical case, to accentuate significant effects of the bending rigidity of the surface the radius of the hole should be less than around 2 nm, however, this size may differ depending on the choice of values for the material parameters. Here, we emphasize that for the model of

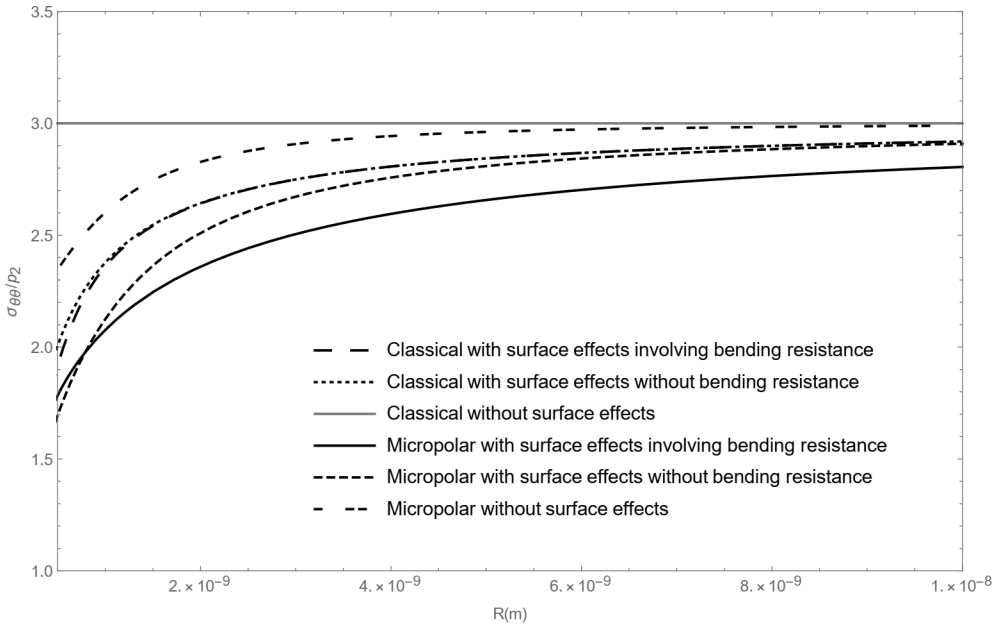

Figure 3.3: Variation of hoop-stress concentration with radius of circular hole

a micropolar bulk with surface effects excluding bending resistance, we assume the surface to be a classical stretching-resistance Gurtin-Murdoch type surface. Therefore, for large circular holes where the bulk micropolar effects are undermined the results approach the classical elasticity with surface incorporation. Also, for a sufficiently large hole radius (e.g. here more than 5 nm) the results with and without surface bending effects essentially agree so that the surface bending resistance becomes insignificant. The most general case of the micropolar model with surface bending resistance is an exception in that sense, since even for large circular holes the intrinsic bending resistance of the surface H_s remains effective.

We sum up this chapter by stating that the surface model gains accuracy via the incorporation of bending resistance in both classical and micropolar theories. We conclude that size-dependence can be captured to a reasonable accuracy by incorporating higher order surface mechanics in both classical and micropolar elasticity. In conclusion, our results indicate several scenarios in which both microstructure and varying degrees of surface elasticity may produce more precise and efficient models of deformation.

We may use the method of the presented solution here to approach problems of more direct application. In particular, problems concerning homogenization of nano-composite materials are of high importance. Studying the effective properties of nano-composite materials using the proposed model is the subject of the next chapter.

Chapter 4

Effective Elastic Properties of Nano-Composites with Interface Effects

In this chapter, we employ the approach from the previous chapter to study the effective shear and bulk moduli of a micropolar nano-composite while taking into account the separate elasticity of the interfaces. Most of the materials we deal with in reality are inhomogeneous as they contain micro/nano-constituents or are formed of micro/nano-structures. Thus, the statistical behavior of micro/nano-constituents determine the overall mechanical responses of the materials. Since the micro/nano-sized constituents of most materials are randomly distributed, the so-called homogenization theories are developed from statistical principles to predict the overall mechanical properties of such materials [93]. Furthermore, it is well-known that the homogenization techniques are strongly influenced by the microstructure and inherent length scales of the heterogeneous material [6]. Classical models of deformation are based on ideas from continuum mechanics which essentially ignore the material's microstructure and any phenomena occurring at smaller length scales. In the recent literature, two different approaches have been taken to address the deficiencies in classical models; the theories of higher-order continua, and the incorporation of surface/interface mechanics. The homogenization techniques have been adopted with the incorporation of the Gurtin-Murdoch surface model, to account for the size-dependency in the effective properties of nano-composites [35],

and nano-voids [37]. The homogenization procedures commonly require knowledge about Eshelby tensors and the stress concentration tensor for inhomogeneities (these are readily derived by Duan et al. [34, 36]) in the presence of surface elasticity. As mentioned previously, however, the Gurtin-Murdoch model is rather limited in that it treats the surface/interface as a membrane incapable of predicting an energy-minimizing configuration under compressive surface/interface stresses. To address the deficiencies of the Gurtin-Murdoch model, the Steigmann-Ogden model has recently attracted extensive attention in refined continuum mechanics models. For example, Chhapadia et al. [17] demonstrated the necessity of the Steigmann-Ogden modification in explaining the discrepancy between the results of atomic simulations and the classical Gurtin-Murdoch model. In the particular case of the homogenization of nano-composites, the work of Zemlyanova and Mogilevskaya [158] is noteworthy. They incorporated the Steigmann-Ogden model into a model of the interface and obtained corresponding stress distributions as well as the effective properties of the composite. They noted, specifically, the contribution of the enhanced model via flexural resistance of the interface.

Adopting a higher-order continuum model is a rather popular alternative approach among the researchers in modifying homogenization techniques to account for size-dependency [134, 97, 155, 96]. Among the aforementioned research, Liu and Hu [96], proposed a formalism in the micropolar theory of elasticity [46] with which the effective properties of materials could be determined in this more general setting. Subsequently, Xun et al. [150] derived the effective in-plane moduli of a micropolar composite by incorporating the analytical solution of the problem into the Mori-Tanaka procedure.

Introducing surface/interface mechanics into the micro-mechanical model of micropolar elasticity combines the two approaches with the objective of providing a comprehensive description of size-dependent composite materials. This approach has been taken by Chen et. al. [15] who based their presentation of the interface on Gurtin-Murdoch model, which as mentioned in the previous chapters, offers no flexural rigidity. Our specific interest in the contribution of flexural effects in the micropolar surface model motivates the study of the

overall mechanical properties of materials in the framework of our presented model.

The approach to the nano-composites problem presented in this chapter, enjoys the advantages of both surface/interface mechanics with flexural effects and the higher order continuum approach in the form of micropolar elasticity with surface/interface effects. We start this chapter with a brief account of the concepts useful in estimating the effective mechanical properties of nano-composites. Subsequently, we obtain the analytical solution of deformations of a circular inhomogeneity in the presence of surface effects in a micropolar medium. We use the analytical solution to evaluate the effective moduli of the nano-composite using the Mori-Tanaka approach. We identify the contribution of surface flexural resistance by comparing a special case of our results with those in [15] in which the interface effect incorporates only membrane type resistance. It should be noted that Chen et. al. [15] simplified their calculations by considering the case of a fiber composed of a classical material. They, as well, imposed zero microrotations on the interface with the micropolar matrix. However, we believe that a perfectly bonded interface which characterizes the influence of a classical fiber material on a micropolar matrix should involve a couple-stress jump condition instead. This is because on the perfectly bonded interface the independent microrotations of a micropolar material must be set aligned with the classical displacement-dependent rotations (marco-rotations) of the classical fiber rather than zero. This choice of boundary conditions is consistent with the fact that couple stresses are zero in the classical fiber but nonzero in the micropolar matrix. However, to present a proper comparison, observe the effects of micropolar flexural resistance and verify our results, we calculate the effective moduli in two different cases of boundary conditions. In the first case, we follow the assumption made in [15], impose microrotations on the interface and demonstrate the additional contribution of interface flexural resistance. In the second case we use the interface couple stress jump conditions rather than fixed rotations. At the end of this chapter, we illustrate the theory by presenting numerical examples in which a plane micropolar medium contains nano-voids with an enhanced surface model. To open the chapter we summarize required preliminary concepts of homogenization theory.

4.1 Preliminary Concepts

We would like to idealize a material consisting of different micro/nano constituents to a homogeneous material whose mechanical properties are uniformly distributed throughout the volume. Consider a space occupied by such a material, S, over which a probability density of the property is defined as, $p(\mathbf{x})$ at a point, $\mathbf{x} \in S$. However, any particular property, $\mathbf{M}$, of an inhomogeneous composite is a function of the point $\mathbf{x}$, in the space S. The ensemble average of this property over the space is defined as,

$$\langle \mathbf{M} \rangle_S \equiv \int_S p(\mathbf{x}) \mathbf{M}(\mathbf{x}) dS \tag{4.1}$$

A representative volume element (RVE) is a volume V, of a heterogeneous material assumed sufficiently large to statistically represent the material in an infinitesimal neighborhood. In other words, an RVE contains a representative sampling of all the inhomogeneities and micro/nano-constituents [93]. Obviously, for a material which is homogeneous at macro-level, we consider associated macro-elements to be micro-spaces or RVEs with statistical information about the micro/nano-structures of the material. The average of a property (e.g. stress, strain, stiffness tensor, etc.) is found, under the assumption that $p(\mathbf{x}) = \frac{1}{V}$. Thus,

$$\langle \mathbf{M} \rangle_V \equiv \frac{1}{V} \int_V \mathbf{M} dV \tag{4.2}$$

The concept of RVE is used in micro/nano-mechanics to estimate the overall elastic properties of materials in terms of the elastic properties of the micro/nano-constituents. The heterogeneous RVE is subjected to prescribed boundary conditions corresponding to the uniform fields. We calculate the overall properties of nano-composite materials based on the RVE response to these boundary conditions. There are several schemes to determine the effective properties of the nano-composite materials. There are two theorems that are used in furnishing the homogenization schemes.

Theorem 4.1. *Suppose an RVE of volume V whose unit outward normal to its boundaries*

is denoted by $\mathbf{N}$*, is subjected to remote traction boundary conditions given by* $\boldsymbol{\Sigma}\mathbf{N}$*, then the average stress field* $\langle\boldsymbol{\sigma}\rangle_V$ *in the RVE equals the remote boundary conditions tensor,* $\boldsymbol{\Sigma}$*.*

Proof. Using the balance equations (2.7) we write the average stress tensor as

$$\begin{aligned}
\langle\boldsymbol{\sigma}\rangle_V &= \frac{1}{V}\int_V \boldsymbol{\sigma} dV \\
&= \frac{1}{V}\int_V \operatorname{div}(\boldsymbol{\sigma}^T \otimes \mathbf{x}) dV \\
&= \frac{1}{V}\int_{\partial V} (\boldsymbol{\sigma}^T \mathbf{N} \otimes \mathbf{x}) dA = \frac{1}{V}\int_{\partial V} (\boldsymbol{\Sigma}\mathbf{N} \otimes \mathbf{x}) dA \\
&= \frac{\boldsymbol{\Sigma}}{V}\int_{\partial V} (\mathbf{n} \otimes \mathbf{x}) dA = \boldsymbol{\Sigma}
\end{aligned}$$

□

Theorem 4.2. *Suppose an RVE of volume* V*, whose boundary conditions are prescribed displacements,* $\mathbf{u}^0$ *which can be described in the form of* $\mathbf{u}^0 = \mathbf{E}\mathbf{x}$ *with* $\mathbf{E}$ *being a constant strain tensor. Then the average strain field in the RVE equals the constant strain tensor,* $\mathbf{E}$*.*

Proof. The proof procedure is similar to the previous theorem. □

Some of the well-known homogenization techniques include dilute suspension approximation, self-consistent method, and Mori-Tanaka method. In this section we summarize the Mori-Tanaka method (MTM) which we use for evaluating the effective elastic moduli of a micropolar nano-composite with surface effects.

4.1.1 Mori-Tanaka Procedure

We briefly reformulate the MTM following Duan et al. [35]. To this end, we define a RVE of a volume V consisting of the medium and inhomogeneities of the same type. The inhomogeneity and the medium occupy the volumes V_1 and V_2 in the RVE, respectively and Γ denotes the interface between the inhomogeneity and the medium. As in the previous

section, the indices 1, 2 again correspond to the inhomogeneity and the medium, respectively. The idea is based on Mori-Tanaka mean field theory which states that for a matrix containing randomly distributed ellipsoidal inhomogeneities the average strain field in the matrix remains the same due to adding a single inhomogeneity to the RVE [108]. There are two strategies for formulating the effective properties of the composite based on MTM. In the first strategy, we calculate the average of strain fields based on prescribed displacement boundary conditions. The second approach is to formulate the average stress fields based on prescribed traction boundary conditions. Since we readily have the analytical solution of the problem of a circular inhomogeneity under prescribed remote loading we adopt the second approach. Note that we are interested in the equivalent classical elastic material moduli so that we take averages over the symmetric parts of the stress/strain fields (denoted by the superscript "sym") [96]. Consequently, we express the uniform remote traction condition on an RVE as,

$$\mathbf{t} = \boldsymbol{\Sigma}\mathbf{N}, \tag{4.3}$$

where, $\mathbf{t}$ represents the uniform traction on the imaginary boundary of the RVE with unit normal $\mathbf{N}$ and $\boldsymbol{\Sigma} = \langle \boldsymbol{\sigma}^{sym} \rangle_V$ is the average of the symmetric part of the stress field which corresponds to the stress field in an equivalent homogeneous classical medium. Under the foregoing traction boundary conditions we define a fourth-order stress concentration tensor, $\mathbf{J}$, which connects the average stress distribution inside the inhomogeneity to the average stress distribution inside the medium in the form

$$\langle \boldsymbol{\sigma}^{sym} \rangle_1 = \mathbf{J} : \langle \boldsymbol{\sigma}^{sym} \rangle_2 . \tag{4.4}$$

In the equation (4.4) and the equations that follow, $\langle . \rangle_1$, $\langle . \rangle_2$, $\langle . \rangle_V$ and $\langle . \rangle_\Gamma$ indicate the average quantities taken over the inhomogeneity, the medium, the total RVE, and the interface, respectively. The notation ":" indicates the double contraction of two tensors. Subsequently, for the average symmetric stress jump over the interface, we adopt the representation given in [8] and [35] and define a concentration tensor, $\mathbf{M}$ such that,

$$\langle [\boldsymbol{\sigma}]^{sym} \rangle_\Gamma = \frac{1}{2V_1} \int_\Gamma \left([\boldsymbol{\sigma}]\mathbf{n} \otimes \mathbf{x} + \mathbf{x} \otimes [\boldsymbol{\sigma}]\mathbf{n} \right) dS = \mathbf{M} : \langle \boldsymbol{\sigma}^{sym} \rangle_2 . \tag{4.5}$$

Here, the vector $\mathbf{x}$ locates the interface's mid-surface, $\mathbf{n}$ is the unit outward normal to the interface, and

$$[\boldsymbol{\sigma}] = \boldsymbol{\sigma}^{(2)}\big|_{\Gamma} - \boldsymbol{\sigma}^{(1)}\big|_{\Gamma}\,,$$

denotes the stress jump across the interface. Also V_1 denotes the volume of the inhomogeneity phase. The concentration tensors are determined from the analytical solution of the problem subject to the prescribed traction boundary conditions. Let f be the volume fraction of the inhomogeneity in the RVE. Then, from the averaging procedure we can express the total average of the stress and strain fields in the form,

$$\langle \boldsymbol{\sigma}^{sym} \rangle_V = (1-f)\,\langle \boldsymbol{\sigma}^{sym} \rangle_2 + f\,\langle \boldsymbol{\sigma}^{sym} \rangle_1 + \frac{f}{2V_1}\int_{\Gamma} \left([\boldsymbol{\sigma}]\boldsymbol{n} \otimes \boldsymbol{x} + \boldsymbol{x} \otimes [\boldsymbol{\sigma}]\mathbf{n}\right) dS, \tag{4.6}$$

$$\langle \boldsymbol{\epsilon}^{sym} \rangle_V = (1-f)\,\langle \boldsymbol{\epsilon}^{sym} \rangle_2 + f\,\langle \boldsymbol{\epsilon}^{sym} \rangle_1\,, \tag{4.7}$$

Upon use of the equations (4.4) and (4.5) in (4.6), we can write,

$$\langle \boldsymbol{\sigma}^{sym} \rangle_V = \left[(1-f)\mathbf{I}^{4th} + f(\mathbf{J}+\mathbf{M})\right] : \langle \boldsymbol{\sigma}^{sym} \rangle_2\,, \tag{4.8}$$

or

$$\langle \boldsymbol{\sigma}^{sym} \rangle_2 = \left[(1-f)\mathbf{I}^{4th} + f(\mathbf{J}+\mathbf{M})\right]^{-1} : \langle \boldsymbol{\sigma}^{sym} \rangle_V\,. \tag{4.9}$$

Here, $\mathbf{I}^{4th}$ is the fourth order unit tensor. We establish the equivalent homogeneous classical material with a uniform equivalent compliance tensor $\overline{\mathbf{D}}$, which arises from the relation between the average symmetric stress and strain tensors in the RVE, formally, $\langle \boldsymbol{\epsilon}^{sym} \rangle_V = \overline{\mathbf{D}} : \langle \boldsymbol{\sigma}^{sym} \rangle_V$. Furthermore, the average stress and strains in each material phase are related through the uniform compliance tensor of that material phase. In other words,

$$\langle \boldsymbol{\epsilon}^{sym} \rangle_2 = \mathbf{D}^{(2)} \colon \langle \boldsymbol{\sigma}^{sym} \rangle_2\,, \quad \langle \boldsymbol{\epsilon}^{sym} \rangle_1 = \mathbf{D}^{(1)} \colon \langle \boldsymbol{\sigma}^{sym} \rangle_1\,. \tag{4.10}$$

Substituting the equations (4.10) in (4.7) and using (4.4), we arrive at,

$$\overline{\mathbf{D}} : \langle \sigma^{sym} \rangle_V = (1-f)\mathbf{D}^{(2)} \colon \langle \sigma^{sym} \rangle_2 + f\mathbf{D}^{(1)} \colon \mathbf{J} : \langle \sigma^{sym} \rangle_2\,. \tag{4.11}$$

The term $(1-f)\langle\sigma^{sym}\rangle_2$ in (4.11) may be replaced by the following expression:

$$(1-f)\langle\boldsymbol{\sigma}^{sym}\rangle_2 = \langle\boldsymbol{\sigma}^{sym}\rangle_V - f\langle\boldsymbol{\sigma}^{sym}\rangle_1 - f\mathbf{M}:\langle\boldsymbol{\sigma}^{sym}\rangle_2 . \tag{4.12}$$

It then follows that,

$$\overline{\mathbf{D}}:\langle\boldsymbol{\sigma}^{sym}\rangle_V = \mathbf{D}^{(2)}:\langle\boldsymbol{\sigma}^{sym}\rangle_V + \left[f\left(\mathbf{D}^{(1)}-\mathbf{D}^{(2)}\right):\mathbf{J}-f\mathbf{D}^{(2)}:\mathbf{M}\right]:\langle\boldsymbol{\sigma}^{sym}\rangle_2 . \tag{4.13}$$

Using the equation (4.9) we express the second term of (4.13) in terms of $\langle\boldsymbol{\sigma}^{sym}\rangle_V$ to obtain,

$$\begin{aligned}\overline{\mathbf{D}} \;:\; \langle\boldsymbol{\sigma}^{sym}\rangle_V = \Big(&\mathbf{D}^{(2)} + \left[f\left(\mathbf{D}^{(1)}-\mathbf{D}^{(2)}\right):\mathbf{J}-f\mathbf{D}^{(2)}:\mathbf{M}\right]: \\ &\left[(1-f)\mathbf{I}^{4th}+f(\mathbf{J}+\mathbf{M})\right]^{-1}\Big):\langle\boldsymbol{\sigma}^{sym}\rangle_V ,\end{aligned}$$

from which we can determine the effective compliance tensor from the Mori-Tanaka formalism,

$$\overline{\mathbf{D}} = \mathbf{D}^{(2)} + \left[f\left(\mathbf{D}^{(1)}-\mathbf{D}^{(2)}\right):\mathbf{J}-f\mathbf{D}^{(2)}:\mathbf{M}\right]:\left[(1-f)\mathbf{I}^{4th}+f(\mathbf{J}+\mathbf{M})\right]^{-1} . \tag{4.14}$$

The effective stiffness tensor or the elastic moduli tensor of the composite may be obtained as the inverse tensor, $\overline{\mathbf{C}}=\overline{\mathbf{D}}^{-1}$. To fully determine the effective elastic moduli, it remains to evaluate the concentration tensors $\mathbf{J}$ and $\mathbf{M}$ which are isotropic tensors of the form,

$$\mathbf{J} = J_b\mathbf{E}_1 + J_s\mathbf{E}_2 \tag{4.15}$$

$$\mathbf{M} = M_b\mathbf{E}_1 + M_s\mathbf{E}_2 \tag{4.16}$$

where

$$\mathbf{E}_1 = \frac{1}{2}\mathbf{I}^{(2d)}\otimes\mathbf{I}^{(2d)},\ \mathbf{E}_2 = -\frac{1}{2}\mathbf{I}^{(2d)}\otimes\mathbf{I}^{(2d)} + \mathbf{I}^{(4th)}. \tag{4.17}$$

Here, $\mathbf{I}^{(2d)}$ is the second order unit tensor and the scalar components J_b, J_s, M_b and M_s are to be determined. We accomplish this task using the exact analytical solution of a circular inhomogeneity in an infinite medium under remote loading. The solution to this problem represents the change in the stress concentration by adding a single inhomogeneity to an infinite RVE of the nano-composite. Note that the stress concentration change can also be found using approximate methods such as Eshelby's equivalent inclusion method [38]. In the next section, we employ the exact analytical solution of the problem to calculate the concentration tensors and subsequently the effective elastic properties.

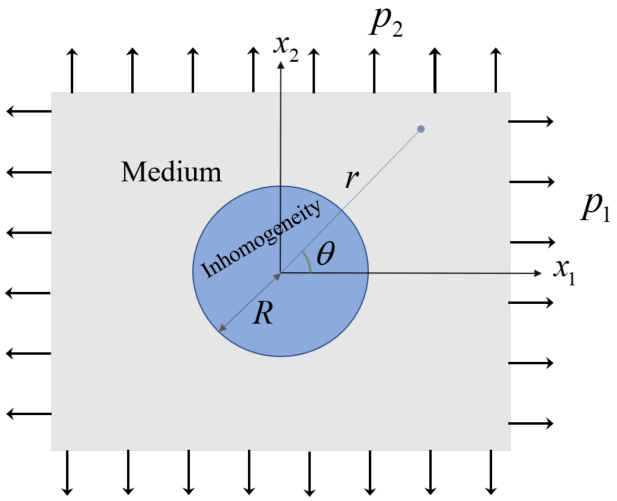

Figure 4.1: Circular inhomogeneity in an infinite plane matrix.

4.2 Circular inhomogeneity in an infinite medium

We consider a micropolar circular inhomogeneity of radius R in an infinite micropolar plane. We describe the interface between the inhomogeneity and the medium by the micropolar elastic interface model presented in chapter 1. This means that the interface of the circular inhomogeneity and the medium is described as a flexural resistant fourth order deformable structure. Consequently, the stress jump boundary conditions (2.49-2.51) hold at the interface. Let $\{o : x_1, x_2, x_3\}$ be a system of Cartesian coordinates and $\{o : r, \theta, x_3\}$ cylindrical coordinates with the common origin o located at the center of the circular inhomogeneity. Expressed in the Cartesian coordinates, the infinite plane medium is subjected to uniform remote normal stresses, $\sigma_{11} = p_1$ and $\sigma_{22} = p_2$, and zero remote couple stresses $\mu_{13} = \mu_{23} = 0$. We set the remote couple stresses to zero, since the remote properties of the infinite medium are assumed in macro-scale level. The configuration of the problem is shown in Figure 4.1. We use the equilibrating in-plane potential functions, ϕ_i and ψ_i, described by [150]

$$
\begin{aligned}
\sigma_{rr}^{(i)} &= \frac{1}{r}\frac{\partial \phi_i}{\partial r} + \frac{1}{r^2}\frac{\partial^2 \phi_i}{\partial \theta^2} - \frac{1}{r}\frac{\partial^2 \psi_i}{\partial r \partial \theta} + \frac{1}{r^2}\frac{\partial \psi_i}{\partial \theta}, \\
\sigma_{\theta\theta}^{(i)} &= \frac{\partial^2 \phi_i}{\partial r^2} + \frac{1}{r}\frac{\partial^2 \psi_i}{\partial r \partial \theta} - \frac{1}{r^2}\frac{\partial \psi_i}{\partial \theta}, \\
\sigma_{r\theta}^{(i)} &= -\frac{1}{r}\frac{\partial^2 \phi_i}{\partial r \partial \theta} + \frac{1}{r^2}\frac{\partial \phi_i}{\partial \theta} - \frac{1}{r}\frac{\partial \psi_i}{\partial r} - \frac{1}{r^2}\frac{\partial^2 \psi_i}{\partial \theta^2}, \\
\sigma_{\theta r}^{(i)} &= -\frac{1}{r}\frac{\partial^2 \phi_i}{\partial r \partial \theta} + \frac{1}{r^2}\frac{\partial \phi_i}{\partial \theta} + \frac{\partial^2 \psi_i}{\partial r^2}, \\
\mu_{r3}^{(i)} &= \frac{\partial \psi_i}{\partial r}, \quad \mu_{\theta 3}^{(i)} = \frac{1}{r}\frac{\partial \psi_i}{\partial \theta}, \quad i = 1, 2,
\end{aligned} \tag{4.18}
$$

In the equation (4.18), the indices $i = 1, 2$ correspond to the inhomogeneity and the medium, respectively. The displacement components can be calculated by combining the kinematic relations (2.11) in cylindrical coordinates and the constitutive relations given by (2.14), in the inverse form. Consequently,

$$
\begin{aligned}
u_r^{(i)} &= -\frac{1}{2\mu_i}\left[\frac{\partial \phi_i}{\partial r} + \frac{1}{r}\frac{\partial \psi_i}{\partial \theta} - (1-\nu_i) r \frac{\partial \eta_i}{\partial \theta}\right], \\
u_\theta^{(i)} &= -\frac{1}{2\mu_i}\left[\frac{1}{r}\frac{\partial \phi_i}{\partial \theta} - \frac{\partial \psi_i}{\partial r} - (1-\nu_i) r^2 \frac{\partial \eta_i}{\partial r}\right], \\
\varphi_3^{(i)} &= \frac{1}{\gamma_i}\psi_i, \quad i = 1, 2,
\end{aligned} \tag{4.19}
$$

where,

$$
\begin{aligned}
\eta_i &= 4B_i\theta + (2C_i r^{-2} + 2F_i r^2)\sin 2\theta, \\
\nu_i &= \frac{\lambda_i}{2(\mu_i + \lambda_i)}
\end{aligned}
$$

and B_i, C_i and F_i , $i = 1, 2$ are constants to be determined. For simplicity in solving the inhomogeneity-matrix problem, we have replaced $\gamma + \varsigma$ by γ for each phase, since only $\gamma + \varsigma$ appears in the in-plane parameters but not $\gamma - \varsigma$. The compatibility equations written in terms of the potential functions ϕ_i and ψ_i, yield the following coupled system of equations,

$$
\begin{aligned}
c_i^2 \frac{\partial}{\partial r}(\Delta - 1)\psi_i &= 2b_i^2(1-\nu_i)\frac{1}{r}\frac{\partial}{\partial \theta}\Delta\phi_i, \\
c_i^2 \frac{1}{r}\frac{\partial}{\partial \theta}(\Delta - 1)\psi_i &= -2b_i^2(1-\nu_i)\frac{\partial}{\partial r}\Delta\phi_i,
\end{aligned} \tag{4.20}
$$

where Δ is the two-dimensional Laplacian and c_i, b_i are the characteristic lengths of a micropolar material defined by,

$$c_i^2 = \frac{\gamma_i(\mu_i + \alpha_i)}{4\mu_i\alpha_i}, \quad b_i^2 = \frac{\gamma_i}{4\mu_i}. \tag{4.21}$$

We solve the system of equations (4.20), to obtain the two uncoupled equations,

$$\Delta\Delta\phi_i = 0, \quad \Delta\left(1 - c_i^2\Delta\right)\psi_i = 0. \tag{4.22}$$

Using the methods of separation of variables and the form of the boundaries [105], general solutions of the equations (4.22) are given in the two material phases through as,

$$\begin{aligned} \phi_i &= A_i \ln r + B_i r^2 + (C_i + D_i r^2 + E_i r^{-2} + F_i r^4)\cos 2\theta, \\ \psi_i &= \left(G_i r^{-2} + H_i r^2 + L_i\ K_2(\frac{r}{c_i}) + J_i\ I_2(\frac{r}{c_i})\right)\sin 2\theta, \quad i = 1, 2, \end{aligned} \tag{4.23}$$

where I_2 and K_2 are the modified Bessel functions of the first and second kind, respectively and $A_i, D_i, E_i, G_i, H_i, L_i$ and J_i are additional constants to be determined. The boundary conditions on the interface include continuity of displacement and rotation in addition to the stress jump arising from the model of the interface. Substituting the arc parameter of the circle $s = R\theta$, and the curvature $b_0 = -R$ in (2.49)-(2.51), and using the simplifying assumption that the micropolar shear parameter of the surface is negligible ($G_s = 0$), we may write the boundary conditions at the perfectly bonded interface as,

$$\begin{aligned} &\frac{A^s}{R^2}\left(\frac{d^2u_s}{d\theta^2} + \frac{du_n}{d\theta}\right) + \frac{B^s}{R^4}\left(-\frac{d^3u_n}{d\theta^3} + \frac{d^2u_s}{d\theta^2}\right) \\ &\quad + \frac{H_s}{R^3}\left(\frac{d^2\varphi_3}{d\theta^2}\right) + \sigma_{r\theta}^{(2)} - \sigma_{r\theta}^{(1)} = 0, \end{aligned} \tag{4.24}$$

$$\begin{aligned} &\frac{A^s}{R^2}\left(\frac{du_s}{d\theta} + u_n\right) - \frac{B^s}{R^4}\left(-\frac{d^4u_n}{d\theta^4} + \frac{d^3u_s}{d\theta^3}\right) \\ &\quad - \frac{H_s}{R^3}\left(\frac{d^3\varphi_3}{d\theta^3}\right) + \sigma_{rr}^{(1)} - \sigma_{rr}^{(2)} = 0, \end{aligned} \tag{4.25}$$

$$\frac{H^s}{R^2}\left(\frac{d^2\varphi_3}{d\theta^2}\right)+\mu_{r3}^{(2)}-\mu_{r3}^{(1)}=0. \tag{4.26}$$

$$u_r^{(1)}(R,\theta)=u_r^{(2)}(R,\theta)=u_n, \tag{4.27}$$

$$u_\theta^{(1)}(R,\theta)=u_\theta^{(2)}(R,\theta)=u_s, \tag{4.28}$$

$$\varphi_3^{(1)}(R,\theta)=\varphi_3^{(2)}(R,\theta)=\varphi_3. \tag{4.29}$$

We note that the first two interface conditions are equivalent to the Steigmann-Ogden interface conditions given in [158] for plane classical elasticity except that in the Steigmann-Ogden model the shear traction couple terms do not appear. Additionally, the remote boundary conditions lead to,

$$\sigma_{rr}^{(2)}(r\to\infty)=\frac{1}{2}(p_2+p_1)+\frac{1}{2}(p_1-p_2)\cos 2\theta, \tag{4.30}$$

$$\sigma_{r\theta}^{(2)}(r\to\infty)=\frac{1}{2}(p_2-p_1)\sin 2\theta, \tag{4.31}$$

$$\mu_{r3}^{(2)}(r\to\infty)=0. \tag{4.32}$$

Again, the compatibility equations (4.20) imply that,

$$G_i=8b_i^2(1-\nu_i)C_i, \tag{4.33}$$

$$H_i=24b_i^2(1-\nu_i)F_i. \tag{4.34}$$

The remote loadings conditions and the boundedness of the stress and couple stress at the center of the inhomogeneity, allow us to calculate the following coefficients:

$$\begin{aligned}
A_1 &= 0,\ C_1=0,\ L_1=0,\ G_1=0,\ E_1=0,\\
J_2 &= 0,\ F_2=0,\ H_2=0,\\
B_2 &= \frac{1}{4}(p_1+p_2),\\
D_2 &= \frac{1}{4}(p_2-p_1).
\end{aligned} \tag{4.35}$$

The remaining ten coefficients are determined using three equations of the interface (Eqs. 4.24-4.26), a condition arising from linear independence of the set $\{1,\cos 2\theta\}$, three equations

describing continuity of the displacement and rotation (Eqs. (4.27-4.29)) and two compatibility relations Eqs. (4.33) and (4.34). The total number of ten available equations make up a linear system of equations with ten unknowns to be determined.

4.3 Effective bulk and shear moduli of plane micropolar nano-composite wth circular nano-inhomogeneities

We apply the analytical solution derived above for the circular inhomogeneity under the remote traction conditions to calculate the effective bulk and shear moduli. The analytical solution was obtained for the most general case in which all of the phases (the inhomogeneity, the medium and the interface) are comprised of micropolar materials. In order to compare our results with the work by Chen et al. [15], we reduce our analytical solution to the same case considered in [15] in which the inhomogeneity is a circular fibre composed of a classical elastic material while the medium and the interface each have micropolar properties. We mention again that Chen et al. [15] assume that this case corresponds to zero microrotations on the interface. We prefer to characterize the influence of a classical elastic fibre on a micropolar matrix using a couple-stress jump condition (so that independent microrotations are aligned with the classical displacement-dependent rotations defined by the anti-symmetric part of the displacement gradient rather than set to zero). However, given that, to the author's knowledge, [15] is the most appropriate paper in the literature to allow an effective comparison with our results, we calculate the effective moduli in two separate cases. In the first case (**Case 1**), we use the same assumption made in [15] and impose zero microrotations on the interface. We then compare the additional contribution of interface flexural resistance from our model to the results in [15]. In the second case (**Case 2**), we do not impose restrictions on the microrotations on the interface but instead introduce the couple stress jump condition (see Eq. (4.26)) at the interface which is based on the requirement that couple stresses are zero in the (classical elastic) fibre but non-zero in the micropolar matrix.

4.3.1 Effective bulk modulus

In order to conveniently estimate the effective bulk modulus of the composite, we impose remote hydrostatic boundary traction, $p_1 = p_2 = p$, on the infinite medium containing a single circular inhomogeneity. In fact, we look for the stress disturbance induced by adding a single circular inhomogeneity to the composite. Consequently, the average stress over the medium can be approximated by the stress induced in an infinite homogeneous medium:

$$\begin{aligned} \langle \sigma_{11}^{sym} \rangle_2 &= p,\ \langle \sigma_{22}^{sym} \rangle_2 = p, \\ \langle \sigma_{12}^{sym} \rangle_2 &= \langle \sigma_{21}^{sym} \rangle_2 = 0. \end{aligned} \tag{4.36}$$

Clearly, since the remote tractions contribute no microrotation, the couple stresses do not play a role under these particular boundary conditions. The average normal stresses inside the inhomogeneity and the medium are related by,

$$\begin{aligned} \langle \sigma_{11}^{sym} \rangle_1 + \langle \sigma_{22}^{sym} \rangle_1 &= J_b(\langle \sigma_{11}^{sym} \rangle_2 + \langle \sigma_{22}^{sym} \rangle_2), \\ &\Rightarrow \quad 4B_1 = 2pJ_b \Rightarrow J_b = \frac{2B_1}{p}. \end{aligned} \tag{4.37}$$

Also, the average stress jump across the interface follows the relation,

$$\begin{aligned} \langle [\sigma_{11}]^{sym} \rangle_\Gamma + \langle [\sigma_{22}]^{sym} \rangle_\Gamma &= M_b(\langle \sigma_{11}^{sym} \rangle_2 + \langle \sigma_{22}^{sym} \rangle_2), \\ &\Rightarrow \quad -4B_1 + 2p + \frac{2A_2}{R^2} = 2pM_b. \end{aligned} \tag{4.38}$$

Note that given the dependence of the coefficients $A_i, B_i, ..$etc, on p**,** J_b and M_b are independent of p as expected**.** The bulk modulus of the two material phases in plane elasticity are defined by $k_i = \mu_i + \lambda_i$, $(i = 1, 2)$, μ_i and λ_i being the classical Lamé coefficients. Using the relations for the stress concentration coefficients (4.37-4.38) into the equation (4.14) and inverting the compliance tensor, the effective bulk modulus, $\overline{k}$ becomes,

$$\frac{\overline{k}}{k_2} = \frac{(1-f) + f(M_b + J_b)}{(1-f) + f\left(\frac{k_2}{k_1}\right) J_b}. \tag{4.39}$$

We employ the coefficients B_1 and A_2 determined from the analytical solution to find J_b and M_b and conclude that,

$$\frac{\overline{k}}{k_2} = \frac{\frac{A^s}{2R}(1 + f\frac{\mu_2}{k_2}) + (1-f)\mu_2 + k_2(1 + f\frac{\mu_2}{k_2})}{(\frac{A^s}{2R} + k_1)(1-f) + \mu_2 + fk_2}, \tag{4.40}$$

for both cases mentioned above. The result coincides with that obtained in [15] since the flexural resistance of the interface does not affect the effective bulk modulus. Also, it is not surprising that in either case we obtain the same results since under the hydrostatic remote traction condition, no point (element) microrotation occurs in the composite. Further, since the points at the interface undergo no microrotation, the bending resistance effects vanish from the solution. Consequently, the use of micropolar elasticity as opposed to classical elasticity seems to make no difference and we obtain the same effective bulk modulus (4.40) as that obtained from the classical model with only surface stretching resistance [37].

4.3.2 Effective shear modulus

For calculations of the effective shear modulus of the composite we impose a pure shear boundary traction $p_1 = -p_2 = p$, on the infinite medium containing a single circular inhomogeneity. As in the calculation of the bulk modulus, since a single inhomogeneity causes very little disturbance in the average stress over the medium, the average stress can be approximated by the stress induced in an infinite homogeneous medium:

$$\begin{aligned} \langle \sigma_{11}^{sym} \rangle_2 &= p,\ \langle \sigma_{22}^{sym} \rangle_2 = -p, \\ \langle \sigma_{12}^{sym} \rangle_2 &= \langle \sigma_{21}^{sym} \rangle_2 = 0. \end{aligned} \tag{4.41}$$

Therefore, the stress concentration tensor component, J_s, relates the average pure shear stress in the medium to the average pure shear stress in the inhomogeneity by,

$$\begin{aligned} \frac{1}{2}(\langle \sigma_{11}^{sym} \rangle_1 - \langle \sigma_{22}^{sym} \rangle_1) = \frac{J_s}{2}(\langle \sigma_{11}^{sym} \rangle_2 - \langle \sigma_{22}^{sym} \rangle_2) = pJ_s, \\ \Rightarrow J_s = (-2D_1 - 3R^2F_1)/p. \end{aligned} \tag{4.42}$$

Similarly, the average pure shear stress jump over the interface satisfies,

$$\frac{1}{2}(\langle\sigma_{11}^{sym}\rangle_{\Gamma} - \langle\sigma_{22}^{sym}\rangle_{\Gamma}) = \frac{M_s}{2}(\langle\sigma_{11}^{sym}\rangle_{2} - \langle\sigma_{22}^{sym}\rangle_{2}) = pM_s,$$

$$\Rightarrow M_s = 1 + \left(2D_1 + 3R^2F_1 - \frac{C_2}{R^2} + \frac{L_2}{2c_2R}K_1\left(\frac{R}{c_2}\right)\right)/p. \tag{4.43}$$

Note that given the dependence of the coefficients $A_i, B_i, ..$etc, on p, J_s and M_s are independent of p, as expected. As mentioned above, we consider two cases enabling us to make a direct comparison with results in the existing literature.

Case 1: Following the assumption made in [15], we adopt the condition of zero micro-rotation at the interface. Thus, using the Mori-Tanaka's effective compliance tensor (4.14) we obtain,

$$\frac{\overline{\mu}}{\mu_2} = \frac{(1-f) + f(M_s + J_s)}{(1-f) + f\left(\frac{\mu_2}{\mu_1}\right)J_s} \tag{4.44}$$

We may calculate the concentration tensor components M_s and J_s using the analytical solution found above under the assumption of applied pure shear remote traction. Consequently,

$$\frac{\overline{\mu}}{\mu_2} = \frac{W_1K_1(\frac{R}{c_2}) + W_2c_2RK_2(\frac{R}{c_2})}{W_1K_1(\frac{R}{c_2}) + W_3c_2RK_2(\frac{R}{c_2})} \tag{4.45}$$

where K_1 and K_2 are again the modified Bessel functions of the second kind and,

$$\begin{aligned} W_1 \;=\; & 4b_2^2(1-f)(1-\nu_2)\left\{4R^4(\mu_1-\mu_2)(\mu_1-\mu_2d_1)\right. \\ & -2R^3h(\mu_1^2-\mu_2^2d_1-8\mu_1\mu_2(1-\nu_1)) \\ & -(8B_sR+2A_sR^3)(\mu_1l_1-\mu_2d_1)-12B_sA_sd_1 \\ & \left.-3hA_sR^2(\mu_1g_1+\mu_2d_1)\right\}, \end{aligned} \tag{4.46}$$

$$\begin{aligned} W_2 \;=\; & 12B_sA_sd_1(f-d_2)+3hA_sR^2\left[\mu_1g_1(f-d_2)+\mu_2d_1(f-g_2)\right] \\ & +(2A_sR^3+8B_sR)\left[\mu_1l_1(f-d_2)-\mu_2d_1(f-2+g_2)\right] \\ & -4R^4(\mu_1-\mu_2d_1)\left[(1-f)\mu_2+\mu_1(f-d_2)\right] \\ & +2hR^3\left[(1-f)d_1\mu_2^2+\mu_1^2(f-d_2)\right. \\ & \left.+8\mu_1\mu_2((d_2-f)(1-\nu_1)+(1-\nu_2))\right], \end{aligned} \tag{4.47}$$

$$
\begin{aligned}
W_3 &= 12B_sA_sd_1d_2(f-1)+3hA_sR^2\left[\mu_1g_1d_2(f-1)+\mu_2d_1(fd_2-g_2)\right] \\
&\quad +(2A_sR^3+8B_sR)\left[\mu_1l_1d_2(f-1)-\mu_2d_1(fd_2-2+g_2)\right] \\
&\quad -4R^4(\mu_1-\mu_2d_1)\left[(1-fd_2)\mu_2+\mu_1(f-1)d_2\right] \\
&\quad -2hR^3\left[(1-f)d_2\mu_1^2+\mu_2^2d_1(fd_2-1)\right. \\
&\quad \left.-8\mu_1\mu_2((1-f)(1-\nu_1)d_2+(1-\nu_2))\right], \qquad (4.48)
\end{aligned}
$$

where,

$$
\begin{aligned}
d_i &= -3+4\nu_i,\ g_i=-1+2\nu_i, \\
l_i &= -5+6\nu_i,\ s_i=-7+8\nu_i, \\
q_i &= -11+12\nu_i,\ i=1,2. \qquad (4.49)
\end{aligned}
$$

By eliminating the flexural resistance of the interface i.e. by assuming $B_s = 0$ and $h = 0$, we recover exactly the result given in [15].

Case 2: In this case, we do not use the assumption of zero microrotation at the interface made in [15] but instead apply the condition expressing the jump in couple stresses across the fibre-matrix interface (Eq. 4.26) (vanishing couple stresses on the classical fibre side versus nonzero couple stresses on the micropolar matrix side) (It is worth noting the difference in results which follow from the subsequent use of the interface condition from Case 1 versus what we believe to be a more precise representation of the interface condition in Case 2.). Applying this boundary condition, we can calculate the concentration tensor components M_s and J_s. Again, using the Mori-Tanaka formula (Eq. 4.14) we obtain the effective shear modulus $\overline{\mu}$ for the Case 2 boundary conditions.

We note here another check of our results: if we allow the stretching, bending and twisting stiffness of the interface, A_s, B_s, and H_s, respectively, tend towards zero, our result recovers exactly that for a micropolar composite without surface effects found in [150]. Specifically,

$$
\frac{\overline{\mu}}{\mu_2} = \frac{Y((1-f)\mu_2+(f-d_2)\mu_1)-X}{Y((1-fd_2)\mu_2-(1-f)d_2\mu_1)-X}, \qquad (4.50)
$$

where,

$$\begin{aligned} Y &= R^2 K_1\left(\frac{R}{c_2}\right) + 2c_2 R K_2\left(\frac{R}{c_2}\right), \\ X &= 8b_2^2(1-f)(\mu_1-\mu_2)(1-\nu_2)K_1\left(\frac{R}{c_2}\right). \end{aligned} \tag{4.51}$$

Also, if we let $R \to \infty$, the size-independent effective shear modulus is given by,

$$\frac{\overline{\mu}}{\mu_2} = \frac{(1-f)\mu_2 + (f-d_2)\mu_1}{(1-fd_2)\mu_2 - (1-f)d_2\mu_1}, \tag{4.52}$$

which again can be verified using the results in Xun et al. [150].

In the following section, we illustrate the size-dependence of the effective shear modulus through some numerical examples.

4.4 Numerical Evaluation

For the numerical evaluation of the foregoing analytical results corresponding to the effective shear modulus of a micropolar nano-composite, we adopt the same material properties used in the paper by Chen et al. [15]. Consequently, we consider a plane aluminum metal containing 20% circular voids ($f = 0.2$). The material constants for such a composite are $\mu_2 = 34.7$GPa, $\mu_1 = 0$, $\nu_2 = 0.3$, $\nu_1 = 0$, $\alpha_2 = 34.7$ GPa and $\alpha_1 = 0$ (refer to the equation (4.21)). The twisting modulus of the medium γ_2 can vary with the first characteristic length c_2 according to,

$$\gamma_2 = \frac{4\mu_2\alpha_2 c_2^2}{\mu_2 + \alpha_2},$$

and consequently the second characteristic length b_2 is determined by,

$$b_2^2 = \frac{\alpha_2 c_2^2}{\mu_2 + \alpha_2},$$

which from the assumed numerical values, $b_2^2 = 0.5c_2^2$. In the paper [15], two types of material properties of the surface are taken from the paper by Sharma et al. [129]. We derive the interface elastic rigidities from the same material properties as given in [129] and [15]. However, we require additional data corresponding to the newly incorporated

parameters of the surface. Consequently, for Case 1 surface conditions (see above), we require the corresponding flexural rigidity of the surface B_s. For Case 2, both bending B_s and twisting H_s rigidities of the surface are required. Accordingly, we choose the following constants for the surface with flexural resistance: $A_s = 6.09\text{N/m}$, $B_s = 5 \times 10^{-18}\text{N.m}$, $H_s = 5 \times 10^{-18}\text{N.m}$ and define an intrinsic length for the surface by, $c_s = A_s/\mu_2 = 0.18\text{nm}$. The values for the bending and twisting rigidities of the surface are chosen based on the order of magnitude expected for this choice of parameters [153, 101]. We acknowledge the fact that our numerical results are limited by the difficulty in obtaining accurate experimental data for the additional bending and twisting rigidities as well as the effective thickness arising in our new curvature-dependent surface model: most of the ongoing experiments in this area are focused on the conventional surface parameters of the classical Gurtin-Murdoch model [77, 120, 95]. For this reason, we have simply chosen suitable numerical values for these parameters for the purpose of comparison with existing results. We follow the procedure in [15]: for the micropolar medium we assign the characteristic length $c_2 = \delta c_s$ and we vary the parameter δ to adjust the micropolar properties of the medium. Consequently, higher values of δ correspond to a higher micropolarity of the medium.

Figures 4.2 and 4.3 illustrate the effects of bending and twisting rigidities of the surface for Case 1 boundary conditions. It is clear that since the microrotations have been set to zero on the interface, the twisting modulus of the surface makes no contribution to the solution. The effect of flexural resistance of the surface dominates when the radius of the voids is in the lower range. For example, when $R < 3.5\text{nm}$, the flexural resistance of the surface plays a significant role in the calculation of the effective shear modulus.

Figures 4.2 and 4.3 demonstrate the effects of bending and twisting rigidities of the surface for Case 2 boundary conditions. Although small, there is an observable difference between the resulting curves for Case 1 and Case 2, which demonstrates the significance of using what we believe to be the more precise boundary condition of a jump in couple stress at the fibre-matrix interface. Again we demonstrate that in the range of sufficiently small void radius, mainly the micropolar twisting resistance of the surface controls the effective

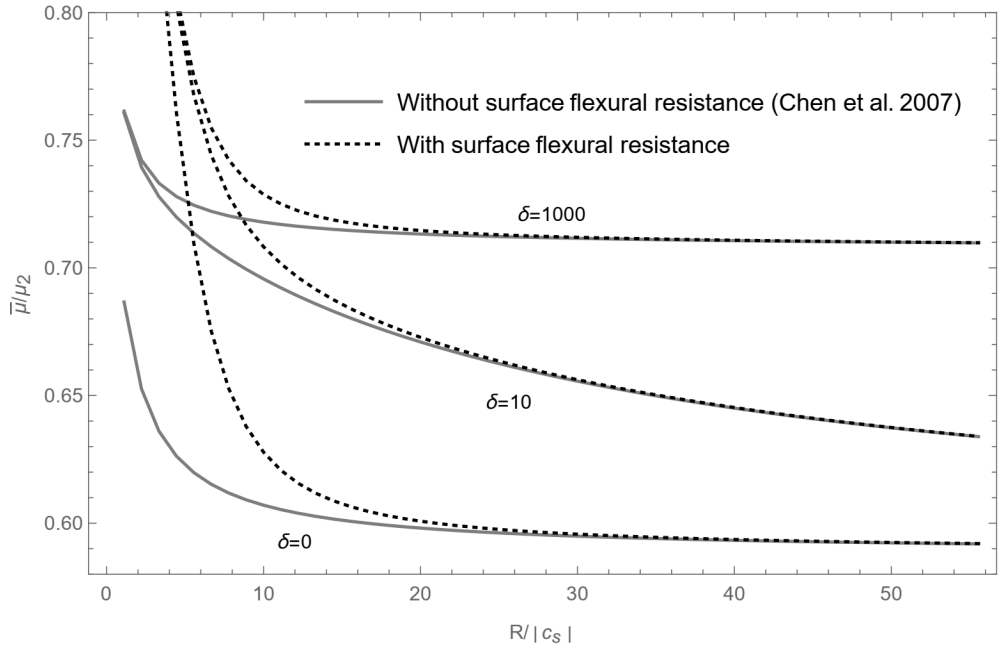

Figure 4.2: Variation of the effective shear modulus ratio with radius of the void for different degrees of micropolarity ($\delta = c_2/c_s$) using Case 1 boundary condition

shear modulus of the composite. By removing the effect of flexural resistance of the surface ($B_s = 0$), we observe that the twisting rigidity of the micropolar surface, H_s, influences the solution slightly in a certain range of micropolar characteristic length. In fact, a remarkable result of this study is that when the characteristic length of the micropolar matrix is of the order of the characteristic length of the surface c_s ($\delta \sim 1$) the effect of micropolar twisting rigidity becomes significant. When the characteristic length of the micropolar matrix is far from the order of magnitude of the characteristic length of the surface c_s, the classical and the micropolar surface models without flexural rigidity (membrane type surfaces) yield similar predictions for the effective shear modulus. Therefore, depending on the value of the twisting rigidity, in the certain micropolarity range (span of characteristic length values) of $\delta \sim 1$ a more significant effect is observed as a result of surface twisting rigidity. This influence is also magnified for very small void radius ($R \sim 1$nm). From the figures, we deduce that considering both micropolarity and flexural rigidity of the void's surfaces increase our

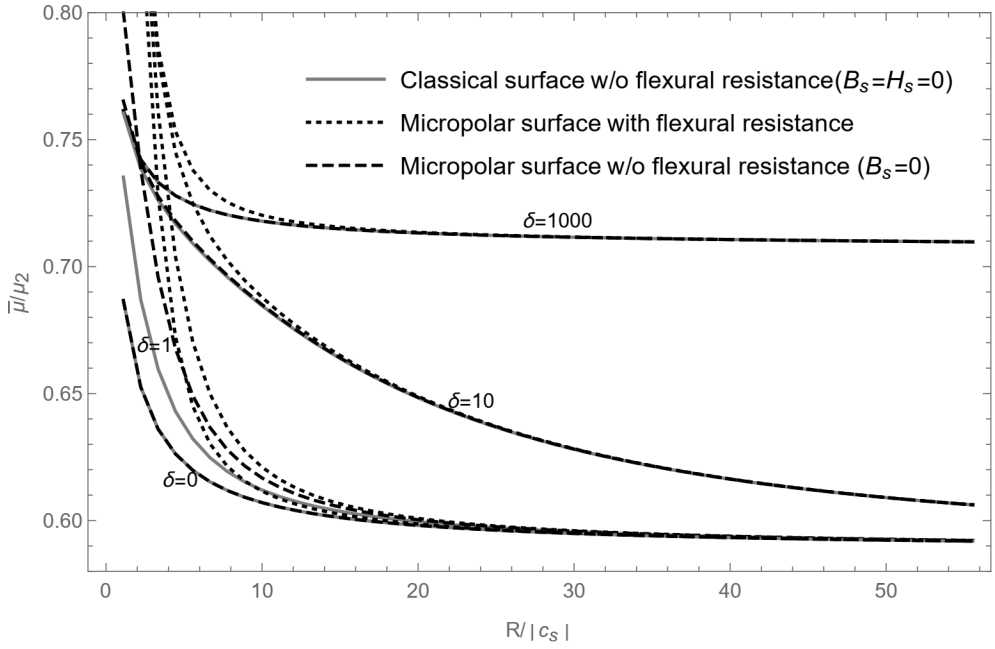

Figure 4.3: Variation of the effective shear modulus ratio with radius of the void for different degrees of micropolarity ($\delta = c_2/c_s$) using Case 2 boundary condition

prediction of the effective shear modulus of the composite. Below that range of void radius the effective shear modulus follows the pattern obtained in the absence of bending rigidity and decreases significantly.

In this chapter, we successfully examined our proposed surface model to the problem of calculating the effective properties of nano-composite materials. The proposed micropolar surface/interface specifically demonstrated the advantage of capturing the concurrent contribution of surface flexural and micropolar twisting resistance. A comparison with a similar research validated our results. In addition, the model enabled us to demonstrate that when the characteristic length of the micropolar material is of the order of the characteristic length of the surface, the micropolar twisting modulus becomes important. In the next chapter we apply our model to a crystal dislocation problem, which is yet another interesting classical problem that appears as a benchmark in the mechanics of small-scale materials.

Chapter 5

Plane Problem of an Edge Dislocation in the Presence of Micropolar Surface Effects

We continue our examination of the model by analyzing the fundamental problem of a micropolar half-plane containing a single edge dislocation. Dislocations play a crucial role in the behavior of crystalline materials and metals, more specifically, they are responsible for the plastic deformation of metals. Dislocations are defects in the perfect arrangement of crystal atoms caused by an abrupt displacement in the arrangement of atoms slipped against each other [117]. In fact, dislocations are defined as the boundary between a slipped plane of particles and the un-slipped ones in a crystal lattice. Study of dislocations, as nano-scale defects, is important in engineering applications and nano-material sciences, since the overall mechanical properties of materials, such as strength and plastic deformation, are highly sensitive to the density of dislocations, their creation, and their motion [70].

The theory of elasticity models dislocations as a discontinuity in the displacement field. The slip of atoms against each other on a plane is described mathematically using a dislocation vector, namely, Burger's vector $\boldsymbol{b}$ or slip vector which determines the strength (magnitude) and the direction of the slippage. Depending on the orientation of discontinuity or slip there are two main types of dislocations. For a "screw dislocation" the dislocation (the boundary of slipped and un-slipped particles) is parallel to the slip vector. An "edge dislo-

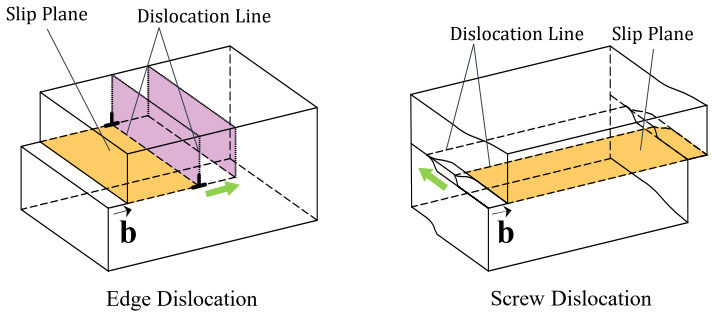

Figure 5.1: Screw and edge dislocations

cation", on the other hand, is formed when the slip vector is perpendicular to the dislocation (see Figure 5.1).

Dislocations disturb the stress fields near the free surface of a crystalline material and increase the potential energy generated from the effects of strain energy. This potential energy is released when the dislocation glides on the slip plane towards the surface and escapes from the surface. This mechanism, as well as the interaction of dislocations with each other, explains many behavioral properties of the plastic deformations of a material [33, 100]. Consequently, the study of interaction between dislocations and surfaces is of high importance and has been the subject of many researches (see for example [51, 148, 28]). The necessity for including size dependence in the analysis of dislocations as a nano-scale phenomenon has triggered intensive research in this area. For example, Lazar et al. [92] employed higher order non-local elasticity theory to eliminate singularities at screw and edge dislocations. Baxevanakis et al. [7] evaluated the interaction of a dislocation with a finite crack in the framework of couple-stress elasticity, and Gharahi et al. [55] investigated the interaction of dislocations near the interfaces and surfaces of couple stress composite materials. Such studies are ongoing using the incorporation of the effects of surfaces and interfaces and applying higher order elasticity and plasticity theories.

In this chapter, we adopt our proposed micropolar surface model to analyze the fundamental problem of the deformation of a micropolar half-space induced by a single edge

dislocation. First, we restate the system of partial differential equations (PDEs) arising from the micropolar elasticity theory and demonstrate the application of Helmholtz decomposition to decoupling the equations into two fourth order standard PDEs. Next, we use Fourier integral transforms to find the analytical solution of the standard PDEs. We validate our results by reducing the problem to the special case of an edge dislocation interacting with a planar surface of the Gurtin-Murdoch (G-M) type and retrieving the results of Intarit et.al [73]. The provided numerical examples illustrate contributions from the enhanced model of deformation which includes the micropolar effects of both bulk and the surface as well as the classical bending resistance of the surface.

5.1 Preliminaries

The theory of dislocations in the micropolar setting is presented in a paper by Nowacki [111] and more recently summarized in [91]. However, a more comprehensive account of the theory is presented in the book "Theory of Asymmetric Elasticity", by Nowacki [112]. Here, we briefly review the theory of dislocations in a micropolar medium and introduce a plan for solving the plane strain problem of an edge dislocation.

5.1.1 Theory of Dislocations: edge dislocation

The classical dislocation is identified by a discontinuity of the displacement field on a given surface S in a micropolar space. This reads mathematically as,

$$[\mathbf{u}(\mathbf{x})] = \mathbf{u}^{+}(\mathbf{x}) - \mathbf{u}^{-}(\mathbf{x}) = \mathbf{b}, \text{ for } \mathbf{x} \longrightarrow \mathbf{x}_0 \in S, \tag{5.1}$$

where, $\boldsymbol{b}$ is the Burger's vector and the superscripts "+" and "−" indicate the sides from which $\mathbf{x}$ approaches S. The microrotation field is continuous and smooth everywhere in the micropolar medium and the displacement field is continuous everywhere except on S. Another main assumption is that the partial derivatives of displacement and microrotation fields are continuous everywhere in the medium including S. Finally, in the absence of body

forces, the homogeneous equilibrium equations of micropolar elasticity (2.15) are satisfied.

5.1.2 Helmholtz Theorem in Plane Micropolar Elasticity

Consider a Cartesian system of coordinates denoted by $\{x_i\}_{i=1}^3$ and formalize plane micropolar elasticity such that the x_1 and x_2 axes lie on the corresponding plane of deformation. As was mentioned in Chapter 2, in plane deformations, the displacement and microrotation vectors take the forms, $\mathbf{u} = (u_1(x_1, x_2), u_2(x_1, x_2), 0)$ and $\boldsymbol{\varphi} = (0, 0, \varphi_3(x_1, x_2))$, respectively, so that the only nonvanishing degrees of freedom, $\{u_1, u_2, \varphi_3\}$, are independent of the out-of-plane axis, x_3. This scenario is referred to as the *first* plane problem in the theory of micropolar elasticity [112]. In this case, in the absence of body forces and body moments, the equilibrium equations (2.7) reduce to,

$$\sigma_{\alpha\beta,\alpha} = 0, \tag{5.2}$$

$$\mu_{\alpha 3,\alpha} + \varepsilon_{3\alpha\beta}\sigma_{\alpha\beta} = 0, \tag{5.3}$$

where the Greek indices take the values $\{1, 2\}$ and, as before, the ongoing convention is summation over repeated indices. The symbols $\varepsilon_{3\alpha\beta}$ are the Cartesian components of the permutation tensor. The microstrain tensor $\epsilon_{\alpha\beta}^{(mi)}$, and the microrotation tensor $\varkappa_{3\alpha}$ are associated with a given displacement and rotation field in plane micropolar elasticity via the relations (2.11), which here become,

$$\epsilon_{\alpha\beta}^{(mi)} = u_{\beta,\alpha} - \varepsilon_{3\alpha\beta}\varphi_3 \tag{5.4}$$

$$\varkappa_{\alpha 3} = \varphi_{3,\alpha}. \tag{5.5}$$

The constitutive relations for a linear homogeneous isotropic micropolar material subjected to plane deformations given by (2.14) are reduced to

$$\sigma_{\alpha\beta} = (\mu + \alpha)\epsilon_{\alpha\beta}^{(mi)} + (\mu - \alpha)\epsilon_{\beta\alpha}^{(mi)} + \lambda\epsilon_{\gamma\gamma}^{(mi)}\delta_{\alpha\beta}, \tag{5.6}$$

$$\sigma_{33} = \lambda\epsilon_{\gamma\gamma}^{(mi)} \tag{5.7}$$

$$\mu_{\alpha 3} = (\gamma + \varsigma)\varphi_{3,\alpha}, \tag{5.8}$$

$$\mu_{3\alpha} = (\gamma - \varsigma)\varphi_{3,\alpha}. \tag{5.9}$$

The parameters μ and λ are the usual Lamé constants from classical elasticity while α, γ and ς are the additional elastic constants introduced in micropolar elasticity. We rewrite the microstrain components in terms of displacement and rotation using (5.4-5.5) and insert the result into the constitutive equations (5.6-5.9). Finally, using the resulting expressions for the stress components in the equilibrium equations (5.2-5.3), we obtain,

$$(\mu+\alpha)\Delta u_1 + (\mu-\alpha+\lambda)\frac{\partial^2 u_1}{\partial x_1^2} + (\mu-\alpha+\lambda)\frac{\partial^2 u_2}{\partial x_1 \partial x_2} + 2\alpha\frac{\partial \varphi_3}{\partial x_2} = 0, \tag{5.10}$$

$$(\mu-\alpha+\lambda)\frac{\partial^2 u_1}{\partial x_1 \partial x_2} + (\mu+\alpha)\Delta u_2 + (\mu-\alpha+\lambda)\frac{\partial^2 u_2}{\partial x_2^2} - 2\alpha\frac{\partial \varphi_3}{\partial x_1} = 0, \tag{5.11}$$

$$-2\alpha\frac{\partial u_1}{\partial x_2} + 2\alpha\frac{\partial u_2}{\partial x_1} + (\gamma+\varsigma)\Delta\varphi_3 - 4\alpha\varphi_3 = 0, \tag{5.12}$$

which are the expanded form of the system of partial differential equations introduced in Chapter 2, Equation (2.17). The set of equations (5.10-5.12) is a system of three coupled partial differential equations in the three kinematic components (two displacements and one rotation), required to be decoupled. We decouple the system (5.10-5.12) by decomposing the displacement field into potential (gradient) and solenoidal (curl) parts based on the Helmholtz theorem. The theorem states that any sufficiently smooth vector field can be represented as the sum of the gradient of a scalar potential and the curl of a vector potential. The gradient term in the field is curl-free (has zero curl) and the curl term has zero divergence. Accordingly, we decompose the displacement field into,

$$\mathbf{u} = \nabla\times\mathbf{\Psi} + \nabla\Phi, \tag{5.13}$$

where $\mathbf{\Psi}(x_1, x_2)$ and $\Phi(x_1, x_2)$ are, respectively, vector and scalar functions to be determined. The displacement components in plane micropolar deformation therefore become

$$u_1 = \Phi_{,1} + \Psi_{3,2}, \tag{5.14}$$

$$u_2 = \Phi_{,2} + \Psi_{3,1}. \tag{5.15}$$

We may write the stress and couple stress components in terms of the functions Φ and Ψ_3:

$$\begin{aligned}
\sigma_{11} &= (2\mu+\lambda)\Delta\Phi + 2\mu\left(\Psi_{3,12} - \Phi_{,22}\right), \\
\sigma_{22} &= (2\mu+\lambda)\Delta\Phi - 2\mu\left(\Psi_{3,12} + \Phi_{,11}\right), \\
\sigma_{12} &= \mu\left(2\Phi_{,12} + \Psi_{3,22} - \Psi_{3,11}\right) - \alpha\Delta\Psi_3 - 2\alpha\varphi_3, \\
\sigma_{21} &= \mu\left(2\Phi_{,12} + \Psi_{3,22} - \Psi_{3,11}\right) + \alpha\Delta\Psi_3 + 2\alpha\varphi_3, \\
\mu_{13} &= (\gamma+\varsigma)\varphi_{3,1},\ \mu_{23} = (\gamma+\varsigma)\varphi_{3,2}, \\
\mu_{31} &= (\gamma-\varsigma)\varphi_{3,1},\ \mu_{32} = (\gamma-\varsigma)\varphi_{3,2}.
\end{aligned} \tag{5.16}$$

Using equations (5.16) into (5.2-5.3) we arrive at,

$$(\Delta\Phi)_{,1} + \frac{2\mu}{2\mu+\lambda}\left(c^2\Delta - 1\right)\varphi_{3,2} = 0, \tag{5.17}$$

$$(\Delta\Phi)_{,2} - \frac{2\mu}{2\mu+\lambda}\left(c^2\Delta - 1\right)\varphi_{3,1} = 0, \tag{5.18}$$

$$(d^2\Delta - 2)\varphi_3 - \Delta\Psi_3 = 0, \tag{5.19}$$

where,

$$d^2 = \frac{(\gamma+\varsigma)}{2\alpha},\ c^2 = \frac{(\gamma+\varsigma)(\mu+\alpha)}{4\mu\alpha}. \tag{5.20}$$

The constants d and c (of dimension "length") are known as the characteristic lengths of the micropolar material. The characteristic lengths are widely recognized to be associated with the length scale of the micro-constituents and identify the micropolar properties of the solid material. We combine derivatives of the two equations (5.17) and (5.18) to obtain,

$$\Delta\Delta\Phi = 0, \tag{5.21}$$

$$\Delta\left(c^2\Delta - 1\right)\varphi_3 = 0. \tag{5.22}$$

Each of these equations contains four integration constants to be determined from the boundary conditions and two relations in the form of Cauchy-Riemann equations. In order to obtain the complete solution of the problem, we solve the equations (5.21) and (5.22) for Φ and φ_3 and carry the resulting φ_3 into the equation (5.19) to find the particular solution, Ψ_3, of the inhomogeneous equation.

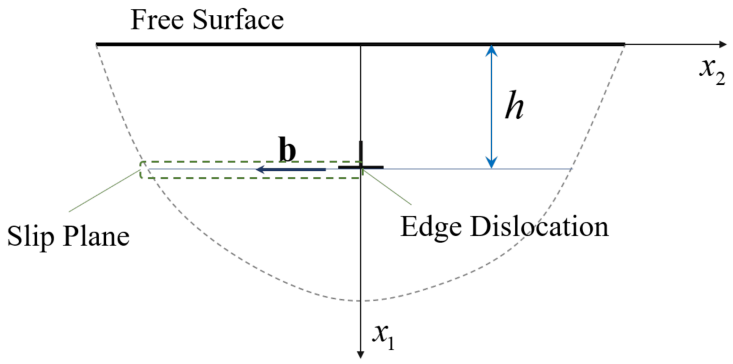

Figure 5.2: Edge dislocation in a depth h of a half-plane with slip plane parallel to the surface

5.2 An Edge Dislocation in a Half-plane Medium with Surface Effects

Consider an elastic micropolar half-plane with an edge dislocation located at a depth h below the surface. As shown in Figure 5.2 the dislocation is oriented such that the slip-plane is parallel to the free surface. To formulate the edge dislocation, we divide the half-plane into two regions; region (1) defined as the strip described by $0 \leq x_1 \leq h$ and region (2), the half-plane where, $h < x_1$. We associate the parameters' correspondence to each region by a superscript $i = 1, 2$ as $(..)^{(i)}$. The free surface of the original half-plane has the surface elastic properties described in the previous section. Consequently, the surface is endowed with classical bending and stretching rigidities as well as two micropolar twisting moduli. The free surface is planar, therefore the radius of curvature $R(s)$ tends to infinity and the curvature tensor component denoted by $b_0 = -1/R(s)$ in (2.49-2.51), approaches zero. The straight edge dislocation under consideration is shown in Figure 5.2.

With respect to the system of coordinates given in Figure 5.2, the arclength variable s coincides with x_2. The free surface implies that, $f_0^- = f_n^- = m_3^- = 0$, while

$$f_0^+ = \sigma_{12}^{(1)}(0, x_2),\ f_n^+ = \sigma_{12}^{(1)}(0, x_2),\ m_3^+ = \mu_{13}^{(1)}(0, x_2), \tag{5.23}$$

in the surface boundary conditions (2.49-2.51). Accordingly, the boundary conditions at the

free surface become,

$$A_s \frac{d^2 u_2^{(1)}}{dx_2^2}\bigg|_{x_1=0} + \sigma_{12}^{(1)}(0, x_2) = 0, \tag{5.24}$$

$$-B_s \frac{d^4 u_1^{(1)}}{dx_2^4}\bigg|_{x_1=0} + H_s \frac{d^3 \varphi_3^{(1)}}{dx_2^3}\bigg|_{x_1=0} + \sigma_{11}^{(1)}(0, x_2) = 0, \tag{5.25}$$

$$H_s \frac{d^2 \varphi_3^{(1)}}{dx_2^2}\bigg|_{x_1=0} + \mu_{13}^{(1)}(0, x_2) = 0. \tag{5.26}$$

In the equations (5.24) to (5.26), we as well, neglect the micropolar shearing stress effects on the surface, i.e. $G_s = 0$, since we assume the thickness of the surface is small enough. In addition, we have the continuity of displacement, microrotations, stresses and couple stresses along the intersection of the two regions at $x_1 = h$. Finally, we characterize the dislocation as a displacement jump across the glide plane ($x_1 = h$, $x_2 < 0$) by the magnitude of a Burgers vector $\mathbf{b} = b\mathbf{e}_2$. Therefore, the jump condition (5.1) created by the edge dislocation becomes,

$$u_2^{(2)}(h, x_2) - u_2^{(1)}(h, x_2) = bH(-x_2) \equiv F(x_2), \tag{5.27}$$

and the remaining the conditions at $x_1 = h$ comply with the assumptions given in Section 5.1.1, the continuity of microrotations, displacement derivative and microrotation derivative. In Eq. (5.27), $H(x)$ denotes the Heaviside step function. We have,

$$u_1^{(2)}(h, x_2) = u_1^{(1)}(h, x_2), \tag{5.28}$$

$$\varphi_3^{(2)}(h, x_2) = \varphi_3^{(1)}(h, x_2) \tag{5.29}$$

$$\sigma_{11}^{(2)}(h, x_2) = \sigma_{11}^{(1)}(h, x_2), \tag{5.30}$$

$$\sigma_{12}^{(2)}(h, x_2) = \sigma_{12}^{(1)}(h, x_2), \tag{5.31}$$

$$\mu_{13}^{(2)}(h, x_2) = \mu_{13}^{(1)}(h, x_2). \tag{5.32}$$

We solve the three governing equations, (5.19), (5.21) and (5.22) for each region using the

following Fourier integral transform:

$$\begin{aligned}\widetilde{f}(x_1,\xi) &= \frac{1}{\sqrt{2\pi}}\int_{-\infty}^{\infty} f(x_1,x_2)e^{-\imath\xi x_2}dx_2,\\ f(x_1,x_2) &= \frac{1}{\sqrt{2\pi}}\int_{-\infty}^{\infty} \widetilde{f}(x_1,\xi)e^{\imath\xi x_2}dx_2,\end{aligned} \tag{5.33}$$

where $\imath=\sqrt{-1}$ is the imaginary unit. The governing equations, consequently, reduce to the ordinary differential equations,

$$\left(\frac{d^2}{dx_1^2}-\xi^2\right)^2\widetilde{\Phi}^{(i)} = 0, \tag{5.34}$$

$$\left(\frac{d^2}{dx_1^2}-\xi^2\right)\left[c^2\left(\frac{d^2}{dx_1^2}-\xi^2\right)-1\right]\widetilde{\varphi_3}^{(i)} = 0, \tag{5.35}$$

$$\left[d^2\left(\frac{d^2}{dx_1^2}-\xi^2\right)-2\right]\widetilde{\varphi_3}^{(i)} = \left(\frac{d^2}{dx_1^2}-\xi^2\right)\widetilde{\Psi}_3^{(i)},\ i=1,2. \tag{5.36}$$

Considering single-valuedness of the functions, the solution to the foregoing system is,

$$\widetilde{\Phi}^{(i)} = A^{(i)}e^{|\xi|x_1}+B^{(i)}x_1e^{|\xi|x_1}+C^{(i)}e^{-|\xi|x_1}+D^{(i)}x_1e^{-|\xi|x_1}, \tag{5.37}$$

$$\widetilde{\varphi}_3^{(i)} = E^{(i)}e^{|\xi|x_1}+F^{(i)}e^{\beta(\xi)x_1}+G^{(i)}e^{-|\xi|x_1}+H^{(i)}e^{-\beta(\xi)x_1}, \tag{5.38}$$

$$\begin{aligned}\widetilde{\Psi}_3^{(i)} &= (d^2-2c^2)F^{(i)}e^{\beta(\xi)x_1}-\frac{E^{(i)}}{|\xi|}x_1e^{|\xi|x_1}+(d^2-2c^2)H^{(i)}e^{-\beta(\xi)x_1}\\ &+ \frac{G^{(i)}}{|\xi|}x_1e^{-|\xi|x_1}, \text{for } i=1,2,\end{aligned} \tag{5.39}$$

where $\beta(\xi)=\sqrt{\xi^2+1/c^2}$. The condition of vanishing response at infinity implies that $A^{(2)}=B^{(2)}=F^{(2)}=E^{(2)}=0$. The remaining coefficients are to be determined from the transformed boundary conditions,

$$\begin{aligned}&A_s\left(-\imath\xi^3\widetilde{\Phi}^{(1)}+\xi^2\widetilde{\Psi}_{3,1}^{(1)}\right)+\mu\left(2\imath\xi\widetilde{\Phi}_{,1}^{(1)}-\xi^2\widetilde{\Psi}_3^{(1)}-\widetilde{\Psi}_{3,11}^{(1)}\right)\\ &-\alpha\left(\widetilde{\Psi}_{3,11}^{(1)}-\xi^2\widetilde{\Psi}_3^{(1)}\right)-2\alpha\widetilde{\varphi}_3^{(1)}\Big|_{x_1=0}=0,\end{aligned} \tag{5.40}$$

$$\begin{aligned}&-B_s\left(\xi^4\widetilde{\Phi}_{,1}^{(1)}+\imath\xi^5\widetilde{\Psi}_3^{(1)}\right)+H_s\left(-\imath\xi^3\widetilde{\varphi}_3^{(1)}\right)+(2\mu+\lambda)\left(\widetilde{\Phi}_{,11}^{(1)}-\xi^2\widetilde{\Phi}^{(1)}\right)\\ &+2\mu\left(\imath\xi\widetilde{\Psi}_{3,1}^{(1)}+\xi^2\widetilde{\Phi}^{(1)}\right)\Big|_{x_1=0}=0,\end{aligned} \tag{5.41}$$

$$H_s\left(-\imath\xi^2\widetilde{\varphi}_3^{(1)}\right)+(\gamma+\varsigma)\widetilde{\varphi}_{3,1}^{(1)}\Big|_{x_1=0}=0, \tag{5.42}$$

$$\left(\imath\xi\widetilde{\Phi}^{(2)}-\widetilde{\Psi}_{3,1}^{(2)}\right)-\left(\imath\xi\widetilde{\Phi}^{(1)}-\widetilde{\Psi}_{3,1}^{(1)}\right)\Big|_{x_1=h}=\widetilde{F}(\xi), \tag{5.43}$$

$$\left(\widetilde{\Phi}_{,1}^{(2)}+\imath s\widetilde{\Psi}_3^{(2)}\right)-\left(\widetilde{\Phi}_{,1}^{(1)}+\imath s\widetilde{\Psi}_3^{(1)}\right)\Big|_{x_1=h}=0, \tag{5.44}$$

$$\widetilde{\varphi}_3^{(2)}-\widetilde{\varphi}_3^{(1)}\Big|_{x_1=h}=0, \tag{5.45}$$

$$\begin{aligned}&(2\mu+\lambda)\left(\widetilde{\Phi}_{,11}^{(2)}-s^2\widetilde{\Phi}^{(2)}\right)+2\mu\left(\imath\xi\widetilde{\Psi}_{3,1}^{(2)}+s^2\widetilde{\Phi}^{(2)}\right)\\&-(2\mu+\lambda)\left(\widetilde{\Phi}_{,11}^{(1)}-s^2\widetilde{\Phi}^{(1)}\right)-2\mu\left(\imath\xi\widetilde{\Psi}_{3,1}^{(1)}+\xi^2\widetilde{\Phi}^{(1)}\right)\Big|_{x_1=h}=0,\end{aligned} \tag{5.46}$$

$$\begin{aligned}&\mu\left(2\imath\xi\widetilde{\Phi}_{,1}^{(2)}-\xi^2\widetilde{\Psi}_3^{(2)}-\widetilde{\Psi}_{3,11}^{(2)}\right)-\alpha\left(\widetilde{\Psi}_{3,11}^{(2)}-\xi^2\widetilde{\Psi}_3^{(2)}\right)-2\alpha\widetilde{\varphi}_3^{(2)}\\&-\mu\left(2\imath\xi\widetilde{\Phi}_{,1}^{(1)}-\xi^2\widetilde{\Psi}_3^{(1)}-\widetilde{\Psi}_{3,11}^{(1)}\right)+\alpha\left(\widetilde{\Psi}_{3,11}^{(1)}-\xi^2\widetilde{\Psi}_3^{(1)}\right)+2\alpha\widetilde{\varphi}_3^{(1)}\Big|_{x_1=h}=0\end{aligned} \tag{5.47}$$

$$\widetilde{\varphi}_{3,1}^{(2)}-\widetilde{\varphi}_{3,1}^{(1)}\Big|_{x_1=h}=0, \tag{5.48}$$

and the transformed Cauchy-Riemann equations,

$$\widetilde{\Phi}_{,111}^{(i)}-\xi^2\widetilde{\Phi}_{,1}^{(i)}+\frac{2\mu\imath\xi}{(2\mu+\lambda)}\left[c^2\left(\widetilde{\varphi}_{3,11}^{(i)}-\xi^2\widetilde{\varphi}_3^{(i)}\right)-\widetilde{\varphi}_3^{(i)}\right]=0, \tag{5.49}$$

$$\imath\xi\left(\widetilde{\Phi}_{,11}^{(i)}-\xi^2\widetilde{\Phi}^{(i)}\right)-\frac{2\mu}{(2\mu+\lambda)}\left[c^2\left(\widetilde{\varphi}_{3,111}^{(i)}-\xi^2\widetilde{\varphi}_{3,1}^{(i)}\right)-\widetilde{\varphi}_{3,1}^{(i)}\right]=0, \tag{5.50}$$

for $i=1,2$. The latter equations enforce the compatibility condition on the problem and lead to three relations between the unknown coefficients:

$$G^{(1)}=\left(\frac{\xi}{\imath}\right)\left(\frac{2\mu+\lambda}{2\mu}\right)D^{(1)}, \tag{5.51}$$

$$G^{(2)}=\left(\frac{\xi}{\imath}\right)\left(\frac{2\mu+\lambda}{2\mu}\right)D^{(2)}, \tag{5.52}$$

$$E^{(1)}=\left(\frac{\xi}{\imath}\right)\left(\frac{2\mu+\lambda}{2\mu}\right)B^{(1)}, \tag{5.53}$$

We find the remaining nine coefficients using the nine boundary conditions presented above. The transformed functions, $\widetilde{\Phi}^{(i)}$, $\widetilde{\varphi}_3^{(i)}$ and $\widetilde{\Psi}_3^{(i)}$ now allow us to determine the displacement and stress field components via their inverse transforms from (5.33), and the expressions (5.14) to (5.16). Thus, the complete analytical solution is given in terms of Fourier integrals.

5.2.1 Special Case of Classical Elasticity

We set the micropolar elastic constants of the bulk material γ, ς, and α as well as the micropolar surface rigidity H_s to zero. The coefficients $F^{(1)}$, $H^{(1)}$ and $H^{(2)}$, in turn, vanish. We normalize the system of linear algebraic equations by taking $\widetilde{F}(\xi) = 1$ and calculate the remaining coefficients. The rest of the coefficients are determined as follows:

$$A^{(1)} = -\frac{\imath h(\mu+\lambda)\,|\xi|\,e^{-h|\xi|}}{2\xi(2\mu+\lambda)} \tag{5.54}$$

$$B^{(1)} = -\frac{\imath\,|\xi|\,\mu e^{-h|\xi|}}{2\xi(2\mu+\lambda)} \tag{5.55}$$

$$C^{(1)} = -\frac{C_1^{(1)}}{D},\; C^{(2)} = -\frac{C_1^{(2)}}{D}, \tag{5.56}$$

$$D^{(1)} = -\frac{D_1^{(1)}}{D},\; D^{(2)} = -\frac{D_1^{(2)}}{D}, \tag{5.57}$$

where,

$$\begin{aligned} C_1^{(1)} &= \imath\,|\xi|\,\xi^2 e^{-h|\xi|}(\mu+\lambda)^2\left\{\frac{2\mu(2\mu+\lambda)}{\mu+\lambda}\,|s|\left(h(B_s\xi^2-A_s)+\frac{A_sB_s\xi^2}{\mu+\lambda}\right)\right. \\ &\quad \left.+h\left(A_sB_s\xi^4-4\mu^2\right)\right\}, \end{aligned} \tag{5.58}$$

$$\begin{aligned} C_1^{(2)} &= \imath\xi^4 e^{-h|\xi|}(\mu+\lambda)^2\left\{\left(\frac{4\mu^2}{|\xi|}+\frac{2\mu(2\mu+\lambda)}{\mu+\lambda}A_s\right)h\left(e^{2h|\xi|}-1\right)\right. \\ &\quad +A_sB_s\xi^2\,|\xi|\left(1+\frac{3\mu+\lambda}{\mu+\lambda}e^{2h|\xi|}\right) \\ &\quad \left.+\xi^2B_s\frac{2\mu(2\mu+\lambda)}{\mu+\lambda}\left(h\left(e^{2h|\xi|}+1\right)+\frac{A_s}{\mu+\lambda}\right)\right\}, \end{aligned} \tag{5.59}$$

$$\begin{aligned} D_1^{(1)} &= \imath\xi^4 e^{-h|\xi|}\mu(\mu+\lambda)\left\{\left(\frac{1}{|\xi|}-2h\right)\left(A_sB_s\xi^4-4\mu^2\right)\right. \\ &\quad \left.-\frac{2\mu(2\mu+\lambda)}{\mu+\lambda}(B_s\xi^2-A_s)\right\}, \end{aligned} \tag{5.60}$$

$$
\begin{aligned}
D_1^{(2)} &= \imath\xi^4 e^{-h|\xi|}\mu(\mu+\lambda)\left\{\left(\frac{4\mu^2}{|\xi|}+\frac{2\mu(2\mu+\lambda)}{\mu+\lambda}\xi^2 B_s\right)\left(e^{2h|\xi|}-1\right)\right. \\
&\quad +A_s B_s\xi^2|\xi|\left(1+\frac{3\mu+\lambda}{\mu+\lambda}e^{2h|\xi|}\right) \\
&\quad \left.+\frac{2\mu(2\mu+\lambda)}{\mu+\lambda}A_s\left(e^{2h|\xi|}+1\right)-2A_s B_s h\xi^4+8\mu^2 h\right\}, \qquad (5.61)
\end{aligned}
$$

$$
\begin{aligned}
D &= 2\xi^3|\xi|(2\mu+\lambda)(\mu+\lambda)\left\{\frac{4\mu^2}{|\xi|}+\frac{3\mu+\lambda}{\mu+\lambda}A_s B_s\xi^2|\xi|\right. \\
&\quad \left.+\frac{2\mu(2\mu+\lambda)}{\mu+\lambda}\left(A_s+2B_s\xi^2\right)\right\}. \qquad (5.62)
\end{aligned}
$$

The stress components are obtained from the inverse integral transform,

$$
\sigma_{\alpha\beta}^{(i)}=\frac{1}{\sqrt{2\pi}}\int_{-\infty}^{\infty}\widetilde{F}(\xi)\widetilde{\sigma}_{\alpha\beta}^{(i)}e^{\imath\xi x_2}dx_2,\ i=1,2,\ \alpha,\beta=1,2. \qquad (5.63)
$$

where $\widetilde{F}(\xi)$ is the Fourier transform of $bH(-x_2)$ and,

$$
\widetilde{\sigma}_{11}^{(i)}=(2\mu+\lambda)\left(\widetilde{\Phi}_{,11}^{(i)}-\xi^2\widetilde{\Phi}^{(i)}\right)+2\mu\left(\imath\xi\widetilde{\Psi}_{3,1}^{(i)}+\xi^2\widetilde{\Phi}^{(i)}\right), \qquad (5.64)
$$

$$
\widetilde{\sigma}_{22}^{(i)}=(2\mu+\lambda)\left(\widetilde{\Phi}_{,11}^{(i)}-\xi^2\widetilde{\Phi}^{(i)}\right)-2\mu\left(\imath\xi\widetilde{\Psi}_{3,1}^{(i)}+\widetilde{\Phi}_{,11}^{(i)}\right), \qquad (5.65)
$$

$$
\widetilde{\sigma}_{12}^{(i)}=\widetilde{\sigma}_{21}^{(i)}=\mu\left(2\imath\xi\widetilde{\Phi}_{,1}^{(i)}-\xi^2\widetilde{\Psi}_3^{(i)}-\widetilde{\Psi}_{3,11}^{(i)}\right),\ i=1,2. \qquad (5.66)
$$

It is not difficult to see that on removing the flexural rigidity of the surface we recover the results presented by Intarit et al. [73].

5.3 Numerical Illustrations

We determine the constants from the system of algebraic equations and hence the transformed functions $\widetilde{\Phi}^{(i)}$, $\widetilde{\Psi}_3^{(i)}$, and $\widetilde{\varphi}_3^{(i)}$. We use these functions and the corresponding inverse integral transforms of the stress components to acquire the complete solution. The solution of the stress field components in the form of improper integrals are then computed using numerical integration methods. In order to compare our results with those in the existing

literature, we adopt classical elastic constants equivalent to that of an Aluminium alloy with surface parameters introduced in [101]. Additionally, we consider hypothetical values for bending rigidity of the surface as well as for the micropolar properties. For the purpose of comparison, we define a surface characteristic length, $l_s = A_s(2\mu + \lambda)/2\mu(\mu + \lambda)$ as in [73]. Accordingly, the numerical values for the most general case are taken as,

$$\begin{aligned} \mu &= 26.1GPa,\ \lambda = 58.1GPa,\ \alpha = 2.6GPa,\ \gamma = 2.6GPa, \varsigma = 0 \\ A_s &= 6.091N/m,\ B_s = 0.024N.m,\ H_s = 0.024N.m. \end{aligned}$$

Again we note that the above values are chosen for illustrative purposes only and to demonstrate the effects of each parameter on the solution. In this area of study, it is almost always the case that the theory is ahead of the experiments making the availability of real parametric data almost impossible to find. We normalize the dimensions in our analysis by the characteristic length of the surface l_s. Therefore, we set the normalized measure of depth of the dislocation to $\overline{h} = h/l_s$, and the normalized coordinates, to $\overline{x}_1 = x_1/l_s$ and $\overline{x}_2 = x_2/l_s$. We illustrate the stress components σ_{11}, σ_{12}, and σ_{22} at two different relative depths along the x_2 direction: $\overline{x}_1 = 0.1$ and $\overline{x}_1 = 1$. We compare five different material models to observe the changes in the solution. The solutions corresponding to classical elastic materials without and with G-M surface effects are published in [73]. Here they are obtained as special cases of our results by letting the micropolar and extra surface parameters B_s, H_s, α, ς, and γ, be set to zero. We introduce three additional cases; a micropolar material without surface effects ($A_s = B_s = H_s = 0$); a classical material with higher order surface effects ($\alpha = \varsigma = \gamma = H_s = 0$); and the most general case of a micropolar material with higher order surface effects incorporating both bending and twisting rigidities.

Figure 5.3 shows the distribution of the normal stress component σ_{11} along the x_2 direction at the depths $\overline{x}_1 = 0.1$ and $\overline{x}_1 = 1$ induced by an edge dislocation at the depth $\overline{h} = 1$. Looking at the stress profile at the relative depth 0.1, we observe that the use of classical and micropolar theories in the absence of surface elasticity intensifies σ_{11} at this depth only slightly, while involving surface flexural and micropolar effects for both classical and microp-

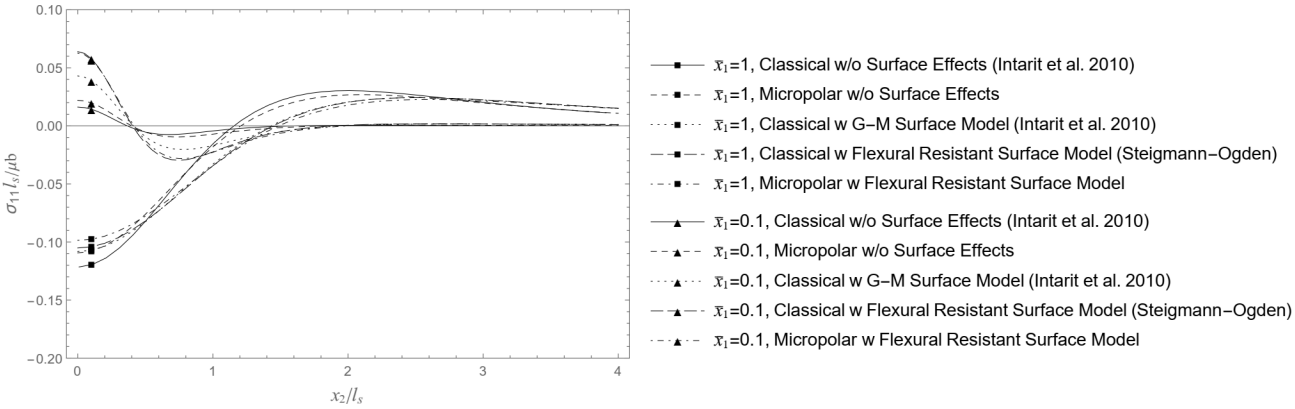

Figure 5.3: Variation of the normalized stress component σ_{11} at relative depth $\bar{x}_1 = 0.1$ and $\bar{x}_1 = 1$, for an edge dislocation at $\bar{h} = 1$.

olar theories significantly affects the solution. The classical G-M model yields higher stress values compared to the absence of surface effects, but lower values compared to the classical and micropolar flexural effects of the surface. Interestingly, the stress distributions for the classical and micropolar surface flexural effects are close to each other. On the other hand, at the relative depth $\overline{x}_1 = 1$, the normal stress component σ_{11} decreases by considerations of micropolarity and surface effects of all kinds. The differences are more pronounced especially near the dislocation core. Among the surface models, the micropolar surface involving all the rigidity aspects presents the lowest intensity of stress distribution along the slip plane, $\overline{x}_1 = 1$, near the dislocation core.

Figure 5.4 shows the distribution of shearing component σ_{12} at two different relative depths, $\overline{x}_1 = 0.1$ and $\overline{x}_1 = 1$. We observe that including micropolar effects of the bulk in the problem decreases the shear stress intensity on the plane $\overline{x}_1 = 0.1$. However, farther away from the dislocation core, the solutions of classical and micropolar elasticity converge. In this case, the classical G-M surface elasticity intensifies the stress, while incorporating micropolar and flexural effects of the surface lowers the results. The classical bending rigidity of the surface has a marginal effect on the stress component, σ_{12}, at this depth. For the shear stress distribution at the slip plane we notice the singularity at the dislocation core for all cases. However, involving micropolarity of the bulk and surfaces effects with various properties

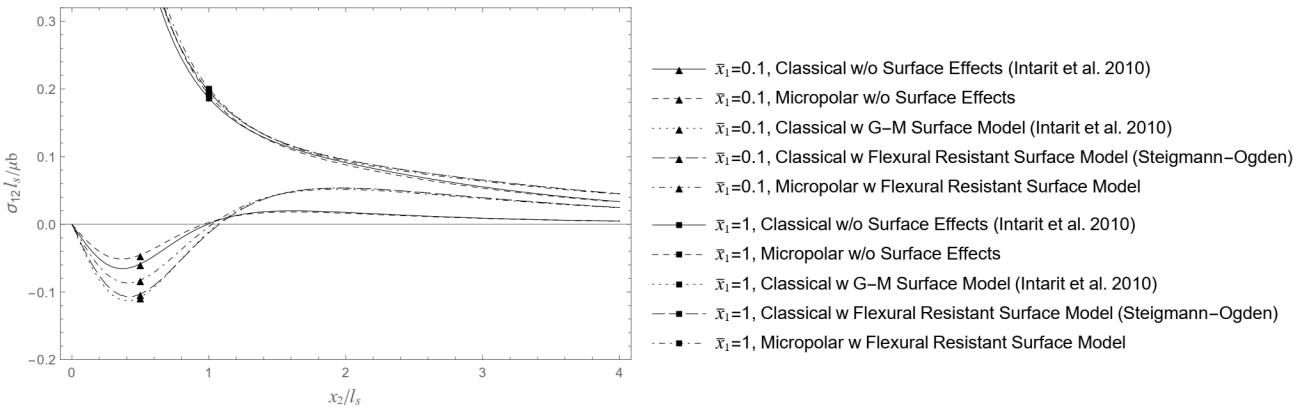

Figure 5.4: Variation of the normalized stress component σ_{12} at relative depth $\bar{x}_1 = 0.1$ and $\bar{x}_1 = 1$, for an edge dislocation at $\bar{h} = 1$.

intensify the singularity rate of the solution. The most extreme case happens for the most general case of a micropolar material with the flexural resistant surface. It is interesting that the micropolar properties of the bulk affect the stress distribution locally near the dislocation core, while all types of surface effects alter the stress distributions even at far away distances from the dislocation core. This is true for the other components of stress as well.

Figure 5.5, shows the distribution profile of the normal stress component σ_{22}. We observe that the incorporation of surface elasticity reduces the stress variation range at the depth $\overline{x}_1 = 0.1$. However, the stress intensity increases near the core by adopting surface effects of any kind. The incorporation of classical bending rigidity in the surface makes an insignificant contribution to the solution compared to analogous results using the regular G-M model. The micropolar surface with bending and twisting rigidities, however, has a higher influence on the profile of the stress component, σ_{22}. At the depth $\overline{x}_1 = 1$,we simply observe that the classical bending rigidity and micropolar effects of the surface do not affect the stress profile. In addition, the micropolarity of the material without surface effects makes no contribution to the stress profile at this depth. For both illustrated depths in Figure 5.3 and also the Figures 5.4 and 5.5, we observe that the surface effects make a global change in the pattern of the stress distribution. Different types of surfaces affect the solution at a certain distance from the dislocation core, however, the type of surface model in use becomes less important

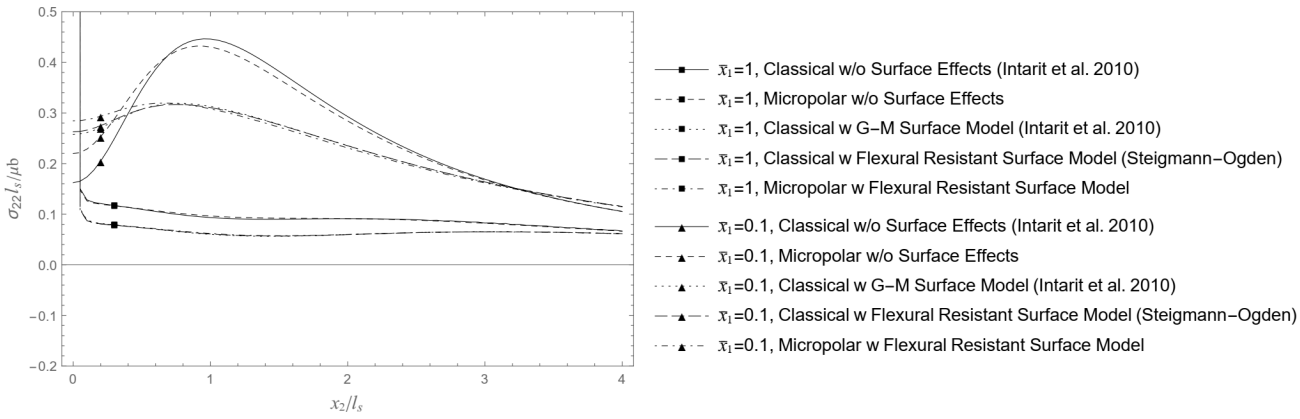

Figure 5.5: Variation of the normalized stress component σ_{22} at relative depth $\bar{x}_1 = 0.1$ and $\bar{x}_1 = 1$, for an edge dislocation at $\bar{h} = 1$.

at distances far from the dislocation core. The same conclusion can be reached when surface effects are ignored altogether in classical and micropolar formulations. Consequently, at relatively far distances from the dislocation core, we have two distinct responses: one arising from the inclusion of surface effects (relatively independent of the surface model used) and one which does not include surface effects irrespective of the type of surface or bulk elasticity model used.

In this chapter, we have demonstrated a successful application of our proposed model to, yet another fundamental problem of plane elasticity. We illustrated the insufficiency of classical approaches such as the G-M model or the sole use of higher order micropolar theory. Also with regards to this specific problem, the incorporation of bending resistance is generally marginal and may alter the solution only for certain cases.

The fundamental problems, presented so far, demonstrate how effectively, we are able to apply the model to approach different problems. However, there remains the question of whether the model is well-posed mathematically. We answer this question through a rigorous analysis of our proposed model in the following chapter.

Chapter 6

Wellposedness Analysis of the Micropolar Surface Model

Before we use a mathematical model to hypothesize a physical phenomenon, we require to ascertain that the mathematical model adequately describes the physics of the problem. In other words, the mathematical model needs to be well-designed in order to be applicable to real physical problems. The adequacy of a model for predicting or describing a physical phenomenon, is evaluated through well-posedness analysis. In the sense of Hadamard [66], a mathematical model of a physical phenomenon is well-posed, if its solution exists, the existing solution is unique, and the solution continuously changes with the boundary data.

A boundary value problem which does not meet Hadamard's conditions, is called ill-posed. An ill-posed model does not adequately represent a non-chaotic physical phenomenon, since it may lead to multiple solutions or no solutions at all for a single physical event, and therefore erroneous results. To avoid the possibility of fruitless attempts to apply an ill-posed model to analyze physics of a phenomenon, it is necessary to investigate the model in terms of the mathematical well-posedness. Well-posedness analysis also uncovers the constraints, limitations, and the range of applicability of the mathematical model.

In this chapter, we consider the well-posedness analysis of the proposed model, in terms of existence and uniqueness theorems. In the first section, we introduce the methods which establish the mathematical framework of the theorems. We employ the commonly used

energy argument to examine the uniqueness of solutions of the model (e.g. [21]). To examine the existence of solutions of the corresponding boundary value problems, we use the boundary-integral equation method (BIEM) [23, 22]. The choice of our approach to the existence theorems is further beneficial in that, it determines the function space in which the solutions are to be sought. Lastly, in this chapter, we determine the conditions under which the existence and uniqueness of solutions of the proposed model are expected.

6.1 Preliminaries

Consider the Cartesian coordinates $\{x_1, x_2, x_3\}$ oriented in such a way that the $\{x_1, x_2\}$ plane coincides with the plane of deformation and x_3, with the antiplane (out-of-plane) direction. We denote a point on the plane of deformation by $\mathbf{x} = (x_1, x_2)$. The analyses in this chapter require transformations between the Cartesian coordinates and the normal-tangential coordinates $(n-t)$. As in Chapter 2, we parameterize a curve in the x_1x_2-plane by an arclength s. We assign to the normal-tangential $(n-t)$ coordinates the orthonormal basis $\{\mathbf{e}_0(s), \mathbf{e}_3, \mathbf{n}(s)\}$ with the unit outward normal denoted by $\mathbf{n}(s)$ and the unit tangent vector denoted by $\mathbf{e}_0(s)$ at an arclength distance s from an origin $s = 0$. The orientation of the tangent to the curve is measured as $\theta(s)$, the angle between the x_1-alignment and $\mathbf{e}_0(s)$. The standard transformation operator defined by

$$\mathbf{A}(\mathbf{x}) = \mathbf{A}^{-\mathbf{1}}(\mathbf{x}) = \begin{bmatrix} \cos\theta(s) & \sin\theta(s) & 0 \\ \sin\theta(s) & -\cos\theta(s) & 0 \\ 0 & 0 & 1 \end{bmatrix}.$$

transforms the coordinates between the normal-tangential and the Cartesian coordinates. We denote by $\mathcal{M}_{m\times n}$ the space of $(m \times n)$ matrices and $\mathbf{I}_n$ is the identity element in $\mathcal{M}_{n\times n}$. We also denote the identity element of $\mathcal{M}_{3\times 3}$, in short, by $\mathbf{I}$. For a space of scalar functions, X, a matrix, $\mathbf{v} \in X$ means that every element of $\mathbf{v}$ belongs to X. In this chapter, we seek the solutions to the corresponding boundary value problems for our model and the determine the requirements of the boundary curves in the function spaces introduced in Section 2.1.2.

6.1.1 Integral Equations

Integral equations are equations which involve unknown functions under integral operators. The simplest integral equation is a Fredholm equation of the first kind wherein the unknown function appears linearly under the integral sign only. For the Fredholm integral equation of the second kind the unknown function appears both inside and outside the integral sign. Fredholm integral equations of the first and second kind over a curve ∂S belonging to the x_1x_2-plane are of the following forms, respectively,

$$\int_{\partial S} K(\mathbf{x},\mathbf{y})\phi(\mathbf{x})d\mathbf{y} = f(\mathbf{x}),\ \phi(\mathbf{x}) - \int_{\partial S} K(\mathbf{x},\mathbf{y})\phi(\mathbf{x})d\mathbf{y} = f(\mathbf{x}),\ \ \mathbf{x},\mathbf{y} \in \partial S.$$

Here, $\phi(\mathbf{x})$ is an unknown function, while $K(\mathbf{x},\mathbf{y})$ is called the "kernel" and $f(\mathbf{x})$ is a prescribed data over the curve ∂S. We regard an integral equation as a linear operator applied to a function $\phi(\mathbf{x})$ to transform it to $f(\mathbf{x})$. Indeed, for a Fredholm integral equation of the second kind this operator is composed of an integral operator,

$$(A\phi)(\mathbf{x}) \equiv \int_{\partial S} K(\mathbf{x},\mathbf{y})\phi(\mathbf{x})d\mathbf{y}$$

$(A\phi)(\mathbf{x})$ and an identity operator, $(I\phi)(\mathbf{x}) = \phi(\mathbf{x})$, i.e $((I-A)\phi)(\mathbf{x}) = f(\mathbf{x})$. We define the adjoint of that linear operator by changing the kernel to $K(\mathbf{y},\mathbf{x})$. Integral equations that involve differential operators as well as the integral operator are known as integro-differential equations.

We call a kernel $K(\mathbf{x},\mathbf{y})$ weakly singular if there exist an $M \in \mathbb{R}$ such that $\forall \mathbf{x},\mathbf{y} \in \mathbb{R}^n$ the product $|\mathbf{x}-\mathbf{y}|^\alpha K(\mathbf{y},\mathbf{x})$ is bounded by M for all $0 \leq \alpha < n$, where n is the dimension of the space $\mathbb{R}^n$ to which $\mathbf{x}$ belongs. In the case of planar problems, we are specifically interested in $\mathbf{x},\mathbf{y} \in \mathbb{R}^2$, hence the condition for α becomes $0 \leq \alpha < 2$.

6.1.2 Analysis Background

In this section, we lay down the useful theorems of functional analysis in application to the integral equations method. The proofs of the stated essential definitions and theorems can be found in references ([83] and [18]).

Linear, Bounded and Compact Operators

Definition 1. *An operator $A : \mathcal{X} \mapsto \mathcal{Y}$ mapping a linear space $\mathcal{X}$ into a linear space $\mathcal{Y}$ is "linear" if $A(\alpha\phi + \beta\psi) = \alpha A(\phi) + \beta A(\psi)$ for all ϕ and $\phi \in \mathcal{X}$ and all α and $\beta \in \mathbb{C}$.*

Definition 2. *An operator $A : (U \subset \mathcal{X}) \mapsto \mathcal{Y}$ mapping a subset U of a normed space $\mathcal{X}$ into a normed space $\mathcal{Y}$ is continuous at an element $\phi \in U$ if*

$$\lim_{n\to\infty} A(\phi_n) = A(\phi) \text{ for all } \phi_n \in U \text{ with } \lim_{n\to\infty} \phi_n = \phi.$$

The operator $A : U \mapsto \mathcal{Y}$ is called continuous if it is continuous for all $\phi \in U$.

Definition 3. *An linear operator $A : \mathcal{X} \mapsto \mathcal{Y}$ mapping a normed space $\mathcal{X}$ into a normed space $\mathcal{Y}$ is called bounded if there exists a $c > 0$ such that for all $\phi \in \mathcal{X}$,*

$$\|A(\phi)\| \leq \ c\|\phi\|.$$

For bounded operators we define the norm of the operator as,

$$\|A\|_{op} \equiv \inf\{c \geq 0 : \|A\phi\| \leq c\,\|\phi\| \ \text{ for all } \phi \in \mathcal{X}\}.$$

Theorem 6.1. *Boundedness of a linear operator is equivalent to its continuity.*

Theorem 6.2. *A linear operator $A : \mathcal{X} \mapsto \mathcal{Y}$ mapping a finite dimensional normed space $\mathcal{X}$ into a normed space $\mathcal{Y}$ is bounded.*

Definition 4. *A relatively compact set U is a set whose closure is compact, i.e. each sequence in $U \subset \mathcal{X}$ contains a convergent subsequence. An linear operator $A : \mathcal{X} \mapsto \mathcal{Y}$ from a normed space $\mathcal{X}$ into a normed space $\mathcal{Y}$ is called compact if it maps any bounded set from $\mathcal{X}$ into a relatively compact set in $\mathcal{Y}$.*

Theorem 6.3. *A linear operator $A : \mathcal{X} \mapsto \mathcal{Y}$ is compact if and only if for each bounded sequence $\{\phi_n\}_{n=1}^{\infty} \in \mathcal{X}$, the mapped $\{A(\phi_n)\}_{n=1}^{\infty}$ contains a convergent subsequence.*

Theorem 6.4. *Compact liner operators are bounded.*

The Riesz Theory

For an operator of the form, $I\phi - A\phi = f$ with, $A : \mathcal{X} \mapsto \mathcal{X}$, a compact linear operator on a normed space $\mathcal{X}$, we define $L \equiv I - A$ as an operator of the second kind.

Theorem 6.5 (Riesz first theorem)**.** *The null-space of the L operator defined by,*

$$N(L) \equiv \{\phi \in \mathcal{X} : L\phi = 0\},$$

is a finite dimensional linear subspace of $\mathcal{X}$.

Theorem 6.6 (Riesz second theorem)**.** *The range of the operator L defined by,*

$$L(\mathcal{X}) \equiv \{L\phi : L\phi \in \mathcal{X}\},$$

is a closed linear subspace of $\mathcal{X}$.

Let us denote by L^k the resultant operator from k times applying the operator L. Then, the statement of the third Riesz theorem follows:

Theorem 6.7 (Riesz third theorem)**.** *There exists a unique non-negative integer r known as "Riesz number" of the operator A, such that,*

$$N(L) \equiv \{\phi \in X : L\phi = 0\}$$

$$\{0\} = N(L^0) \subsetneqq N(L^1) \subsetneqq N(L^2) ... \subsetneqq N(L^r) = N(L^{r+1}) = ...$$

$$\mathcal{X} = L^0(\mathcal{X}) \supsetneqq L^1(\mathcal{X}) \supsetneqq ... \supsetneqq L^r(\mathcal{X}) = L^{r+1}(\mathcal{X}) = ...$$

Theorem 6.8. *Let $\mathcal{X}$ be a normed space, $A : \mathcal{X} \mapsto \mathcal{X}$ a compact linear operator and let $L \equiv I - A$ be injective. Then, the inverse operator $L^{-1} \equiv (I - A)^{-1}$ exists and it is bounded.*

Proof. Because $L = I - A$ is injective then $N(L) = \{0\}$. Therefore, Riesz number $r = 0$. It follows that $L(\mathcal{X}) = \mathcal{X}$ which means L is surjective, hence, L^{-1} exists.

Now, assume L^{-1} is not bounded. Then there must exist a sequence $\{\phi_n\}_{n=1}^{\infty}$ with $\|\phi_n\| = 1$ such that $f_n \equiv L^{-1}\phi_n$ is not bounded. Let us define

$$\psi_n \equiv \frac{\phi_n}{\|f_n\|}, g_n \equiv \frac{f_n}{\|f_n\|},$$

then $\psi_n \to 0$ as $n \to \infty$, while $\|g_n\| = 1$. Since A is compact we can choose a subsequence $\{g_{n(k)}\}_{k=1}^{\infty}$ such that, $Ag_{n(k)} \to g \in \mathcal{X}$, as $k \to \infty$. Then, because $\psi_n = g_n - Ag_n$, we see that $g_{n(k)} \to g$ as $k \to \infty$. In conclusion, g belongs to the null-space of L, i.e., $g \in N(L)$, and therefore, $g = 0$ which contradicts the fact that $\|g_n\| = 1$. □

Corollary 1. *For a normed space $\mathcal{X}$ and a compact linear operator $A : \mathcal{X} \mapsto \mathcal{X}$ if the homogeneous equation,*

$$\phi - A\phi = 0,$$

only has the trivial solution $\phi = 0$, then for all $f \in \mathcal{X}$ the inhomogeneous equation,

$$\phi - A\phi = f,$$

has a unique solution $\phi \in \mathcal{X}$ and this solution depends continuously on f.

Corollary 2. *If the homogeneous equation $\phi - A\phi = 0$ has a nontrivial solution, then the non-homogeneous equation $\phi - A\phi = f$ is either unsolvable or its general solution is of the form,*

$$\phi = \phi^* + \sum_{k=1}^{m} \alpha_k \phi_k,$$

where, ϕ^* is the particular solution of the non-homogeneous equation and $\{\phi_k\}_{k=1}^{m}$ are linearly independent solutions of the homogeneous equation and α_k are scalar constants.

Fredholm Theory

The last corollary indicates a limitation of Riesz theory. Albeit, in the case of a homogeneous equation with non-trivial solution, we can use Fredholm theory to find whether the non-homogeneous equation, $\phi - A\phi = f$, for a given f is solvable or not. Before stating the elements of the Fredholm theory we need to define some terms:

Definition 5. *Two normed spaces $\mathcal{X}$ and $\mathcal{Y}$ equipped with a bounded, nondegenerate bilinear form denoted by $\langle \mathcal{X}, \mathcal{Y} \rangle$ are called "dual system". Here, we define the biliear form as a mapping $\langle \cdot, \cdot \rangle : \mathcal{X} \times \mathcal{Y} \longrightarrow \mathbb{C}$. The bilinearity specifies the conditions,*

$$\begin{aligned} \langle \alpha_1 \phi_1 + \alpha_2 \phi_2, \psi \rangle &= \alpha_1 \langle \phi_1, \psi \rangle + \alpha_2 \langle \phi_2, \psi \rangle \\ \langle \phi, \beta_1 \psi_1 + \beta_2 \psi_2 \rangle &= \beta_1 \langle \phi, \psi_1 \rangle + \beta_2 \langle \phi, \psi_2 \rangle , \end{aligned}$$

The bilinear form is bounded if there is a $\gamma > 0$ such that,

$$|\langle \phi, \psi \rangle| \leq \gamma \|\phi\| \|\psi\| , \text{ for } \phi \in \mathcal{X} \text{ and } \psi \in \mathcal{Y}.$$

The norm of the bilinear form, $\langle \phi, \psi \rangle$ as an operator is therefore defined as,

$$\|\langle \phi, \psi \rangle\| \equiv \sup_{\|\phi\|=1} |\langle \phi, \psi \rangle| > 0, \text{ for } \psi \neq 0, \text{ or } \sup_{\|\psi\|=1} |\langle \phi, \psi \rangle| > 0, \text{ for } \phi \neq 0.$$

The nondegeneracy condition implies that for any $\phi \neq 0$ there exists a $\psi \in \mathcal{Y}$ such that $\langle \phi, \psi \rangle \neq 0$ and for any $\psi \neq 0$ there exists a $\phi \in \mathcal{X}$ such that $\langle \phi, \psi \rangle \neq 0$. In finite dimensional spaces it means that $\langle \phi, \psi \rangle = 0$ for all $\psi \in \mathcal{Y}$ if and only if $\phi = 0$, and vice versa.

Theorem 6.9. *A normed space $\mathcal{X}$ and its dual space $\mathcal{X}^*$ form a dual system $\langle \mathcal{X}, \mathcal{X}^* \rangle$ with the bilinear form, $\langle \phi, \phi^* \rangle$, where, $\phi \in \mathcal{X}$ and $\phi^* \in \mathcal{X}^*$. It is called a "natural dual system".*

Definition 6. *Let $\langle \mathcal{X}, \mathcal{Y} \rangle$ be a dual system. Then, two operators, $A : \mathcal{X} \to \mathcal{X}$ and $B : \mathcal{Y} \to \mathcal{Y}$ are called "adjoint" if for every $\phi \in \mathcal{X}$ and $\psi \in \mathcal{Y}$, $\langle A\phi, \psi \rangle = \langle \phi, B\psi \rangle$.*

Definition 7. *A set $G \in \mathbb{R}^m$, $m \in \mathbb{N}$, is called "Jordan-measurable" if a function,*

$$X_G(\mathbf{x}) \equiv \begin{cases} 1 & \mathbf{x} \in G, \\ 0 & \mathbf{x} \notin G, \end{cases}$$

is Riemann integrable.The Jordan measure $|G|$ is the integral of X_G over G.

Theorem 6.10. *Let G be a Jordan-measurable compact subset, for example $G \subset \mathbb{R}^2$. Then, $\langle C(G), C(G) \rangle$, where $C(G)$ is the space of continuous functions on G, is a dual system with the bilinear form defined by,*

$$\langle \phi, \psi \rangle \equiv \int_G \phi(x)\psi(x)dx, \quad \phi, \psi \in C(G). \tag{6.1}$$

Theorem 6.11. *Let $\langle \mathcal{X}, \mathcal{Y} \rangle$ be a dual system. If an operator $A : \mathcal{X} \to \mathcal{X}$ has an adjoint $B : \mathcal{Y} \to \mathcal{Y}$, then B is uniquely determined and A and B are linear.*

Theorem 6.12. *In the dual system $\langle C(G), C(G) \rangle$ with the bilinear form (6.1), the integral operators: the integral operators,*

$$(A\phi)(x) \equiv \int_G K(x,y)\phi(y)dy \text{ and } (B\psi)(x) \equiv \int_G K(x,y)\psi(y)dy, \tag{6.2}$$

with continuous or weakly singular kernel K are adjoint operators.

Proof. We can prove this theorem by directly using the bilinear form,

$$\begin{aligned} \langle A\phi, \psi \rangle &= \int_G \left[\int_G K(x,y)\phi(y)dy \right] \psi(x)dx \\ &= \int_G \int_G K(x,y)\phi(y)\psi(x)dydx. \end{aligned}$$

Since K is weakly singular or continuous then the integral operator is compact, i.e. $A_n\phi \to A$ as $n \to \infty$, therefore,

$$\begin{aligned} \int_G \int_G K(x,y)\phi(y)\psi(x)dydx &= \int_G \phi(y) \left[\int_G K(x,y)\psi(x)dx \right] dy \\ &= \langle \phi, B\psi \rangle \end{aligned}$$

□

Lemma 1 (Orthogonality)**.** *In a dual system $\langle \mathcal{X}, \mathcal{Y} \rangle$ for every set of linearly independent elements $\phi_1, ..., \phi_n \in \mathcal{X}$, there exists a set $\psi_1, ..., \psi_n \in \mathcal{Y}$ such that $\langle \phi_i, \psi_j \rangle = \delta_{ij}$, where $i, j = 1, ..., n$.*

Theorem 6.13 (Fredholm's first theorem)**.** *Let $\langle \mathcal{X}, \mathcal{Y} \rangle$ be a dual system and $A : \mathcal{X} \to \mathcal{X}$ and $B : \mathcal{Y} \to \mathcal{Y}$ be compact adjoint operators. Then the null-space of the operator $I - A$ and $I - B$ have the same finite dimensions.*

Proof. First, by the Riesz first theorem we know that the null-spaces of both $I - A$ and $I - B$ are finite dimensional. Let us take the finite dimensions of the null-spaces as $m = \dim\{N(I-A)\}$ and $n = \dim\{N(I-B)\}$ such that that $n > m$. We choose a basis $\{\phi_i\}_{i=1}^m$ for the null-space $N(I-A)$ and a basis $\{\psi_i\}_{i=1}^n$ for the null-space $N(I-B)$. By the orthogonality lemma (1), there exist $\{a_k\}_{k=1}^m$ and $\{b_k\}_{k=1}^n$ such that

$$\begin{aligned} \langle \phi_i, a_k \rangle &= \delta_{ik}, \quad i,k = 1, ..., m \\ \langle b_k, \psi_i \rangle &= \delta_{ik}, \quad i,k = 1, ..., n. \end{aligned}$$

We define a linear operator $T : \mathcal{X} \to \mathcal{X}$ with a finite dimensional range as,

$$T\phi \equiv \begin{cases} 0 & m = 0 \\ \displaystyle\sum_{i=1}^{m} \langle \phi, a_i \rangle \, b_i & m > 0 \end{cases} \tag{6.3}$$

Next, let a $\phi \in N(I - A + T)$, then for $m > 0$,

$$\phi - A\phi + \sum_{i=1}^{m} \langle \phi, a_i \rangle \, b_i = 0, \tag{6.4}$$

hence,

$$\left\langle \phi - A\phi + \sum_{i=1}^{m} \langle \phi, a_i \rangle \, b_i, \psi_k \right\rangle = 0.$$

Using linearity property of the bilinear form and the definition of an adjoint operator, we have

$$\langle \phi, \psi_k - B\psi_k \rangle + \sum_{i=1}^{m} \langle \phi, a_i \rangle \, \langle b_i, \psi_k \rangle = 0,$$

and since $\langle b_i, \psi_k \rangle = \delta_{ik}$, then

$$\langle \phi, \psi_k - B\psi_k \rangle + \langle \phi, a_k \rangle = 0.$$

On the other hand, ψ_k is in $N(I - B)$, consequently, $\langle \phi, a_k \rangle = 0$, for all $k = 1, ...m$, which by (6.4), it means that, $\phi - A\phi = 0$, or in other words, $\phi \in N(I - A)$. Since we may write

ϕ in terms of the basis $\{\phi_i\}_{i=1}^m$ as

$$\phi = \sum_{i=1}^{m} \langle \phi, a_i \rangle \, \phi_i,$$

by $\langle \phi, a_k \rangle = 0$, we conclude that $\phi = 0$. As a result, the null-space $N(I - A - T) = \{0\}$ which means, $I - A - T$ is injective. By the corollary (1), the non-homogeneous equation,

$$\phi - A\phi + T\phi = b_{m+1},$$

has a unique solution ϕ. Also, by the orthogonality condition,

$$1 = \langle b_{m+1}, \psi_{m+1} \rangle = \langle \phi - A\phi + T\phi, \psi_{m+1} \rangle \,, \tag{6.5}$$

and again, from (6.3),

$$\langle T\phi, \psi_{m+1} \rangle = \left\langle \sum_{i=1}^{m} \langle \phi, a_i \rangle \, b_i, \psi_{m+1} \right\rangle = \sum_{i=1}^{m} \langle \phi, a_i \rangle \, \langle b_i, \psi_{m+1} \rangle = 0,$$

since $i \neq m+1$ ever. Therefore, equation (6.5) translates into,

$$1 = \langle b_{m+1}, \psi_{m+1} \rangle = \langle \phi - A\phi, \psi_{m+1} \rangle = \langle \phi, \psi_{m+1} - B\psi_{m+1} \rangle = 0,$$

which is obviously a contradiction. The same argument follows when $m > n$, then $m = n$. $\square$

Theorem 6.14 (Fredholm's second theorem)**.** *We assume the usual conditions from the first theorem for A and B, that is, $A : \mathcal{X} \to \mathcal{X}$ and $B : \mathcal{Y} \to \mathcal{Y}$ are compact adjoint operators. Then, the non-homogeneous equations,*

$$\phi - A\phi = f,$$

is solvable if and only of, $\langle f, \psi \rangle = 0$, for all solutions of the homogeneous adjoint equation,

$$\psi - B\psi = 0.$$

Similarly, the non-homogeneous equations,

$$\psi - B\psi = g,$$

is solvable if and only of, $\langle g, \phi \rangle = 0$, for all solutions of the homogeneous adjoint equation,

$$\phi - A\phi = 0.$$

Proof. Consider the equation $\phi - A\phi = f$ with ϕ being a solution. Then for all solutions of $\psi - B\psi = 0$ we have,

$$\langle f, \psi \rangle = \langle \phi - A\phi, \psi \rangle = \langle \phi, \psi - B\psi \rangle = 0.$$

On the other hand, from the first Fredholm theorem (theorem 6.13), we take the common null-spaces dimension,

$$m \equiv \dim N(I - A) = \dim N(I - B) < \infty.$$

For the special case of $m = 0$, $\langle f, \psi \rangle = 0$ is satisfied for all $f \in \mathcal{X}$ and therefore, by the corollary (1), $\phi - A\phi = f$ is solvable for all $f \in \mathcal{X}$. However, in the case of $m > 0$, let us assume $\langle f, \psi_k \rangle = 0$ $(k = 1, ..., m)$ for a basis $\{\psi_i\}_{i=1}^m$ in the null-space $N(I - B)$. We already proved that for the defined,

$$T\phi \equiv \sum_{i=1}^{m} \langle \phi, a_i \rangle \, b_i,$$

the null-space $N(I - A + T) = \{0\}$. Hence, there exists a unique solution ϕ for the equation, $\phi - A\phi + T\phi = f$. Then, it follows that,

$$\begin{aligned} 0 = \langle f, \psi_k \rangle &= \langle \phi - A\phi + T\phi, \psi_k \rangle \\ &= \langle \phi - A\phi, \psi_k \rangle + \langle T\phi, \psi_k \rangle \\ &= \left\langle \phi, \underbrace{\psi_k - B\psi_k}_{0} \right\rangle + \langle T\phi, \psi_k \rangle = \langle T\phi, \psi_k \rangle . \end{aligned}$$

Now, since $\langle T\phi, \psi_k \rangle = 0$, ϕ also satisfies $\phi - A\phi = f$ which proves the statement. □

The latter theorem is known as the "Fredholm Alternative" and may be summarized as follows:

> Let $\langle \mathcal{X}, \mathcal{Y} \rangle$ be a dual system and $A : \mathcal{X} \to \mathcal{X}$ and $B : \mathcal{Y} \to \mathcal{Y}$ be compact adjoint operators. Then either,
>
> $$\begin{array}{ll} N(I - A) = \{0\} & \text{and } N(I - B) = \{0\} \\ (I - A)(\mathcal{X}) = \{\mathcal{X}\} & \text{and } (I - B)(\mathcal{Y}) = \{\mathcal{Y}\} \end{array}$$

or

$$\begin{gathered}\dim N(I-A) = \dim N(I-B) \in \mathbb{N} \\ \text{and } (I-A)(\mathcal{X}) = \{f \text{ such that, } \langle f, \psi\rangle = 0,\ \psi \in N(I-B)\} \\ \text{and } (I-B)(\mathcal{Y}) = \{g \text{ such that, } \langle g, \phi\rangle = 0,\ \phi \in N(I-A)\}\end{gathered}$$

If we define the dual system $\langle \mathcal{X}, \mathcal{Y}\rangle$ by the bilinear form of an integral in (6.1) and A and B as integral operators (6.2), then the results of the Fredholm Alternative theorem are useful for integral equations of the second kind. A special case is known as Schauder theory when, $\mathcal{Y} = \mathcal{X}^*$ ($\mathcal{X}^*$: dual of $\mathcal{X}$) and the bilinear form is defined as the operator $\langle \phi, \psi\rangle = \psi(\phi)$ for all $\phi \in \mathcal{X}$ and bounded linear functionals, $\psi \in \mathcal{X}^*$. The statement of Fredholm Alternative theorem for integral equations follows as:

Let $G \subset \mathbb{R}^m$ be a Jordan-measurable domain and let $K : \mathcal{X} \times \mathcal{X} \to \mathbb{C}$ be a continuous or weakly singular kernel. Then **either**,

$$\phi(x) - \int_G K(x,y)\phi(y)dy = 0 \text{ and } \psi(x) - \int_G K(x,y)\psi(y)dy = 0,$$

have only the trivial continuous solutions $\phi = 0$ and $\psi = 0$ and

$$\phi(x) - \int_G K(x,y)\phi(y)dy = f(x) \text{ and } \psi(x) - \int_G K(x,y)\psi(y)dy = g(x),$$

have a unique continuous solution for any continuous f and g, **or**

$$\phi(x) - \int_G K(x,y)\phi(y)dy = 0 \text{ and } \psi(x) - \int_G K(x,y)\psi(y)dy = 0,$$

have the same number of linearly independent solutions, $\phi_1, ..., \phi_n$ and $\psi_1, ..., \psi_n$ and

$$\phi(x) - \int_G K(x,y)\phi(y)dy = f(x) \text{ and } \psi(x) - \int_G K(x,y)\psi(y)dy = g(x),$$

are solvable if and only if,

$$\int_G f(x)\psi_i(x)dx = 0, \text{ and } \int_G g(x)\phi_i(x)dx = 0, \text{ for all } i = 1, ..., n.$$

6.1.3 Singular Integral Equations

Let $\mathbf{x} \in \mathbb{R}^2$ characterize a generic point in $\mathbb{R}^2$ plane, and as before, ∂S a curve in $\mathbb{R}^2$. Equations of the form,

$$A(\mathbf{x})\phi(\mathbf{x}) + \frac{B(\mathbf{x})}{\imath\pi}\int\limits_{\partial S}\frac{\phi(\mathbf{y})d\mathbf{y}}{\mathbf{x}-\mathbf{y}} + \frac{1}{i\pi}\int\limits_{\partial S}k(\mathbf{x},\mathbf{y})\phi(\mathbf{y})d\mathbf{y} = f(\mathbf{x}), \mathbf{x} \in \partial S, \tag{6.6}$$

are called singular integral equations if the following conditions are satisfied. The contour curve ∂S, consists of a finite number of smooth closed curves, the functions $A(\mathbf{x})$, $B(\mathbf{x})$, f and $|\mathbf{x}-\mathbf{y}|^a k(\mathbf{x},\mathbf{y})$, with $a \in (0,1]$, satisfy Hölder continuity condition. Additionally, the functions $A(\mathbf{x}) - B(\mathbf{x})$ and $A(\mathbf{x}) + B(\mathbf{x})$ do not vanish anywhere on ∂S. The general singular integral equation in the form of (6.6) is decomposed into an integral with a singular Cauchy kernel, $1/(\mathbf{x}-\mathbf{y})$, and an integral with a weakly singular kernel, $k(\mathbf{x},\mathbf{y})$. The two first terms of the equation (6.6) form the dominant part of the singular integral equation, and $A(\mathbf{x})$ and $B(\mathbf{x})$ are known as the coefficients of the dominant part. Another important concept that plays role in the theory of singular integral equations is the integer,

$$\varkappa = \frac{1}{2\pi}\arg\left[\frac{A(\mathbf{x})-B(\mathbf{x})}{A(\mathbf{x})+B(\mathbf{x})}\right]_{\partial S}, \tag{6.7}$$

which is known as the index of the corresponding singular integral operator, where, $\arg[...]_{\partial S}$ denotes the increment of the argument of the function in brackets on one circuit of ∂S in the positive direction. It is obvious that the index depends only on the dominant part of the singular integral equation. In the special case of $B(\mathbf{x}) = 0$ the singular integral equation reduces to a Fredholm integral equation of the second kind whose index is obviously zero. It is easy to show the adjoint of equation (6.6) is

$$A(\mathbf{x})\phi(\mathbf{x}) - \frac{1}{\imath\pi}\int\limits_{\partial S}\frac{B(\mathbf{y})\phi(\mathbf{y})d\mathbf{y}}{\mathbf{x}-\mathbf{y}} + \frac{1}{i\pi}\int\limits_{\partial S}k(\mathbf{y},\mathbf{x})\phi(\mathbf{y})d\mathbf{y} = g(\mathbf{x}), \mathbf{x} \in \partial S, \tag{6.8}$$

where $g(\mathbf{x})$ is also Hölder continuous. The extension of Fredholm theory to singular integral equations is developed by Noether [110] which can be summarized in the following three theorems [109],

Theorem 6.15 (Noether's first theorem)**.** *The necessary and sufficient condition for solvability of the equation (6.6) is*

$$\int_{\partial S} f(\mathbf{x})\psi_i(\mathbf{x})d\mathbf{x} = 0, \quad \textit{for } i = 1, ..., n,$$

where $\{\psi_i\}_{i=1}^n$ *is the set of linearly independent solutions of of the adjoint homogeneous equation (homogeneous form of equation (6.8)), i.e.*

$$A(\mathbf{x})\phi(\mathbf{x}) - \frac{1}{\imath\pi}\int_{\partial S} \frac{B(\mathbf{y})\phi(\mathbf{y})d\mathbf{y}}{\mathbf{x}-\mathbf{y}} + \frac{1}{i\pi}\int_{\partial S} k(\mathbf{y},\mathbf{x})\phi(\mathbf{y})d\mathbf{y} = 0, \mathbf{x} \in \partial S,$$

Theorem 6.16 (Noether's second theorem)**.** *The difference between the number of linearly independent solutions of a homogeneous singular integral equation,* m*, and the number of linearly independent solutions of the homogeneous adjoint equation,* n*, i.e.* $m - n$ *depends only on the dominant part of the singular integral equation.*

Theorem 6.17 (Noether's third theorem)**.** *The aforementioned difference* $m - n = \varkappa$ *is equal to the index of the equation (6.6).*

It follows from the latter theorem that when index of a singular integral equation equals zero ($\varkappa = 0$) the number of linearly independent solutions of the homogeneous equation and its adjoint are equal. In that case, the Fredholm Alternative theorem applies to the singular integral equation and determines the solvability of the equation.

6.1.4 Singular Integro-differential Equation

Similar theorems for singular integro-differential equations are given in Isahanov [74]. Consider the following general form of a singular integro-differential equation,

$$\sum_{r=0}^{p}\left[A_r(\mathbf{x})\phi^{(r)}(\mathbf{x}) + \frac{B_r(\mathbf{x})}{\imath\pi}\int_{\partial S}\frac{\phi^{(r)}(\mathbf{y})d\mathbf{y}}{\mathbf{x}-\mathbf{y}} + \frac{1}{\imath\pi}\int_{\partial S} k_r(\mathbf{x},\mathbf{y})\phi^{(r)}(\mathbf{y})d\mathbf{y}\right] = f(\mathbf{x}), \tag{6.9}$$

where the functions $A_r(\mathbf{x})$ and $K_r(\mathbf{x},\mathbf{y}) = B_r(\mathbf{x}) + (\mathbf{x}-\mathbf{y})k_r(\mathbf{x},\mathbf{y})$ have the following Hölder continuous derivatives:

$$\frac{d^r A_r(\mathbf{x})}{d\mathbf{x}^r}, \ \frac{\partial^r K_r(\mathbf{x},\mathbf{y})}{\partial\mathbf{x}^j d\mathbf{y}^{r-j}} \ (r = 0, ..., p; \ j = 0, ..., r), \ \frac{\partial^p k_p(\mathbf{x},\mathbf{y})}{\partial\mathbf{x}^p},$$

Theorem 6.18. *The necessary and sufficient conditions for solvability of the singular integro-differential equation (6.9) are that*

$$\int_{\partial S} f(\mathbf{x})\psi_i(\mathbf{x})d\mathbf{x} = \mathbf{0}, \quad \textit{for } i = 1, ..., n,$$

where $\{\psi_i\}_{i=1}^n$ *is the complete set linearly independent solutions of the associated adjoint homogeneous equation (i.e. adjoint of (6.9)),*

$$\sum_{r=0}^{p}(-1)^r \left[\left(A_r(\mathbf{x})\psi(\mathbf{x})\right)^{(r)} - \frac{1}{\imath\pi}\int_{\partial S} \frac{\left((\partial/\partial\mathbf{x} + \partial/\partial\mathbf{y})^r K_r(\mathbf{y},\mathbf{x})\right)\psi(\mathbf{y})d\mathbf{y}}{\mathbf{x}-\mathbf{y}} \right] = 0. \tag{6.10}$$

Similar to Noether's theory of singular integral equations, the difference between the number "m" of linearly independent solutions of the homogeneous equation $(6.9)^0$ *(the superscript* 0 *denotes the homogeneous form of the referenced equation) and the number "n" of linearly independent solutions of homogeneous equation* $(6.10)^0$ *equals the index of the equation (6.9),* $\varkappa$*, which is defined by*

$$m - n = \varkappa = \frac{1}{2\pi}\arg\left[\frac{A_p(\mathbf{x}) - B_p(\mathbf{x})}{A_p(\mathbf{x}) + B_p(\mathbf{x})}\right]_{\partial S}. \tag{6.11}$$

It is evident that in the case of $\varkappa = 0$ the number of linearly independent solutions of the homogeneous equation and its adjoint are the same and Fredholm alternative theorem determines solvability of the equation.

The above theorem for the singular integro-differential equation is also valid for systems of singular integro-differential equations [74, 144, 109]. A system of l singular integro-differential equations for the unknown matrix $\boldsymbol{\phi} = (\phi_1, ..., \phi_l)^T$ is given as,

$$\sum_{r=0}^{p}\left[\mathbf{A}_r(\mathbf{x})\boldsymbol{\phi}^{(r)}(\mathbf{x}) + \frac{\mathbf{B}_r(\mathbf{x})}{\imath\pi}\int_{\partial S}\frac{\boldsymbol{\phi}^{(r)}(\mathbf{y})d\mathbf{y}}{\mathbf{x}-\mathbf{y}} + \frac{1}{\imath\pi}\int_{\partial S}\mathbf{k}_r(\mathbf{x},\mathbf{y})\boldsymbol{\phi}^{(r)}(\mathbf{y})d\mathbf{y}\right] = \mathbf{f}(\mathbf{x}), \tag{6.12}$$

where the elements of the matrices $\mathbf{A}(\mathbf{x}), \mathbf{B}(\mathbf{x}), \mathbf{k}(\mathbf{x},\mathbf{y}) \in \mathcal{M}_{l\times l}$, and $\boldsymbol{\phi} \in \mathcal{M}_{l\times 1}$, have the same conditions as their counterparts in the equation (6.9). The adjoint homogeneous equation for (6.9) is defined by

$$\sum_{r=0}^{p}(-1)^r \left[\left(\mathbf{A}_r^T(\mathbf{x})\boldsymbol{\psi}(\mathbf{x})\right)^{(r)} - \frac{1}{\imath\pi}\int_{\partial S} \frac{(\partial/\partial\mathbf{x} + \partial/\partial\mathbf{y})^r \mathbf{K}_r^T(\mathbf{y},\mathbf{x})\boldsymbol{\psi}(\mathbf{y})d\mathbf{y}}{\mathbf{x}-\mathbf{y}} \right] = 0, \tag{6.13}$$

where, likewise $\mathbf{K}_r(\mathbf{y},\mathbf{x}) = \mathbf{B}_r(\mathbf{y}) + (\mathbf{x}-\mathbf{y})\mathbf{k}_r(\mathbf{y},\mathbf{x})$. Also, the difference between the number of linearly independent solutions of the homogeneous equation $(6.12)^0$ and the number of linearly independent solutions of its adjoint (6.13) is given by the index of the system of integro-differential equations (6.12), i.e.

$$\varkappa = \frac{1}{2\pi} \arg \left[\frac{\det \left(\mathbf{A}_p(\mathbf{x}) - \mathbf{B}_p(\mathbf{x}) \right)}{\det \left(\mathbf{A}_p(\mathbf{x}) + \mathbf{B}_p(\mathbf{x}) \right)} \right]_{\partial S}, \tag{6.14}$$

where $\det \left(\mathbf{A}_p(\mathbf{x}) \pm \mathbf{B}_p(\mathbf{x}) \right) \neq 0$. Evidently, solvability of such system of equations depends on the coefficients of the highest order of derivative of the unknown function $\boldsymbol{\phi}$ which form the dominant part of the integro-differential equation.

6.2 Uniqueness of the Solution

6.2.1 (a) Interior boundary value problem

Let S again be a bounded multiply-connected domain enclosed by ∂S which, for simplicity, here consists of two sufficiently smooth closed curves Γ and ∂S_1 ($\partial S = \Gamma \cup \partial S_1$), denoting reinforced (representing surface effects) and non-reinforced (without surface effects) boundaries, respectively (see Fig. 6.1). The non-reinforced boundary is divided into two open curves $\partial S_{\mathbf{w}}$ and $\partial S_{\mathbf{t}}$ ($\partial S_1 = \partial S_{\mathbf{t}} \cup \partial S_{\mathbf{w}}$) with common end points a and b, on which the boundary values for displacement/microrotations $\mathbf{w}^{(0)}$, and stress/couple-stress tractions, $\mathbf{t}^{(0)}$ are prescribed, respectively. We note that in the special case when a and b coincide, $\partial S_{\mathbf{t}}$ and $\partial S_{\mathbf{w}}$ are closed curves. A simple example of an interior problem is shown in Fig. 6.1.

We pose the interior mixed-boundary value problem of micropolar plane elasticity with surface reinforcement as follows: find a vector $\mathbf{w}$ belonging to an admissible function space $C^2(S) \cap C^1(\overline{S} \backslash \{a,b\})$, such that,

$$\mathbf{L}(\partial\mathbf{x})\mathbf{w}(\mathbf{x}) = \mathbf{0}, \quad \mathbf{x} \in S,$$

$$\mathbf{T}(\partial\mathbf{x})\mathbf{w}(\mathbf{x}) = \mathbf{t}^0(\mathbf{x}), \quad \mathbf{x} \in \partial S_{\mathbf{t}},$$

$$\mathbf{w}(\mathbf{x}) = \mathbf{w}^0(\mathbf{x}), \quad \mathbf{x} \in \partial S_{\mathbf{w}},$$

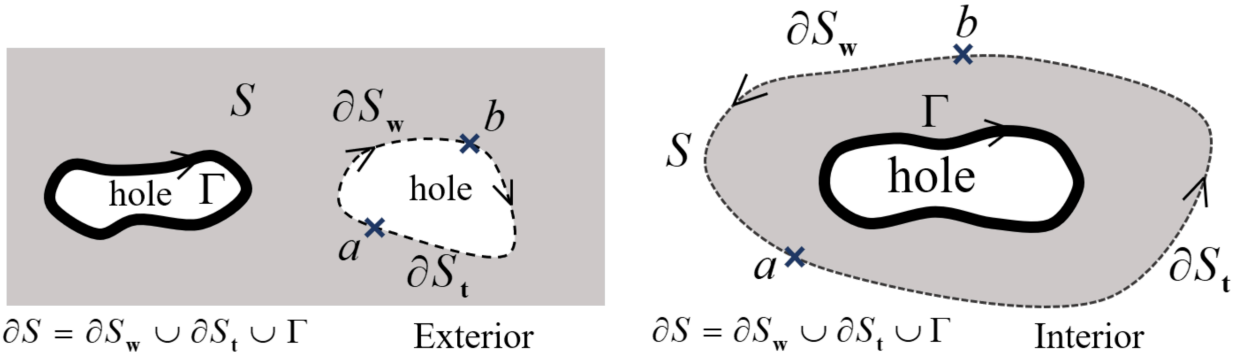

Figure 6.1: Interior and exterior problems

$$\mathbf{T}^{(i)}(\partial\mathbf{x})\mathbf{w}(\mathbf{x}) = \mathbf{A}(\mathbf{x})\mathbf{R}^{(i)}(d/ds)\mathbf{A}^{-1}(\mathbf{x})\mathbf{w} + \mathbf{A}(\mathbf{x})\mathbf{t}^{(i)}(\mathbf{x}), \quad \mathbf{x} \in \Gamma, \ i = 1, 2, \tag{6.15}$$

where $\mathbf{T}$ denotes the boundary stress operator defined in (2.19), and the superscript $i = 1, 2$, indicates the association of the corresponding quantity with the fourth and second order models, respectively.

6.2.2 (b) Exterior boundary value problem

The exterior problem is defined similarly to the interior problem except that S is now an unbounded domain with ∂S described by $\partial S = \Gamma \cup \partial S_1$. Here, again each one of the non-reinforced ($\partial S_1 = \partial S_{\mathbf{t}} \cup \partial S_{\mathbf{w}}$) and the reinforced ($\Gamma$) parts of ∂S consist of closed curves. The exterior mixed-boundary value problem of plane micropolar elasticity with surface reinforcement is as to find a vector $\mathbf{w} \in C^2(S) \cap C^1(\overline{S}\backslash\{a, b\}) \cap \mathcal{A}^*$ such that,

$$\mathbf{L}(\partial\mathbf{x})\mathbf{w}(\mathbf{x}) = \mathbf{0}, \quad \mathbf{x} \in S,$$

$$\mathbf{T}(\partial\mathbf{x})\mathbf{w}(\mathbf{x}) = \mathbf{t}^0(\mathbf{x}), \quad \mathbf{x} \in \partial S_{\mathbf{t}},$$

$$\mathbf{w}(\mathbf{x}) = \mathbf{w}^0(\mathbf{x}), \quad \mathbf{x} \in \partial S_{\mathbf{w}},$$

$$\mathbf{T}^{(i)}(\partial\mathbf{x})\mathbf{w}(\mathbf{x}) = \mathbf{A}(\mathbf{x})\mathbf{R}^{(i)}(d/ds)\mathbf{A}^{-1}(\mathbf{x})\mathbf{w} + \mathbf{A}(\mathbf{x})\mathbf{t}^{(i)}(\mathbf{x}), \quad \mathbf{x} \in \Gamma, \ i = 1, 2. \tag{6.16}$$

Note that $\mathcal{A}^*$ represents the asymptotic behavior of the solution $\mathbf{w}$ and has been defined in (2.27).

6.2.3 Uniqueness of Solutions of Interior and Exterior Problems

Theorem: Both the interior and the exterior mixed boundary-value problems (6.15 and 6.16) have at most one solution.

Proof: Let $\mathbf{w}_1$ and $\mathbf{w}_2$ be any two solutions of either the interior or exterior boundary value problem (6.15 or 6.16). The difference $\mathbf{v}^*= \mathbf{w}_1 - \mathbf{w}_2$ satisfies the following form of the problem in either case,

$$\mathbf{L}(\partial\mathbf{x})\mathbf{v}^* = \mathbf{0}, \quad \mathbf{x} \in S,$$

$$\mathbf{T}(\partial\mathbf{x})\mathbf{v}^* = \mathbf{0}, \quad \mathbf{x} \in \partial S_{\mathbf{t}},$$

$$\mathbf{v}^*= \mathbf{0}, \quad \mathbf{x} \in \partial S_{\mathbf{w}},$$

$$\mathbf{T}^{(i)}(\partial\mathbf{x})\mathbf{v}^* = \mathbf{A}(\mathbf{x})\mathbf{R}^{(i)}(d/ds)\mathbf{A}^{-1}(\mathbf{x})\mathbf{v}^*, \quad \mathbf{x} \in \Gamma, \ i = 1, 2. \tag{6.17}$$

Here, ∂S_1 and Γ represent single closed curves as shown in Figure 3. Consider the following integral over the boundary of the domain S,

$$\int\limits_{\partial S} \mathbf{v}^* \cdot \mathbf{T}^{(i)}(\partial\mathbf{x})\mathbf{v}^* ds = \int\limits_{\Gamma} \mathbf{v}^* \cdot \mathbf{T}^{(i)}(\partial\mathbf{x})\mathbf{v}^* ds + \int\limits_{\partial S_1} \mathbf{v}^* \cdot \mathbf{T}^{(i)}(\partial\mathbf{x})\mathbf{v}^* ds.$$

Using the boundary conditions in (6.17) as well as the first Betti formula given in (2.23) (or 2.29), we obtain,

$$2\int\limits_{S} E(\mathbf{v}^*, \mathbf{v}^*) dv = \int\limits_{\Gamma} \mathbf{v}^* \cdot \left(\mathbf{A}(\mathbf{x})\mathbf{R}^{(i)}(d/ds)\mathbf{A}^{-1}(\mathbf{x})\mathbf{v}^*\right) ds. \tag{6.18}$$

Using the reinforced boundary conditions (boundary conditions associated with surface effects) of the first type ($i = 1$) (2.49-2.51) and integrating by parts, the integrand on the

right-hand side of the equation (6.18) can be expanded in $(n-t)$ coordinates as

$$\begin{aligned}
&\int_{\Gamma} \mathbf{v}^*_{nt} \cdot \mathbf{R}^{(1)}(d/ds)\mathbf{v}^*_{nt} ds \\
= \; & -\int_{\Gamma} A_s \left(F_1'(s)\right)^2 ds - \int_{\Gamma} B_s \left(F_2'(s)\right)^2 ds \\
& + \int_{\Gamma} H_s F_2'(s)\varphi_3'(s) ds - \int_{\Gamma} H_s \left(\varphi_3'(s)\right)^2 ds - \int_{\Gamma} 2G_s \varphi_3 (F_2(s) + \varphi_3) ds \\
& - \int_{\Gamma} \frac{t}{2} u_0 b_0 T_0^{(1)^{nt}} \mathbf{v}^*_{nt} ds + \int_{\Gamma} \frac{t}{2} u_n \frac{d(T_0^{(1)^{nt}} \mathbf{v}^*_{nt})}{ds} ds + \int_{\Gamma} \frac{t}{2} \varphi_3 T_0^{(1)^{nt}} \mathbf{v}^*_{nt} ds, \qquad (6.19)
\end{aligned}$$

where $\mathbf{v}^*_{nt} = \mathbf{A}^{-1}(\mathbf{x})\mathbf{v}^*$ denotes the displacement/rotation expression in the $(n-t)$ coordinates. In integrating by parts, the boundary terms vanish since Γ is closed. The functions $F_1(s)$ and $F_2(s)$ are defined as,

$$F_1(s) = \frac{du_0}{ds} - u_n b_0, \qquad (6.20)$$

$$F_2(s) = u_0 b_0 + \frac{du_n}{ds}. \qquad (6.21)$$

With the assumption of a perfectly bonded interface between the reinforcement and the bulk, the continuity of stress across the interface leads to $T_0^{(1)^{nt}} \mathbf{v}^*_{nt} = 2\alpha_s \left(F_2(s) + \varphi_3\right)$. It follows that,

$$\begin{aligned}
2\int_S E(\mathbf{v}^*, \mathbf{v}^*) dv = & -\int_{\Gamma} A_s \left(F_1(s)\right)^2 ds - \int_{\Gamma} B_s \left(F_2'(s)\right)^2 ds \\
& + \int_{\Gamma} H_s F_2'(s)\varphi_3'(s) ds - \int_{\Gamma} H_s \left(\varphi_3'(s)\right)^2 ds \\
& - \int_{\Gamma} G_s (F_2(s) + \varphi_3)^2 ds. \qquad (6.22)
\end{aligned}$$

It can shown that the right-hand side of the equation (6.22) is negative definite provided that,

$$A_s > 0,\ G_s > 0,\ B_s - \frac{H_s}{4} > 0,\ H_s > 0, \qquad (6.23)$$

The foregoing conditions restrict the classical surface bending rigidity B_s and the micropolar surface twisting rigidity H_s accordingly. Another implication of the conditions (6.23) is that the fourth order surface representation confines the model to a sufficiently high surface bending rigidity, B_s, which occurs when the effective thickness t of the surface is significant. Noting that $B_s \sim t^3$ and $H_s \sim t$, the second order model appears to be preferable for a surface with small effective thickness. Eliminating the classical shear deformation removes the direct effects of surface shear rigidity M_s from the equations and the given conditions (6.23). Instead the condition $G_s > 0$ corresponding to the deviation of microstrains from classical strains plays an independent role here. From the first Betti formula and the positive definiteness of $E(\mathbf{v}^*, \mathbf{v}^*)$, the equation (6.22) holds only if both sides are set to zero. Thus, the strain energy density $E(\mathbf{v}^*, \mathbf{v}^*) = 0$ which by standard arguments implies that,

$$\mathbf{v}^* = (c_1 - c_3 x_2, c_2 + c_3 x_1, c_3),$$

for some c_1, c_2, and c_3 constants. The boundary condition $\mathbf{v}^* = \mathbf{0}$ on $\partial S_{\mathbf{w}}$ and the continuity of the solution up to the boundary enforces $\mathbf{v}^* = \mathbf{0}$ in the domain S, so any solution of the interior (and exterior) boundary value problem is unique for the type $i = 1$ boundary reinforcement (surface).

Consider the alternative second order boundary reinforcement ($i = 2$) condition (Eremeyev-Lebedev-Altenbach shell), the right-hand side of the equation (6.18) becomes

$$\begin{aligned} \int_\Gamma \mathbf{v}^*_{nt} \cdot \mathbf{R}^{(2)} (d/ds) \mathbf{v}^*_{nt} ds &= -\int_\Gamma A_s \left(F_1(s)\right)^2 ds - \int_\Gamma \left(M_s + G_s\right) \left(F_2(s) + \varphi_3(s)\right)^2 ds \\ &\quad - \int_\Gamma \left(H_s + B_s\right) \left(\varphi_3'(s)\right)^2 ds \\ &= 2 \int_S E(\mathbf{v}^*, \mathbf{v}^*) dv, \end{aligned} \tag{6.24}$$

which using the same argument and positive definiteness of the strain energy enforces $E(\mathbf{v}^*, \mathbf{v}^*) = 0$ when,

$$A_s > 0,\ M_s + G_s > 0,\ H_s + B_s > 0. \tag{6.25}$$

The conditions (6.25) are similar to the positive definiteness conditions of internal energy in micropolar shells and plates [47, 2] in the special case when the drilling component of both rotation and microrotation vectors vanish (in our notation $\varphi_n = 0$) and the in-surface rotation and microrotations coincide. In other words, the surface shell is regarded as a couple stress material in this case. Therefore, the contribution of classical bending and micropolar twisting rigidities appear as a sum $H_s + B_s$ in material surface parameters [1]. Notice the slightly different conditions placed on the surface moduli in this case. The foregoing theorem can be generalized in a straightforward manner to the cases when each of ∂S_1 and Γ consist of a union of a finite number of closed curves as well as when ∂S_1 consists of more than two partitions $\partial S_{\mathbf{w}}$ and $\partial S_{\mathbf{t}}$.

6.3 Existence of Solutions

6.3.1 Reduction to singular integral equations

In the following representations the superscript "0" denotes the homogeneous version of the corresponding equation and the subscripts, "I" and "E", the correspondence to the interior and exterior formulations. In addition, the superscript (i) on the parameters no longer means the correspondence to the fourth and second order models. Instead, we will investigate each model in a separate section. Following the approach in Schiavone and Ru [125], using known solutions for the related Dirichlet and Neumann problems of the equation (2.17), we can reduce the interior and exterior boundary value problems to simpler forms with homogeneous conditions on $\partial S_{\mathbf{t}}$ and $\partial S_{\mathbf{w}}$. Consequently, we may consider the following mixed boundary value problem:

find $\mathbf{w} \in C^2(S) \cap C^1(\overline{S} \backslash \{a, b\})$ such that,

$$\begin{aligned}
\mathbf{L}(\partial\mathbf{x})\mathbf{w}(\mathbf{x}) &= \mathbf{0}, \quad \mathbf{x} \in S, \\
\mathbf{T}(\partial\mathbf{x})\mathbf{w}(\mathbf{x}) &= \mathbf{0}, \quad \mathbf{x} \in \partial S_{\mathbf{t}}, \\
\mathbf{w}(\mathbf{x}) &= \mathbf{0}, \ \ \mathbf{x} \in \partial S_{\mathbf{w}}, \\
\mathbf{T}(\partial\mathbf{x})\mathbf{w}(\mathbf{x}) &= \mathbf{A}(\mathbf{x})\mathbf{R}\mathbf{A}^{-1}(\mathbf{x})\mathbf{w}(\mathbf{x}) + \mathbf{A}(\mathbf{x})\mathbf{t}(\mathbf{x}), \ \ \mathbf{x} \in \Gamma.
\end{aligned} \tag{6.26}$$

The foregoing system describes the interior problem when S is bounded and the exterior problem when S is unbounded and the requirement $\mathbf{w} \in \mathcal{A}^*$ is added.

(a) Interior problem

We begin by constructing an auxilliary solution $\mathbf{D}_1 \in \mathcal{M}_{3\times 3}$ for use later in the existence results. Let Ω_1 be a multiply-connected domain with sufficiently smooth boundary $\partial\Omega_1$ such that,

$$S \subset \Omega_1, \;\; \Gamma \subset \Omega_1, \;\; (\partial S_{\mathbf{t}} \cup \partial S_{\mathbf{w}}) \subseteq \partial\Omega_1.$$

We define a matrix $\mathbf{D}_1(\mathbf{x},\mathbf{y}) \in \mathcal{M}_{3\times 3}$ with $\mathbf{y} \in \Gamma$ whose columns $\mathbf{D}_1^{(i)}(\mathbf{x},\mathbf{y})$, $i = 1,2,3$, satisfy the following mixed boundary value problem:

$$\begin{aligned}
\mathbf{L}(\partial\mathbf{x})\mathbf{D}_1^{(i)}(\mathbf{x},\mathbf{y}) &= \mathbf{0}, \qquad \mathbf{x} \in \Omega_1, \\
\mathbf{T}(\partial\mathbf{x})\mathbf{D}_1^{(i)}(\mathbf{x},\mathbf{y}) &= \mathbf{T}(\partial\mathbf{x})\mathbf{D}^{(i)}(\mathbf{x},\mathbf{y}), \qquad \mathbf{x} \in \partial S_{\mathbf{t}}, \\
\mathbf{D}_1^{(i)}(\mathbf{x},\mathbf{y}) &= \mathbf{D}^{(i)}(\mathbf{x},\mathbf{y}), \;\; \mathbf{x} \in \partial\Omega_1 \backslash \partial S_{\mathbf{t}}.
\end{aligned} \tag{6.27}$$

Clearly, the boundary values $\mathbf{D}^{(i)}(\mathbf{x},\mathbf{y})$ are smooth since $\mathbf{x} \neq \mathbf{y}$ ever. Consequently, from the existence results in [123] for a homogeneous mixed boundary value problem with smooth boundary conditions there exists a unique smooth solution $\mathbf{D}_1^{(i)}(\mathbf{x},\mathbf{y})$ for all $\mathbf{y} \in \Gamma$ in the class $C^2(\Omega_1) \cap C^1(\overline{\Omega}_1/\{a,b\})$.

We look for a solution of $(6.26)_I$ in the form of a modified single layer potential:

$$\mathbf{w}(\mathbf{x}) = (V\boldsymbol{\phi})_I(\mathbf{x}) = \int_\Gamma \left(\mathbf{D}(\mathbf{x},\mathbf{y}) - \mathbf{D}_1(\mathbf{x},\mathbf{y})\right) \mathbf{A}(\mathbf{y})\boldsymbol{\phi}(\mathbf{y}) dS_{\mathbf{y}}, \;\; \mathbf{x} \in S, \tag{6.28}$$

where $\boldsymbol{\phi} \in \mathcal{M}_{3\times 1} \cap C^{3,\alpha}(\Gamma)$ with $0 < \alpha < 1$ is an unknown density matrix function on Γ in $(n-\tau)$ coordinates. From the properties of the single layer potential of plane-strain micropolar elasticity [123], it is not difficult to check that the following conditions of $(6.26)_I$ are satisfied:

$$\mathbf{L}(\partial\mathbf{x})\mathbf{w}(\mathbf{x}) = \int_\Gamma \mathbf{L}\left(\mathbf{D}(\mathbf{x},\mathbf{y}) - \mathbf{D}_1(\mathbf{x},\mathbf{y})\right) \mathbf{A}(\mathbf{y})\boldsymbol{\phi}(\mathbf{y}) dS_{\mathbf{y}} = \mathbf{0}, \;\; \mathbf{x} \in S,$$

$$\mathbf{T}(\partial\mathbf{x})\mathbf{w}(\mathbf{x}) = \int_\Gamma \mathbf{T}\left(\mathbf{D}(\mathbf{x},\mathbf{y}) - \mathbf{D}_1(\mathbf{x},\mathbf{y})\right) \mathbf{A}(\mathbf{y})\boldsymbol{\phi}(\mathbf{y}) dS_{\mathbf{y}} = \mathbf{0}, \;\; (\Omega_1 \ni \mathbf{x} \to \partial S_{\mathbf{t}}),$$

$$\mathbf{w}(\mathbf{x})=\int_{\Gamma}\left(\mathbf{D}(\mathbf{x},\mathbf{y})-\mathbf{D}_1(\mathbf{x},\mathbf{y})\right)\mathbf{A}(\mathbf{y})\boldsymbol{\phi}(\mathbf{y})dS_{\mathbf{y}}=\mathbf{0},\ \ (\Omega_1\ni\mathbf{x}\to\partial S_{\mathbf{w}}).$$

The remaining traction boundary condition on Γ leads to a system of singular integral equations when we approach $\Omega_1\ni\mathbf{x}\to\mathbf{x}\in\Gamma$, and since $\mathbf{y}\in\Gamma$, we use the Sokhotski-Plemelj theorem to find,

$$\mathbf{T}(V^{+}\boldsymbol{\phi})=\left(W_0^{*}+\frac{1}{2}\mathbf{I}\right)\boldsymbol{\phi}$$

where W_0^{*} indicates the adjoint of a modified double layer potential defined by,

$$(W\boldsymbol{\phi})_I(\mathbf{x})=\int_{\Gamma}\mathbf{T}(\partial\mathbf{y})\left(\mathbf{D}(\mathbf{x},\mathbf{y})-\mathbf{D}_1(\mathbf{x},\mathbf{y})\right)\mathbf{A}(\mathbf{y})\boldsymbol{\phi}(\mathbf{y})dS_{\mathbf{y}},\ \mathbf{x}\in\Gamma. \tag{6.29}$$

Based on this fact, the boundary condition on Γ can be written as,

$$\begin{aligned}&\frac{1}{2}\boldsymbol{\phi}(\mathbf{x})+\mathbf{A}^{-1}(\mathbf{x})\int_{\Gamma}\mathbf{T}(\partial\mathbf{x})\mathbf{D}(\mathbf{x},\mathbf{y})\mathbf{A}(\mathbf{y})\boldsymbol{\phi}(\mathbf{y})dS_{\mathbf{y}}-\mathbf{R}^{*}(d_{\mathbf{x}})d_{\mathbf{x}}\mathbf{A}^{-1}(\mathbf{x})\int_{\Gamma}\mathbf{D}(\mathbf{x},\mathbf{y})\mathbf{A}(\mathbf{y})\boldsymbol{\phi}(\mathbf{y})dS_{\mathbf{y}}\\&=-\mathbf{R}^{*}(d_{\mathbf{x}})d_{\mathbf{x}}\mathbf{A}^{-1}(\mathbf{x})\int_{\Gamma}\mathbf{D}_1(\mathbf{x},\mathbf{y})\mathbf{A}(\mathbf{y})\boldsymbol{\phi}(\mathbf{y})dS_{\mathbf{y}}+\mathbf{A}^{-1}(\mathbf{x})\int_{\Gamma}\mathbf{T}(\partial\mathbf{x})\mathbf{D}_1(\mathbf{x},\mathbf{y})\mathbf{A}(\mathbf{y})\boldsymbol{\phi}(\mathbf{y})dS_{\mathbf{y}}\\&+\mathbf{R}_0\mathbf{A}^{-1}(\mathbf{x})\int_{\Gamma}\left(\mathbf{D}(\mathbf{x},\mathbf{y})-\mathbf{D}_1(\mathbf{x},\mathbf{y})\right)\mathbf{A}(\mathbf{y})\boldsymbol{\phi}(\mathbf{y})dS_{\mathbf{y}}+\mathbf{t}(\mathbf{x}),\ \mathbf{x}\in\Gamma.\end{aligned} \tag{6.30}$$

The integrals on the right-hand side are Fredholm-type integrals with at most weakly singular kernels. The first integral on the left-hand side has a singular kernel. However, this integral has already been investigated in detail by Schiavone [123] and Ieşan [71]. In the next section we shall focus on the second integral on the left-hand side in order to reduce it to a standard singular integro-differential form which we can evaluate in terms of the results given in [144].

Theorem 6.19. *The homogeneous form of the equation (6.30)^0 (i.e. when $\mathbf{t}(\mathbf{x})=\mathbf{0}$) has only the trivial solution.*

Proof. Let $\boldsymbol{\phi}_0\in C^{3,\alpha}(\Gamma)$ be a solution of $(6.30)_I^0$. Then,

$$(V\boldsymbol{\phi}_0)_I(\mathbf{x})=\int_{\Gamma}\left(\mathbf{D}(\mathbf{x},\mathbf{y})-\mathbf{D}_1(\mathbf{x},\mathbf{y})\right)\mathbf{A}(\mathbf{y})\boldsymbol{\phi}_0(\mathbf{y})dS_{\mathbf{y}},$$

solves the homogeneous interior problem from $(6.26)_I^0$ (i.e. when $\mathbf{t}(\mathbf{x})=\mathbf{0}$). The theorem of uniqueness of solutions for the mixed boundary value problem asserts that $(V\boldsymbol{\phi}_0)_I(\mathbf{x})=\mathbf{0}$ in

$\mathbf{x} \in S$ and the continuity of a single layer potential [123] establishes $(V\boldsymbol{\phi}_0)_I(\mathbf{x}) = \mathbf{0}$, on the boundary $\mathbf{x} \in \partial S$, which means $(V\boldsymbol{\phi}_0)_I(\mathbf{x}) = \mathbf{0}$, $\mathbf{x} \in \Gamma$. The definition of $\mathbf{D}_1(\mathbf{x}, \mathbf{y})$ implies that,

$$\begin{aligned} \mathbf{L}(\partial\mathbf{x})(V\boldsymbol{\phi}_0)_I(\mathbf{x}) &= \mathbf{0},\ \mathbf{x} \in \Omega_1\backslash S, \\ (V\boldsymbol{\phi}_0)_I(\mathbf{x}) &= \mathbf{0},\ \mathbf{x} \in \partial\Omega_1\backslash\partial S, \\ (V\boldsymbol{\phi}_0)_I(\mathbf{x}) &= \mathbf{0},\ \mathbf{x} \in \Gamma. \end{aligned} \tag{6.31}$$

The solution to the resulting interior Dirichlet problem of micropolar elasticity is unique (see [123]); hence $(V\boldsymbol{\phi}_0)_I(\mathbf{x}) = \mathbf{0}$ in the bounded domain $\Omega_1\backslash S$. The Sokhotski-Plemelj theorem for jump relations appear upon applying the $\mathbf{T}(\partial\mathbf{x})$-operator to the single layer potential (see [123]) and yield

$$(\mathbf{T}V)_I^+(\boldsymbol{\phi}_0)(\mathbf{x}') - (\mathbf{T}V)_I^-(\boldsymbol{\phi}_0)(\mathbf{x}') = \boldsymbol{\phi}_0(\mathbf{x}) = 0,\ \mathbf{x} \in \Gamma.$$

This completes the proof. The superscripts $+$ and $-$ indicate $\mathbf{x}' \to \mathbf{x} \in \Gamma$ ($\mathbf{x}' \notin \Gamma$) approaching from interior and exterior of Γ, respectively.

(b) Exterior problem

Let Ω_2 be a multiply connected infinite domain with sufficiently smooth boundary $\partial\Omega_2$. For the exterior problem of $(6.26)_E$, we assume

$$S \subset \Omega_2,\ \ \Gamma \subset \Omega_2,\ \ (\partial S_{\mathbf{t}} \cup \partial S_{\mathbf{w}}) \subseteq \partial\Omega_2,\ \{0\} \notin \overline{\Omega}_2.$$

We define a matrix $\mathbf{D}_2(\mathbf{x}, \mathbf{y}) \in \mathcal{M}_{3\times 3}$ for which $\mathbf{y} \in \Gamma$, and the columns $\mathbf{D}_2^{(i)}$ each satisfy the following mixed boundary value problem:

$$\begin{aligned} \mathbf{L}(\partial\mathbf{x})\mathbf{D}_2^{(i)}(\mathbf{x}, \mathbf{y}) &= \mathbf{0}, \qquad \mathbf{x} \in \Omega_2, \\ \mathbf{T}(\partial\mathbf{x})\mathbf{D}_2^{(i)}(\mathbf{x}, \mathbf{y}) &= \mathbf{T}(\partial\mathbf{x})\boldsymbol{\Psi}^{(i)}(\mathbf{x}, \mathbf{y}), \qquad \mathbf{x} \in \partial S_{\mathbf{t}}, \\ \mathbf{D}_2^{(i)}(\mathbf{x}, \mathbf{y}) &= \boldsymbol{\Psi}^{(\mathbf{i})}(\mathbf{x}, \mathbf{y}),\ \ \mathbf{x} \in \partial\Omega_2\backslash\partial S_{\mathbf{t}}, \end{aligned} \tag{6.32}$$

where $\mathbf{\Psi} \in \mathcal{M}_{3\times 3}$ is given by

$$\mathbf{\Psi}(\mathbf{x},\mathbf{y}) = \mathbf{D}(\mathbf{x},\mathbf{y}) - \mathbf{M}^{\infty}(\mathbf{x})\mathbf{F}^{T}(\mathbf{y}),$$

where $\mathbf{M}^{\infty}(\mathbf{x}) \in \mathcal{M}_{3\times 3}$ is written in polar coordinates as [123],

$$\mathbf{M}^{\infty}(r,\theta) = \frac{1}{4\pi\mu(\beta+1)} \begin{bmatrix} -2\beta(\ln r + 1) + \cos 2\theta & \sin 2\theta & r^{-1}(\beta+1)\sin\theta \\ \sin 2\theta & -2\beta(\ln r + 1) - \cos 2\theta & -r^{-1}(\beta+1)\cos\theta \\ r^{-1}(\beta+1)\sin\theta & -r^{-1}(\beta+1)\cos\theta & 0 \end{bmatrix}, \tag{6.33}$$

with $r = |\mathbf{x}|$, $\theta = \tan^{-1}(x_2/x_1)$, and β defined as in (2.26). The existence results for the exterior mixed problems of asymmetric elasticity [123] prove that for each $\mathbf{y} \in \Gamma$, $\mathbf{D}_2^{(i)}(\mathbf{x},\mathbf{y})$ exists uniquely in the class $C^2(\Omega_1) \cap C^1(\overline{\Omega}_1 \backslash \{a,b\}) \cap \mathcal{A}^*$.

We seek the solution of $(6.26)_E$ in the form of the following modified single-layer potential:

$$\mathbf{w}(\mathbf{x}) = (V\boldsymbol{\phi})_E(\mathbf{x}) = \int_{\Gamma} \left(\mathbf{\Psi}(\mathbf{x},\mathbf{y}) - \mathbf{D}_2(\mathbf{x},\mathbf{y})\right) \mathbf{A}(\mathbf{y})\boldsymbol{\phi}(\mathbf{y}) dS_{\mathbf{y}}, \tag{6.34}$$

where $\boldsymbol{\phi} \in \mathcal{M}_{3\times 1} \cap C^{3,\alpha}(\Gamma)$ on Γ with $0 < \alpha < 1$ is again an unknown density matrix function in $(n-\tau)$ coordinates. Clearly, from the properties of the single-layer potential, $(V\boldsymbol{\phi})_E(\mathbf{x})$ in (6.34) satisfies the conditions of the exterior problem $(6.26)_E$ except the traction boundary conditions on Γ, which leads to a system of singular integral equations. It also remains to show that $(V\boldsymbol{\phi})_E(\mathbf{x}) \in \mathcal{A}^*$. Following the method given by Constanda [20], as $|\mathbf{x}| \longrightarrow \infty$,

$$\begin{aligned} \int_{\Gamma} \mathbf{\Psi}(\mathbf{x},\mathbf{y})\mathbf{A}(\mathbf{y})\boldsymbol{\phi}(\mathbf{y}) dS_{\mathbf{y}} &= \int_{\Gamma} \mathbf{D}(\mathbf{x},\mathbf{y})\mathbf{A}(\mathbf{y})\boldsymbol{\phi}(\mathbf{y}) dS_{\mathbf{y}} - \mathbf{M}^{\infty}(\mathbf{x}) \int_{\Gamma} \mathbf{F}^{T}(\mathbf{y})\mathbf{A}(\mathbf{y})\boldsymbol{\phi}(\mathbf{y}) dS_{\mathbf{y}} \\ &= \mathbf{w}^{\mathcal{A}} + \mathbf{M}^{\infty}(\mathbf{x}) \int_{\mathbf{\Gamma}} \mathbf{F}^{\mathbf{T}}(\mathbf{y})\mathbf{A}(\mathbf{y})\boldsymbol{\phi}(\mathbf{y}) \mathbf{dS}_{\mathbf{y}} \\ &\quad -\mathbf{M}^{\infty}(\mathbf{x}) \int_{\Gamma} \mathbf{F}^{T}(\mathbf{y})\mathbf{A}(\mathbf{y})\boldsymbol{\phi}(\mathbf{y}) dS_{\mathbf{y}} \\ &= \mathbf{w}^{\mathcal{A}} \in \mathcal{A}. \end{aligned}$$

Also since $\mathbf{D}_2^{(i)}(\mathbf{x},\mathbf{y}) \in \mathcal{A}^*$, for all $\mathbf{y} \in \Gamma$, then

$$\int_{\Gamma} \mathbf{D}_2(\mathbf{x},\mathbf{y})\mathbf{A}(\mathbf{y})\boldsymbol{\phi}(\mathbf{y}) dS_{\mathbf{y}} = \int_{\Gamma} \mathbf{D}_2^{(i)}(\mathbf{x},\mathbf{y})(\mathbf{A}\boldsymbol{\phi})_i(\mathbf{y}) dS_{\mathbf{y}} \in \mathcal{A}^*.$$

In the above, $(\mathbf{A}\boldsymbol{\phi})_i$ are the components of the matrix $\mathbf{A}\boldsymbol{\phi} \in \mathcal{M}_{3\times 1}$. Consequently, $\mathbf{w}$ will be of the class $\mathcal{A}^*$. Using the boundary integral form of the solution and application of the $\mathbf{T}(\partial\mathbf{x})$-operator to the single layer potential, as with the interior problem, the remaining boundary condition of the exterior problem on Γ is reduced to the following system of singular integral equations on Γ:

$$\begin{aligned}
&\frac{1}{2}\boldsymbol{\phi}(\mathbf{x})+\mathbf{A}^{-1}(\mathbf{x})\int_\Gamma \mathbf{T}(\partial\mathbf{x})\mathbf{D}(\mathbf{x},\mathbf{y})\mathbf{A}(\mathbf{y})\boldsymbol{\phi}(\mathbf{y})dS_{\mathbf{y}} - \mathbf{R}^*(d_{\mathbf{x}})d_{\mathbf{x}}\mathbf{A}^{-1}(\mathbf{x})\int_\Gamma \mathbf{D}(\mathbf{x},\mathbf{y})\mathbf{A}(\mathbf{y})\boldsymbol{\phi}(\mathbf{y})dS_{\mathbf{y}}\\
=\;& -\mathbf{R}^*(d_{\mathbf{x}})d_{\mathbf{x}}\mathbf{A}^{-1}(\mathbf{x})\int_\Gamma \left(\mathbf{M}^\infty(\mathbf{x})\mathbf{F}^T(\mathbf{y})+\mathbf{D}_2(\mathbf{x},\mathbf{y})\right)\mathbf{A}(\mathbf{y})\boldsymbol{\phi}(\mathbf{y})dS_{\mathbf{y}}\\
+\;& \mathbf{A}^{-1}(\mathbf{x})\int_\Gamma \mathbf{T}(\partial\mathbf{x})\left(\mathbf{D}_2(\mathbf{x},\mathbf{y})+\mathbf{M}^\infty(\mathbf{x})\mathbf{F}^T(\mathbf{y})\right)\mathbf{A}(\mathbf{y})\boldsymbol{\phi}(\mathbf{y})dS_{\mathbf{y}}\\
+\;& \mathbf{R}_0\mathbf{A}^{-1}(\mathbf{x})\int_\Gamma \left(\boldsymbol{\Psi}(\mathbf{x},\mathbf{y})-\mathbf{D}_2(\mathbf{x},\mathbf{y})\right)\mathbf{A}(\mathbf{y})\boldsymbol{\phi}(\mathbf{y})dS_{\mathbf{y}}+\mathbf{t}(\mathbf{x}),\ \mathbf{x}\in\Gamma. \qquad (6.35)
\end{aligned}$$

The integrals on the left-hand side of (6.35) are interpreted in the sense of principal value as they have Cauchy-type singularities, while the integrals on the right-hand side are improper integrals with Fredholm kernels. Again, knowing that the first integral on the left-hand side has been studied in [71] and [123], we focus our attention on the second integral on the left-hand side and reduce it to a more familiar singular integro-differential form. Before ending this section, however, we establish the following theorem which is required later in the analysis.

Theorem 6.20. *The homogeneous form of the equation (6.35)^0 (i.e. when $\mathbf{t}(\mathbf{x})=\mathbf{0}$) has only the trivial solution.*

Proof. Let $\boldsymbol{\phi}_0 \in C^{3,\alpha}(\Gamma)$ be a solution of $(6.35)^0$. Then,

$$(V\boldsymbol{\phi}_0)_E(\mathbf{x}) = \int_\Gamma \left(\boldsymbol{\Psi}(\mathbf{x},\mathbf{y})-\mathbf{D}_2(\mathbf{x},\mathbf{y})\right)\mathbf{A}(\mathbf{y})\boldsymbol{\phi}_0(\mathbf{y})dS_{\mathbf{y}},$$

solves the homogeneous exterior problem of $(6.26)^0_E$ (i.e. when $\mathbf{t}(\mathbf{x})=\mathbf{0}$). The uniqueness theorem for the exterior problem [59] now asserts that $(V\boldsymbol{\phi}_0)_E(\mathbf{x})=\mathbf{0}$, $\mathbf{x}\in S$. Analogous to the proof of the theorem for the interior problem, we show that $(V\boldsymbol{\phi}_0)_E(\mathbf{x})=\mathbf{0}$, $\mathbf{x}\in\Omega_2\backslash S$, and therefore, $(V\boldsymbol{\phi}_0)_E(\mathbf{x})$ vanishes on both sides of Γ. By applying the $\mathbf{T}(\partial\mathbf{x})$-operator to

the single-layer potential, and considering the Sokhotski-Plemelj theorem for jump relations we will have,

$$(\mathbf{T}V)^{+}_{E}(\boldsymbol{\phi}_0)(\mathbf{x}')-(\mathbf{T}V)^{-}_{E}(\boldsymbol{\phi}_0)(\mathbf{x}')=\boldsymbol{\phi}_0(\mathbf{x})=0,\ \mathbf{x}\in\Gamma,$$

which proves the theorem. The superscripts $+$ and $-$ indicate $\mathbf{x}'\to\mathbf{x}\in\Gamma$ ($\mathbf{x}'\notin\Gamma$) approaching from the interior and exterior of Γ, respectively.

6.3.2 Singular Integro-differential Equation in the Standard Form

In this section we focus on the term

$$\mathbf{R}^{*}(d_{\mathbf{x}})d_{\mathbf{x}}\mathbf{A}^{-1}(\mathbf{x})\int_{\Gamma}\mathbf{D}(\mathbf{x},\mathbf{y})\mathbf{A}(\mathbf{y})\boldsymbol{\phi}(\mathbf{y})dS_{\mathbf{y}}, \tag{6.36}$$

which appears in both interior and exterior problems. Before analyzing the foregoing integral, we remind ourselves that the first integral on the left-hand side of both equations (6.30) and (6.35) has been investigated by Ieşan [71] and Schiavone [124]:

$$\begin{aligned}&\mathbf{A}^{-1}(\mathbf{x})\int_{\Gamma}\mathbf{T}(\partial\mathbf{x})\mathbf{D}(\mathbf{x},\mathbf{y})\mathbf{A}(\mathbf{y})\boldsymbol{\phi}(\mathbf{y})dS_{\mathbf{y}}\\ =\ &-\frac{c}{2\pi}\begin{bmatrix}0&1&0\\-1&0&0\\0&0&0\end{bmatrix}\int_{\Gamma}\frac{\phi(\mathbf{y})}{\mathbf{x}-\mathbf{y}}dS_{\mathbf{y}}+\int_{\Gamma}\mathbf{K}_0(\mathbf{x},\mathbf{y})\phi(\mathbf{y})dS_{\mathbf{y}},\end{aligned} \tag{6.37}$$

where,

$$c=\frac{(\mu+\alpha)(\mu-\alpha)-\alpha\lambda}{(\mu+\alpha)(2\mu+\lambda)},$$

and $\mathbf{K}_0$ is a weakly singular (Fredholm) kernel.

Let us now consider the second integral in the left-hand side (6.36) which can be represented as

$$\begin{aligned}&\mathbf{R}^{*}(d_{\mathbf{x}})d_{\mathbf{x}}\mathbf{A}^{-1}(\mathbf{x})\int_{\Gamma}\mathbf{D}(\mathbf{x},\mathbf{y})\mathbf{A}(\mathbf{y})\boldsymbol{\phi}(\mathbf{y})dS_{\mathbf{y}}\\ =\ &\mathbf{R}_4\int_{\Gamma}(d^4/ds_x^4)\left[\mathbf{A}^{-1}(\mathbf{x})\mathbf{D}(\mathbf{x},\mathbf{y})\right]\mathbf{A}(\mathbf{y})\boldsymbol{\phi}(\mathbf{y})dS_{\mathbf{y}}+\mathbf{R}_3\int_{\Gamma}(d^3/ds_x^3)\left[\mathbf{A}^{-1}(\mathbf{x})\mathbf{D}(\mathbf{x},\mathbf{y})\right]\mathbf{A}(\mathbf{y})\boldsymbol{\phi}(\mathbf{y})dS_{\mathbf{y}}\\ &+\mathbf{R}_2\int_{\Gamma}(d^2/ds_x^2)\left[\mathbf{A}^{-1}(\mathbf{x})\mathbf{D}(\mathbf{x},\mathbf{y})\right]\mathbf{A}(\mathbf{y})\boldsymbol{\phi}(\mathbf{y})dS_{\mathbf{y}}\\ &+\mathbf{R}_1\int_{\Gamma}(d/ds_x)\left[\mathbf{A}^{-1}(\mathbf{x})\mathbf{D}(\mathbf{x},\mathbf{y})\right]\mathbf{A}(\mathbf{y})\boldsymbol{\phi}(\mathbf{y})dS_{\mathbf{y}}.\end{aligned} \tag{6.38}$$

It is convenient to evaluate the terms of the foregoing representation in complex form. We regard the plane of the problem as a complex plane where points corresponding to $\mathbf{x}$ and $\mathbf{y}$ are defined as $x = x_1 + \imath x_2$ and $y = y_1 + \imath y_2$, and, without loss of generality, we write for a function f on Γ that $f(z) = f(x)$, where $z = x_1 + \imath x_2$. Note that,

$$\begin{aligned} e^{\imath\theta(\mathbf{y})} dS_{\mathbf{y}} &= dy,\ e^{\imath\theta(\mathbf{x})} dS_{\mathbf{x}} = dx,\ x - y = |x - y|\, e^{\imath\beta(\mathbf{x}-\mathbf{y})}, \\ &\lim_{\mathbf{x}\to\mathbf{y}} \cos\left[\theta(\mathbf{x}) - \beta(\mathbf{x}-\mathbf{y})\right] e^{\imath(\beta(\mathbf{x}-\mathbf{y})-\theta(\mathbf{y}))} = 1, \end{aligned}$$

where $\beta(\mathbf{x}-\mathbf{y})$ is the angle between x_1-axis and vector $\mathbf{x}-\mathbf{y}$ so that,

$$\cos\beta = \frac{x_1 - y_1}{|x-y|},\ \sin\beta = \frac{x_2 - y_2}{|x-y|}.$$

The procedure of finding the fundamental solution is given by [19], and in our case $\mathbf{D}(\mathbf{x},\mathbf{y}) = \mathbf{L}^* t(\mathbf{x},\mathbf{y})$. The matrix of fundamental solution therefore can be written as

$$\mathbf{D}(\mathbf{x},\mathbf{y}) = -\frac{1}{2\pi} \begin{bmatrix} b & 0 & 0 \\ 0 & b & 0 \\ 0 & 0 & \frac{1}{\gamma} \end{bmatrix} \ln(|\mathbf{x}-\mathbf{y}|) + \mathbf{D}_0(\mathbf{x},\mathbf{y}), \tag{6.39}$$

where $\mathbf{D}_0(\mathbf{x},\mathbf{y})$ is a matrix of non-singular terms and

$$b = \frac{3\mu + \lambda - \alpha}{2(2\mu+\lambda)(\mu+\alpha)}.$$

It can be shown that $\mathbf{R}^*(d_{\mathbf{x}}) d_{\mathbf{x}} \left[\mathbf{A}^{-1}(\mathbf{x}) \mathbf{D}_0(\mathbf{x},\mathbf{y})\right] \mathbf{A}(\mathbf{y})$ is a Fredholm kernel for $\theta \in C^4(\Gamma)$. Therefore, the system of singular integral equations on Γ for both interior and the exterior problems are represented by

$$\begin{aligned} &\frac{1}{2}\boldsymbol{\phi}(\mathbf{x}) + \mathbf{A}^{-1}(\mathbf{x}) \int_\Gamma \mathbf{T}(\partial\mathbf{x}) \mathbf{D}(\mathbf{x},\mathbf{y}) \mathbf{A}(\mathbf{y}) \boldsymbol{\phi}(\mathbf{y}) dS_{\mathbf{y}} \\ &+ \frac{1}{2\pi} \begin{bmatrix} b & 0 & 0 \\ 0 & b & 0 \\ 0 & 0 & \frac{1}{\gamma} \end{bmatrix} \int_\Gamma \mathbf{R}^*(d_{\mathbf{x}}) d_{\mathbf{x}} \left[\mathbf{A}^{-1}(\mathbf{x}) \ln(|\mathbf{x}-\mathbf{y}|)\right] \mathbf{A}(\mathbf{y}) \boldsymbol{\phi}(\mathbf{y}) dS_{\mathbf{y}} \\ = &\int_\Gamma \boldsymbol{\Lambda}(\mathbf{x},\mathbf{y}) \boldsymbol{\phi}(\mathbf{y}) dS_{\mathbf{y}} + \mathbf{t}(\mathbf{x}),\ \mathbf{x} \in \Gamma. \end{aligned} \tag{6.40}$$

Here, the weakly singular kernel $\mathbf{\Lambda}(\mathbf{x},\mathbf{y})$ assumes different forms for the interior and exterior problems. Through the conversion of integrals into complex representation, we find that,

$$
\begin{aligned}
&\int_\Gamma d_{\mathbf{x}}^4 \left[\mathbf{A}^{-1}(\mathbf{x})\ln(|\mathbf{x}-\mathbf{y}|)\right]\mathbf{A}(\mathbf{y})\boldsymbol{\phi}(\mathbf{y})dS_{\mathbf{y}}\\
=\;& \left\{d_{\mathbf{x}}\left[\left(d_{\mathbf{x}}\mathbf{A}^{-1}(\mathbf{x})\right)\mathbf{A}(\mathbf{x})e^{\imath\theta(\mathbf{x})}+d_{\mathbf{x}}e^{\imath\theta(\mathbf{x})}\right]\right\}\int_\Gamma\frac{\boldsymbol{\phi}'(y)}{x-y}dy\\
&+\left[d_{\mathbf{x}}\left(e^{2\imath\theta(\mathbf{x})}\right)\right]\int_\Gamma\frac{\boldsymbol{\phi}''(y)}{x-y}dy+e^{3\imath\theta(\mathbf{x})}\int_\Gamma\frac{\boldsymbol{\phi}'''(y)}{x-y}dy\\
&+\left\{2d_{\mathbf{x}}\left[\left(d_{\mathbf{x}}^2\mathbf{A}^{-1}(\mathbf{x})\right)\mathbf{A}(\mathbf{x})\right]+d_{\mathbf{x}}\left[\left(d_{\mathbf{x}}\mathbf{A}^{-1}(\mathbf{x})\right)\left(d_{\mathbf{x}}\mathbf{A}(\mathbf{x})\right)\right]\right\}\int_\Gamma\frac{\boldsymbol{\phi}(y)}{x-y}dy\\
&+\left\{2\left[d_{\mathbf{x}}^2\mathbf{A}^{-1}(\mathbf{x})\right]\mathbf{A}(\mathbf{x})+\left(d_{\mathbf{x}}\mathbf{A}^{-1}(\mathbf{x})\right)\left(d_{\mathbf{x}}\mathbf{A}(\mathbf{x})\right)\right\}e^{\imath\theta(\mathbf{x})}\int_\Gamma\frac{\boldsymbol{\phi}'(y)}{x-y}dy\\
&+\left\{\left(d_{\mathbf{x}}e^{i\theta(\mathbf{x})}\right)+\left(d_{\mathbf{x}}\mathbf{A}^{-1}(\mathbf{x})\right)\mathbf{A}(\mathbf{x})e^{\imath\theta(\mathbf{x})}\right\}e^{\imath\theta(\mathbf{x})}\int_\Gamma\frac{\boldsymbol{\phi}''(y)}{x-y}dy\\
&+\left(d_{\mathbf{x}}^3\mathbf{A}^{-1}(\mathbf{x})\right)\mathbf{A}(\mathbf{x})\int_\Gamma\frac{\boldsymbol{\phi}(y)}{x-y}dy+\int_\Gamma\mathbf{K}_4(\mathbf{x},\mathbf{y})\boldsymbol{\phi}(\mathbf{y})dS_{\mathbf{y}},
\end{aligned}
$$

$$
\begin{aligned}
&\int_\Gamma d_{\mathbf{x}}^3\left[\mathbf{A}^{-1}(\mathbf{x})\ln(|\mathbf{x}-\mathbf{y}|)\right]\mathbf{A}(\mathbf{y})\boldsymbol{\phi}(\mathbf{y})dS_{\mathbf{y}}\\
=\;&\left(d_{\mathbf{x}}e^{\imath\theta(\mathbf{x})}\right)\int_\Gamma\frac{\boldsymbol{\phi}'(y)}{x-y}dy+e^{2\imath\theta(\mathbf{x})}\int_\Gamma\frac{\boldsymbol{\phi}''(y)}{x-y}dy\\
&+\left\{2\left(d_{\mathbf{x}}^2\mathbf{A}^{-1}(\mathbf{x})\right)\mathbf{A}(\mathbf{x})+\left(d_{\mathbf{x}}\mathbf{A}^{-1}(\mathbf{x})\right)\left(d_{\mathbf{x}}\mathbf{A}(\mathbf{x})\right)\right\}\int_\Gamma\frac{\boldsymbol{\phi}(y)}{x-y}dy\\
&+\left[d_{\mathbf{x}}\mathbf{A}^{-1}(\mathbf{x})\right]\mathbf{A}(\mathbf{x})e^{\imath\theta(\mathbf{x})}\int_\Gamma\frac{\boldsymbol{\phi}'(y)}{x-y}dy+\int_\Gamma\mathbf{K}_3(\mathbf{x},\mathbf{y})\boldsymbol{\phi}(\mathbf{y})dS_{\mathbf{y}},
\end{aligned}
$$

$$
\begin{aligned}
&\int_\Gamma d_{\mathbf{x}}^2\left[\mathbf{A}^{-1}(\mathbf{x})\ln(|\mathbf{x}-\mathbf{y}|)\right]\mathbf{A}(\mathbf{y})\boldsymbol{\phi}(\mathbf{y})dS_{\mathbf{y}}\\
=\;&e^{\imath\theta(\mathbf{x})}\int_\Gamma\frac{\boldsymbol{\phi}'(y)}{x-y}dy+\left[d_{\mathbf{x}}\mathbf{A}^{-1}(\mathbf{x})\right]\mathbf{A}(\mathbf{x})\int_\Gamma\frac{\boldsymbol{\phi}(y)}{x-y}dy\\
&+\int_\Gamma\mathbf{K}_2(\mathbf{x},\mathbf{y})\boldsymbol{\phi}(\mathbf{y})dS_{\mathbf{y}},
\end{aligned}
$$

$$
\begin{aligned}
&\int_\Gamma d_{\mathbf{x}}\left[\mathbf{A}^{-1}(\mathbf{x})\ln(|\mathbf{x}-\mathbf{y}|)\right]\mathbf{A}(\mathbf{y})\boldsymbol{\phi}(\mathbf{y})dS_{\mathbf{y}}\\
=\;&\int_\Gamma\frac{\boldsymbol{\phi}(y)}{x-y}dy+\int_\Gamma\mathbf{K}_1(\mathbf{x},\mathbf{y})\boldsymbol{\phi}(\mathbf{y})dS_{\mathbf{y}},
\end{aligned}
$$

where $\mathbf{K}_i(\mathbf{x},\mathbf{y})$ $(i=1,...,4)$ are weakly singular kernels and $\boldsymbol{\phi}^{(n)}(y)$ $(n=0,...,3)$ denotes the nth complex directional derivative with respect to y on Γ. Noting that,

$$\mathbf{A}^{-1}(\mathbf{x})\mathbf{A}(\mathbf{x}) = \begin{bmatrix} 1 & 0 & 0 \\ 0 & 1 & 0 \\ 0 & 0 & 1 \end{bmatrix},$$

$$\left[d_{\mathbf{x}}\mathbf{A}^{-1}(\mathbf{x})\right]\mathbf{A}(\mathbf{x}) = \theta_{,s}\begin{bmatrix} 0 & -1 & 0 \\ 1 & 0 & 0 \\ 0 & 0 & 0 \end{bmatrix},$$

$$\left[d_{\mathbf{x}}\mathbf{A}^{-1}(\mathbf{x})\right]\left[d_{\mathbf{x}}\mathbf{A}(\mathbf{x})\right] = \theta_{,s}^2\begin{bmatrix} 1 & 0 & 0 \\ 0 & 1 & 0 \\ 0 & 0 & 1 \end{bmatrix},$$

$$\left[d_{\mathbf{x}}^2\mathbf{A}^{-1}(\mathbf{x})\right]\mathbf{A}(\mathbf{x}) = \theta_{,ss}\begin{bmatrix} 0 & -1 & 0 \\ 1 & 0 & 0 \\ 0 & 0 & 0 \end{bmatrix} - \theta_{,s}^2\begin{bmatrix} 1 & 0 & 0 \\ 0 & 1 & 0 \\ 0 & 0 & 0 \end{bmatrix},$$

$$\begin{aligned}\left[d_{\mathbf{x}}^3\mathbf{A}^{-1}(\mathbf{x})\right]\mathbf{A}(\mathbf{x}) &= \theta_{,sss}\begin{bmatrix} 0 & -1 & 0 \\ 1 & 0 & 0 \\ 0 & 0 & 0 \end{bmatrix} - 3\theta_{,ss}\theta_{,s}\begin{bmatrix} 1 & 0 & 0 \\ 0 & 1 & 0 \\ 0 & 0 & 0 \end{bmatrix} \\ &\quad -\theta_{,s}^3\begin{bmatrix} 0 & -1 & 0 \\ 1 & 0 & 0 \\ 0 & 0 & 0 \end{bmatrix},\end{aligned}$$

we obtain the following system of singular integro-differential equation on Γ. The system of integral equations reduces to the following system of integro-differential equations,

$$\begin{aligned}&\frac{1}{2}\boldsymbol{\phi}(\mathbf{x}) + \sum_{n=0}^{3}\mathbf{M}_n(\mathbf{x})\int_\Gamma \frac{\boldsymbol{\phi}^{(n)}(y)}{x-y}dy \\ &= \int_\Gamma \mathbf{N}(\mathbf{x},\mathbf{y})\boldsymbol{\phi}(\mathbf{y})dS_{\mathbf{y}} + \mathbf{t}(\mathbf{x}), \quad \mathbf{x}\in\Gamma. \end{aligned} \tag{6.41}$$

where,

$$\mathbf{M}_0(\mathbf{x}) = \frac{1}{2\pi}\begin{bmatrix} 0 & G_s b\theta_{,s} - c & \frac{H_s}{\gamma}\theta_{,s} \\ c - A_s b\theta_{,s} & 0 & \frac{G_s}{\gamma} \\ 0 & -G_s & 0 \end{bmatrix},$$

$$\mathbf{M}_1(\mathbf{x}) = \frac{e^{\imath\theta(\mathbf{x})}}{2\pi}\begin{bmatrix} A_s b & -B_s b\imath\theta_{,s}^2 & \frac{H_s}{\gamma}\theta_{,s} \\ 0 & -B_s b\imath\theta_{,s} + G_s b & \frac{H_s}{\gamma}\imath\theta_{,s} \\ 0 & 0 & \frac{H_s}{\gamma} \end{bmatrix},$$

$$\mathbf{M}_2(\mathbf{x}) = \frac{e^{2\imath\theta(\mathbf{x})}}{2\pi}\begin{bmatrix} 0 & -B_s b\theta_{,s} & 0 \\ 0 & -3B_s b\imath\theta_{,s} & \frac{H_s}{\gamma} \\ 0 & 0 & 0 \end{bmatrix},$$

$$\mathbf{M}_3(\mathbf{x}) = \frac{e^{3\imath\theta(\mathbf{x})}}{2\pi}\begin{bmatrix} 0 & 0 & 0 \\ 0 & -B_s b & 0 \\ 0 & 0 & 0 \end{bmatrix}.$$

6.3.3 Existence Theorems

The system (6.41) is not well adapted to the classical existence theory for singular integro-differential equations presented in [74] (see also [144] and [135]). The reason is that the coefficient matrix corresponding to the highest-order derivative $M_3(\mathbf{x})$ is always singular. However, it is still possible to write the system (6.41) in the classical form for which the existence theorems for the interior and exterior problems can be established. To do so, we introduce the unknown matrix function $\boldsymbol{\rho} \in \mathcal{M}_{5\times 1}$ on Γ with components defined as

$$\begin{aligned} \rho_1(\mathbf{y}) &= \phi_1(\mathbf{y}),\ \rho_2(\mathbf{y}) = \phi_2(\mathbf{y}),\ \rho_3(\mathbf{y}) = \phi_3(\mathbf{y}), \\ \rho_4(\mathbf{y}) &= \phi_2'(\mathbf{y}),\ \rho_5(\mathbf{y}) = \phi_2''(\mathbf{y}) + \frac{H_s}{\gamma B_s b} e^{-\imath\theta(\mathbf{y})}\phi_3'(\mathbf{y}). \end{aligned}$$

To ensure compatibility between the equations in terms of the new variable $\boldsymbol{\rho}$ and those in terms of $\boldsymbol{\phi}$ we require the conditions,

$$\rho_4(\mathbf{y}) = \rho_2'(\mathbf{y}),\ \rho_5(\mathbf{y}) = \rho_4'(\mathbf{y}) + \frac{H_s}{\gamma B_s b} e^{-\imath\theta(\mathbf{y})}\rho_3'(\mathbf{y}).$$

Under the assumption $\theta \in C^4(\Gamma)$, and using the relations,

$$\begin{aligned} \int_\Gamma \frac{e^{-\imath\theta(\mathbf{x})} - e^{-\imath\theta(\mathbf{y})}}{x-y}\phi_3''(y)dy &= \int_\Gamma \left(\frac{e^{-\imath\theta(\mathbf{x})} - e^{-\imath\theta(\mathbf{y})}}{x-y}\right)'' \phi_3(y)dy, \\ \int_\Gamma \frac{\imath\theta_{,s}(\mathbf{x})e^{-2\imath\theta(\mathbf{x})} - \imath\theta_{,s}(\mathbf{y})e^{-2\imath\theta(\mathbf{y})}}{x-y}\phi_3'(y)dy &= -\int_\Gamma \left(\frac{\imath\theta_{,s}(\mathbf{x})e^{-2\imath\theta(\mathbf{x})} - \imath\theta_{,s}(\mathbf{y})e^{-2\imath\theta(\mathbf{y})}}{x-y}\right)' \phi_3(y)dy, \end{aligned}$$

we remove singularity from some of the terms on the left-hand side of (6.41) and move them to the right-hand side as improper integrals. Finally, we obtain,

$$\mathbf{A}_0(\mathbf{x})\boldsymbol{\rho}(\mathbf{x}) + \mathbf{A}_1(\mathbf{x})\boldsymbol{\rho}'(\mathbf{x}) + \frac{1}{\imath\pi}\int_\Gamma \frac{\mathbf{B}_1(\mathbf{x})\boldsymbol{\rho}'(y) + \mathbf{B}_0(\mathbf{x})\boldsymbol{\rho}(y)}{x-y}dy = \int_\Gamma \mathbf{M}(\mathbf{x},\mathbf{y})\boldsymbol{\rho}(\mathbf{y})dS_{\mathbf{y}} + \mathbf{t}(\mathbf{x}),\ \mathbf{x}\in\Gamma, \tag{6.42}$$

where,

$$\mathbf{B}_1(\mathbf{x}) = \frac{\imath}{2}\begin{bmatrix} A_s b e^{\imath\theta(\mathbf{x})}\theta_{,s}^2 & -B_s b\imath e^{\imath\theta(\mathbf{x})} & \frac{H_s}{\gamma}\theta_{,s}e^{\imath\theta(\mathbf{x})} & -B_s b\theta_{,s}e^{2\imath\theta(\mathbf{x})} & 0 \\ 0 & (-B_s b\imath\theta_{,s}+G_s b)e^{\imath\theta(\mathbf{x})} & 2\frac{H_s}{\gamma}\imath\theta_{,s}e^{\imath\theta(\mathbf{x})} & -3B_s b\imath\theta_{,s}e^{2\imath\theta(\mathbf{x})} & -B_s b e^{3\imath\theta(\mathbf{x})} \\ 0 & 0 & \frac{H_s}{\gamma}e^{\imath\theta(\mathbf{x})} & 0 & 0 \\ 0 & 0 & 0 & 0 & 0 \\ 0 & 0 & 0 & 0 & 0 \end{bmatrix},$$

$$\mathbf{B}_0(\mathbf{x}) = \frac{\imath}{2}\begin{bmatrix} 0 & G_s b\theta_{,s}-c & \frac{H_s}{\gamma}\theta_{,s} & 0 & 0 \\ c-A_s b\theta_{,s} & 0 & \frac{G_s}{\gamma} & 0 & 0 \\ 0 & -G_s b & 0 & 0 & 0 \\ 0 & 0 & 0 & 0 & 0 \\ 0 & 0 & 0 & 0 & 0 \end{bmatrix},$$

$$\mathbf{A}_1(\mathbf{x}) = \begin{bmatrix} 0 & 0 & 0 & 0 & 0 \\ 0 & 0 & 0 & 0 & 0 \\ 0 & 0 & 0 & 0 & 0 \\ 0 & 0 & \frac{H_s}{\gamma B_s b}e^{-\imath\theta(\mathbf{x})} & 1 & 0 \\ 0 & 1 & 0 & 0 & 0 \end{bmatrix},$$

$$\mathbf{A}_0(\mathbf{x}) = \begin{bmatrix} \frac{1}{2} & 0 & 0 & 0 & 0 \\ 0 & \frac{1}{2} & 0 & 0 & 0 \\ 0 & 0 & \frac{1}{2} & 0 & 0 \\ 0 & 0 & 0 & 0 & -1 \\ 0 & 0 & 0 & -1 & 0 \end{bmatrix},$$

and $\mathbf{M}(\mathbf{x},\mathbf{y})$ is a weakly singular kernel of the form,

$$\mathbf{M}(\mathbf{x},\mathbf{y}) = \begin{bmatrix} * & * & * & 0 & 0 \\ * & * & * & 0 & 0 \\ * & * & * & 0 & 0 \\ 0 & 0 & 0 & 0 & 0 \\ 0 & 0 & 0 & 0 & 0 \end{bmatrix},$$

where "$*$" denotes a (possibly) non-zero component whose specific form does not affect the analysis. The system of integro-differential equation in the standard form of (6.42) can be investigated through the well-documented theorems [74, 109, 144]. It is clear that the index of the system (6.42) is

$$\varkappa = \arg\left[\frac{\det(\mathbf{A}_1-\mathbf{B}_1)}{\det(\mathbf{A}_1+\mathbf{B}_1)}\right]_\Gamma = 0.$$

Consequently, in the case of (6.42), Noether's theorems reduce to Fredholm's theorems which paves the way to proving the existence results.

Theorem 6.21. *(Existence of the interior problem $(6.26)_I$) The system of singular integral equations (6.30) has a unique solution $\boldsymbol{\phi} \in C^{3,\alpha}(\Gamma)$, with $0 < \alpha < 1$ whenever $\mathbf{t} \in C^{1,\alpha}(\Gamma)$. In addition, if $\mathbf{t} \in C^{1,\alpha}(\Gamma)$, the interior problem of (6.26) with C^4 boundary Γ incorporating bending and micropolar twisting rigidities has a unique solution describable in the form (6.28) with $\boldsymbol{\phi} \in C^{3,\alpha}(\Gamma)$ being the unique solution of $(6.26)_I$.*

Proof. The system of integral equations (6.30) is equivalent to the system (6.42) and since the index of the corresponding dominant operator is zero, Fredholm's theorems apply to (6.42) and its adjoint system. From Theorem 1 we deduce that the homogeneous system $(6.42)^0$ (with $\mathbf{t}(\mathbf{x}) = \mathbf{0}$) has only the trivial solution, $\boldsymbol{\rho}_0 = \mathbf{0}$. Therefore, from the Fredholm alternative, there exists a unique solution of (6.42), which is $\boldsymbol{\rho} \in C^{1,\alpha}(\Gamma)$. The latter implies that $\boldsymbol{\phi} \in C^{3,\alpha}(\Gamma)$ exists as the unique solution of (6.30) for $\mathbf{t} \in C^{1,\alpha}(\Gamma)$. We may construct the solution of $(6.26)_I$ by (6.28) and the uniqueness of the solution of $(6.26)_I$ completes the proof.

Following the same procedure, we can establish an analogous theorem for the exterior problem:

Theorem 6.22. *(Existence of the exterior problem $(6.26)_E$) The system of singular integral equations (6.35) has a unique solution $\boldsymbol{\phi} \in C^{3,\alpha}(\Gamma)$, with $0 < \alpha < 1$ whenever $\mathbf{t} \in C^{1,\alpha}(\Gamma)$. In addition, if $\mathbf{t} \in C^{1,\alpha}(\Gamma)$, the exterior problem of (6.26) with C^4 boundary Γ incorporating bending and micropolar twisting rigidities has a unique solution describable in the form (6.34) with $\boldsymbol{\phi} \in C^{3,\alpha}(\Gamma)$ being the unique solution of $(6.26)_E$.*

6.3.4 Existence Theorem for the Case of Second Order Boundary Conditions

In the second chapter of this thesis, we introduced an alternative version of the of micropolar surface model utilizing second order boundary conditions [59]. This model is based on the

Altenbach-Eremeyev-Lebedov shell representation [43, 2] and still incorporates bending and twisting resistance of the surface. For that case, the boundary differential operator matrix on the curve Γ (which incorporates surface elasticity) will become:

$$\mathbf{R}(d_{\mathbf{x}}) = \mathbf{R}^*(d_{\mathbf{x}})d_{\mathbf{x}} + \mathbf{R}_0,\ \mathbf{R}^*(d_{\mathbf{x}}) = \mathbf{R}_2 d_{\mathbf{x}} + \mathbf{R}_1, \tag{6.43}$$

where

$$\mathbf{R}_2 = \begin{bmatrix} A_s & 0 & 0 \\ 0 & M_s + G_s & 0 \\ 0 & 0 & H_s + B_s \end{bmatrix},\ \mathbf{R}_1 = \begin{bmatrix} 0 & (A_s + M_s + G_s)\theta_{,s} & 0 \\ -(A_s + M_s + G_s)\theta_{,s} & 0 & M_s + G_s \\ 0 & -(M_s + G_s) & 0 \end{bmatrix},$$

$$\mathbf{R}_0 = \begin{bmatrix} -(M_s + G_s)\theta_{,s}^2 & A_s\theta_{,ss} & (M_s + G_s)\theta_{,s} \\ -(M_s + G_s)\theta_{,ss} & -A_s\theta_{,s}^2 & 0 \\ (M_s + G_s)\theta_{,s} & 0 & -(M_s + G_s) \end{bmatrix}.$$

Here, $\theta(\mathbf{x})$ belongs to a broader set of admissible functions $\theta(\mathbf{x}) \in C^4(\Gamma)$. The boundary integral equation method proceeds as before and leads to the following system of integro-differential equations:

$$\begin{aligned} \frac{1}{2}\boldsymbol{\phi}(\mathbf{x}) + \sum_{n=0}^{1} \mathbf{M}_n(\mathbf{x}) \int_\Gamma \frac{\boldsymbol{\phi}^{(n)}(y)}{x - y} dy \\ = \int_\Gamma \mathbf{N}(\mathbf{x}, \mathbf{y})\boldsymbol{\phi}(\mathbf{y}) dS_{\mathbf{y}} + \mathbf{t}(\mathbf{x}), \quad \mathbf{x} \in \Gamma. \end{aligned} \tag{6.44}$$

where

$$\mathbf{M}_0(\mathbf{x}) = \frac{1}{2\pi} \begin{bmatrix} 0 & (M_s + G_s)\theta_{,s} b & 0 \\ -A_s\theta_{,s} b & 0 & \frac{M_s + G_s}{\gamma} \\ 0 & -(M_s + G_s) b & 0 \end{bmatrix},$$

$$\mathbf{M}_1(\mathbf{x}) = \frac{e^{\imath\theta(\mathbf{x})}}{2\pi} \begin{bmatrix} A_s b & 0 & 0 \\ 0 & (M_s + G_s) b & 0 \\ 0 & 0 & \frac{H_s + B_s}{\gamma} \end{bmatrix}.$$

The singular integro-differential equation (6.44) is of Vekua's standard form [74] and can be examined by comparing (6.44) with the class of equations given in (6.42). We find that the index of the singular operator in (6.44) is again zero as in the standard form (6.42),

$$\mathbf{A}_1(\mathbf{x}) = \mathbf{0},\ \mathbf{B}_1(\mathbf{x}) = \frac{\imath e^{\imath\theta(\mathbf{x})}}{2} \begin{bmatrix} A_s b & 0 & 0 \\ 0 & (M_s + G_s) b & 0 \\ 0 & 0 & \frac{H_s + B_s}{\gamma} \end{bmatrix},$$

and therefore,

$$\varkappa = \arg\left[\frac{\det(\mathbf{A}_1 + \mathbf{B}_1)}{\det(\mathbf{A}_1 - \mathbf{B}_1)}\right]_\Gamma = 0,$$

assuming the surface material coefficients are non-zero ($A_s, M_s, G_s, H_s, B_s \neq 0$). Consequently, the Fredholm alternative holds for (6.44) and its adjoint.

We readily have the following existence theorems for the alternative case of the second order boundary conditions of the surface.

Theorem 6.23. *(Existence of the interior problem (6.26)$_I$ with second order $\mathbf{R}(d_\mathbf{x})$ given in (6.43)) The system of singular integral equations (6.30) has a unique solution $\boldsymbol{\phi} \in C^{1,\alpha}(\Gamma)$, with $0 < \alpha < 1$ whenever $\mathbf{t} \in C^{1,\alpha}(\Gamma)$. In addition, if $\mathbf{t} \in C^{1,\alpha}(\Gamma)$, the interior problem of (6.26) with C^2 boundary Γ incorporating bending and micropolar twisting rigidities has a unique solution describable in the form (6.28) with $\boldsymbol{\phi} \in C^{1,\alpha}(\Gamma)$ being the unique solution of (6.26)$_I$.*

Theorem 6.24. *(Existence of the exterior problem (6.26)$_E$ with second order $\mathbf{R}(d_\mathbf{x})$ given in (6.43)) The system of singular integral equations (6.35) has a unique solution $\boldsymbol{\phi} \in C^{1,\alpha}(\Gamma)$, with $0 < \alpha < 1$ whenever $\mathbf{t} \in C^{1,\alpha}(\Gamma)$. In addition, if $\mathbf{t} \in C^{1,\alpha}(\Gamma)$, the exterior problem of (6.26) with C^2 boundary Γ incorporating bending and micropolar twisting rigidities has a unique solution describable in the form (6.34) with $\boldsymbol{\phi} \in C^{1,\alpha}(\Gamma)$ being the unique solution of (6.26)$_E$.*

Proof. The proofs of the existence theorems can be found the same way through Fredholm theorems. □

We mention in closing that the case in which the entire boundary of the solid is coated gives rise to a Neumann-type problem (similar to the one studied in [126]) in which the corresponding homogeneous systems of singular integral equations give rise to nontrivial solutions that affect the solvability of both the interior and exterior boundary value problems. This case is not covered by the results in the present thesis since it requires further analysis

of the corresponding integral equations. This can form the basis of future research in this area[1].

[1]A. Gharahi and P. Schiavone recently addressed this problem in *Math. Mech. Solids* (The Neumann problem in plane deformations of a micropolar elastic solid with micropolar surface effects: Accepted for publication)

Chapter 7

Conclusions

In this thesis, we have proposed a comprehensive model of plane deformations of micropolar solids with micropolar surface effects. In our model, we described the surface as a micropolar elastic shell perfectly bonded to the surface (or the interface) of a micropolar material bulk. We introduced two surface models based on two different micropolar shell theories to mimic the deformations of the surface. The presented models use micropolar shell theories of the Kirchhoff's type as their bases for the surface mechanism in conjunction with the classical theory of micropolar elasticity. We demonstrated that a slight difference in the kinematic assumptions of Kirchhoff-type shell theories leads to two different orders of surface conditions; one of them leads to second order and the other leads to fourth order boundary conditions. In either cases, the effects of bending and twisting modes of deformation of the surface are captured in the model. This is, on its own, a substantial improvement since these effects are commonly missing from surface mechanics. In the first part of the thesis, we successfully applied the mathematical model to three widely interesting micro/nano-mechanics problems. We examined the fourth order boundary conditions model which is more challenging in terms of analysis. The second order surface models of the same problems involve less complexity and are expected to be solvable by the same analytical techniques.

First, we determined the analytical solutions of the stress fields around a circular cavity under remote loading and evaluated variations in the stress concentration due to the size-dependence effects. We demonstrated that the stress field can be calculated with a higher

precision when more information is carried into the model. In particular, the hoop stress around a cavity is important since it corresponds to the failure mechanisms and the emergence of plastic zone. Generally, for a smaller hole the hoop stress intensity factor is shown to be lower compared to the predictions of models which incorporate less size-dependent variables. Furthermore, we find that when the hole radius is sufficiently small, the bending rigidity of the surface contributes significantly to the solution.

Next, we proceeded by examining the contribution of our model to the effective properties of a nano-composite containing material inhomogeneities. We illustrated that for nano-scale inhomogeneities, all the size-dependent components of our model become important in the calculation of the effective shear modulus. However, the degree to which these effects dominate depends on the ratio of their corresponding characteristic length to the size of the inhomogeneities in a representative volume element. In particular, we demonstrated the surface/interface flexural resistance effects as well as the surface micropolar twisting effects by comparing our results with a similar study in the existing literature. Thus, we validated our model by showing that in a special case, our formulations reduces to the existing model in which flexural effects are absent from the micropolar surface/interface. In addition, we concluded that the bending and twisting rigidities of the interface, as well as the micropolar properties of the bulk exert no influence on the overall bulk modulus of the composite.

As the final test, we applied our model to the fundamental problem of an edge dislocation close to the surface of a micropolar half-plane. Once again, we demonstrated that the proposed model can indeed be successfully applied to fundamental problems of plane elasticity. In particular, the contribution of micropolar surface effects and other size-dependent variables were examined and shown to be significant in a sufficiently small-scale level. In addition, we concluded that the classical G–M surface model may not be sufficient for materials in which micropolar bulk effects and surface twisting rigidities are significant. In contrast, the classical bending resistance of the planar surface only marginally affects the stress distribution induced by a nearby edge dislocation. Nevertheless, the incorporation of this surface effect in the model of deformation may still prove to be useful in certain cases, for

example, in the presence of a reinforcement attached to the boundary of the solid. Finally, we concluded that the particular choice of surface and bulk models become important for calculations of stress near the dislocation core but not as important farther away.

We dedicated the second part of the thesis to a rigorous analysis of the design and the mathematical adequacy of the two models. We organized the mathematical models in the form of mixed boundary value problems in the interior and exterior domains. These proposed formats of the models make them well-suited for analysis by the integral equation methods. However, the corresponding boundary value problems involve highly non-standard boundary conditions due to either surface model that incorporates surface effects. In pursuit of an answer to the question of well-posedness, we established that for each of the two presented models any smooth solutions of the corresponding interior and exterior boundary mixed value problems are necessarily unique. Furthermore, we demonstrated that the corresponding interior and exterior problems can be reduced to systems of singular integro-differential equations by expressing the solutions in the form of modified single layer potentials. We further proved that Noether's theorems apply to the existing models according to which the models fit into Fredholm's theorems. Consequently, we established solvability of the corresponding mixed boundary value problems in the appropriate function spaces. Furthermore, we found the underlying restrictions on the boundary and the prescribed data. Thus, considering the appropriate function spaces, and the restrictions on the data and the boundary, the statements of well-posedness in the sense of Hadamard hold true for both models.

7.1 Future Work

The present work opens the gate to several new possibilities. First, the proposed mathematical model can be applied to various popular problems of micro/nano-mechanics. For example, it is well-known that in fracture mechanics the incorporation of surface effects ameliorates the order of singularity of stress fields at the crack tip and reduces the anomalies that follow from the classical models. It would be interesting to investigate the stress distribution at the crack tip using the proposed model and compare the results with other

popular surface elastic models. Equally attractive is the calculations of micropolar elastic moduli which has remained challenging to theoretical and experimental studies. The model at hand can pave a way for further research about finding the effective micropolar elastic properties of materials.

Further ideas can be considered for expansion of this project. For instance, developing a combined model of non-linear elastic micropolar plane deformations coupled with surface effects of micropolar type would be an idea to pursue. The linear theory degenerated from such a model, then can be compared to the model proposed in this thesis. A similar model can be developed for torsional deformation in micropolar elasticity with the incorporation of surface mechanics. Also, micropolar theories of plates and shells can be combined with the micropolar surface elasticity. Introducing time-dependence and generalizing the model to encompass three dimensional deformations are other possibilities that, although challenging, could be topics of further studies. Of course, any newly proposed model creates a topic of research for investigating the design and validating the model in terms of its well-posedness and applicability limitations. Any such investigation requires a rigorous mathematical analysis which will create a subject of study for further research.

References

[1] H. Altenbach and V. A. Eremeyev. On the linear theory of micropolar plates. *ZAMM - J. Appl. Math. Mech.*, 89(4):242–256, 2013.

[2] J. Altenbach, H. Altenbach, and V. A. Eremeyev. On generalized Cosserat-type theories of plates and shells: a short review and bibliography. *Archive of Applied Mechanics*, 80(1):73–92, 2010.

[3] W. B. Anderson and R. A. Lakes. Size effects due to Cosserat elasticity and surface damage in closed-cell polymethacrylimide foam. *J. Mater. Sci.*, 29:6413– 6419, 1994.

[4] Y. A. Antipov and P. Schiavone. Integro-differential equation for a finite crack in a strip with surface effects. *Q. J. Mech. Appl. Math.*, 64(1):87–106, feb 2011.

[5] Attila Askar. Molecular crystals and the polar theories of the continua Experimental values of material coefficients for KNO3. *Int. J. Eng. Sci.*, 10(3):293–300, mar 1972.

[6] A. Bacigalupo and L. Gambarotta. Second-order computational homogenization of heterogeneous materials with periodic microstructure. *ZAMM - Journal of Applied Mathematics and Mechanics / Zeitschrift für Angewandte Mathematik und Mechanik*, 90(10-11):796–811, 2010.

[7] K. P. Baxevanakis, P. A. Gourgiotis, and H. G. Georgiadis. Interaction of cracks with dislocations in couple-stress elasticity. Part II: Shear modes. *Int. J. Solids Struct.*, 118-119:192–203, jul 2017.

[8] Y. Benveniste and T. Miloh. Imperfect soft and stiff interfaces in two-dimensional elasticity. *Mech. Mater.*, 33(6):309–323, 2001.

[9] Y. Benveniste and T. Miloh. Soft neutral elastic inhomogeneities with membrane-type interface conditions. *J. Elast.*, 88(2):87–111, jul 2007.

[10] A. J. Beveridge, M. A. Wheel, and D. H. Nash. The micropolar elastic behaviour of model macroscopically heterogeneous materials. *Int. J. Solids Struct.*, 50(1):246–255, jan 2013.

[11] O. Brulin. *Mechanics of Micropolar Media*. World Scientific Publishing Co Pte Ltd, 1982.

[12] I. Chasiotis. Experimental mechanics of MEMS and thin films. In *ICASE/LaRC Interdisciplinary Series in Science and Engineering*, pages 3–37. Springer Netherlands, 2004.

[13] C. P. Chen and R. S. Lakes. Holographic study of conventional and negative Poisson's ratio metallic foams: elasticity, yield and micro-deformation. *J. Mater. Sci.*, 26(20):5397–5402, oct 1991.

[14] C. Q. Chen, Y. Shi, Y. S. Zhang, J. Zhu, and Y. J. Yan. Size dependence of young's modulus in ZnO nanowires. *Phys. Rev. Lett.*, 96(7), feb 2006.

[15] H. Chen, G. Hu, and Z. Huang. Effective moduli for micropolar composite with interface effect. *Int. J. Solids Struct.*, 44(25-26):8106–8118, 2007.

[16] H. Chen, X. Liu, and G. Hu. Overall plasticity of micropolar composites with interface effect. *Mech. Mater.*, 40(9):721 – 728, 2008.

[17] P. Chhapadia, P. Mohammadi, and P. Sharma. Curvature-dependent surface energy and implications for nanostructures. *J. Mech. Phys. Solids*, 59(10):2103–2115, 2011.

[18] D. Colton and R. Kress. *Integral Equation Methods in Scattering Theory*. Society for Industrial and Applied Mathematics, nov 2013.

[19] C. Constanda. Some comments on the integration of certain systems of partial differential equations in continuum mechanics. *ZAMP*, 29(5):835–839, Sep 1978.

[20] C. Constanda. The boundary integral equation method in plane elasticity. *Proc. Am. Math. Soc.*, 123(11):3385–3396, 1995.

[21] C. Constanda. *Mathematical Methods for Elastic Plates*. Springer-Verlag GmbH, 2014.

[22] C. Constanda. *Direct and Indirect Boundary Integral Equation Methods*. Chapman and Hall/CRC, jan 2020.

[23] C. Constanda, D. Doty, and W. Hamill. *Boundary Integral Equation Methods and Numerical Solutions*. Springer-Verlag GmbH, 2016.

[24] E. Cosserat and F. Cosserat. *Theorie des Corps Deformables*. Paris, A. Herman et fils, 1909.

[25] M. Dai, A. Gharahi, and P. Schiavone. Analytic solution for a circular nano-inhomogeneity with interface stretching and bending resistance in plane strain deformations. *Appl. Math. Modell.*, 55:160–170, 2018.

[26] M. Dai, P. Schiavone, and C. F. Gao. Uniqueness of neutral elastic circular nano-inhomogeneities in antiplane shear and plane deformations. *J. Appl. Mech.*, 83(10), jul 2016.

[27] Ming Dai, P. Schiavone, and C. F. Gao. Screw dislocation in a thin film with surface effects. *Int. J. Solids Struct.*, 110-111:89–93, 2017.

[28] Ming Dai and Peter Schiavone. Edge dislocation interacting with a Steigmann–Ogden interface incorporating residual tension. *Int. J. Eng. Sci.*, 139:62–69, jun 2019.

[29] René de Borst. Numerical modelling of bifurcation and localisation in cohesive-frictional materials. *Pure Appl. Geophys.*, 137(4):367–390, dec 1991.

[30] Patrick de Buhan and Bruno Sudret. Micropolar multiphase model for materials reinforced by linear inclusions. *Eur. J. Mech. A. Solids*, 19(4):669–687, jul 2000.

[31] S. Diebels. A micropolar theory of porous media: constitutive modelling. *Transp. Porous Media*, 34(1/3):193–208, 1999.

[32] T. Dillard, S. Forest, and P. Ienny. Micromorphic continuum modelling of the deformation and fracture behaviour of nickel foams. *Eur. J. Mech. A. Solids*, 25(3):526–549, may 2006.

[33] J. E. Dorn, J. Mitchell, and F. Hauser. Dislocation dynamics. *Experimental Mechanics*, 5(11):353–362, nov 1965.

[34] H. L. Duan, J. Wang, Z. P. Huang, and B. L. Karihaloo. Eshelby formalism for nano-inhomogeneities. *Proc. R. Soc. London, Ser. A*, 461(2062):3335–3353, 2005.

[35] H. L. Duan, J. Wang, Z. P. Huang, and B. L. Karihaloo. Size-dependent effective elastic constants of solids containing nano-inhomogeneities with interface stress. *J. Mech. Phys. Solids*, 53(7):1574–1596, 2005.

[36] H. L. Duan, J. Wang, Z. P. Huang, and Z. Y. Luo. Stress concentration tensors of inhomogeneities with interface effects. *Mech. Mater.*, 37:7, 2005.

[37] H. L. Duan, J. Wang, B. L. Karihaloo, and Z. P. Huang. Nanoporous materials can be made stiffer than non-porous counterparts by surface modification. *Acta Mater.*, 54(11):2983–2990, 2006.

[38] H. L. Duan, X. Yi, Z. P. Huang, and J. Wang. Eshelby equivalent inclusion method for composites with interface effects. *Key Eng. Mater.*, 312:161–166, 2006.

[39] W. Ehlers. Theoretical and numerical modelling of granular liquid-saturated elastoplastic porous media. *ZAMM - Journal of Applied Mathematics and Mechanics/Zeitschrift fuer Angewandte Mathematik und Mechanik*, 77, 1997.

[40] W. Ehlers and W. Volk. On shear band localization phenomena of liquid-saturated granular elastoplastic porous solid materials accounting for fluid viscosity and micropolar solid rotations. *Mech. Cohesive-frict. Mater.*, 2(4):301–320, 1997.

[41] R. W. Ellis and C. W. Smith. A thin-plate analysis and experimental evaluation of couple-stress effects. *Experimental Mechanics*, 7(9):372–380, sep 1967.

[42] V. A. Eremeyev and H. Altenbach. *Basics of Mechanics of Micropolar Shells*, pages 63–111. Springer, 2016.

[43] V. A. Eremeyev and L. P. Lebedev. Existence theorems in the linear theory of micropolar shells. *ZAMM - J. Appl. Math. Mech.*, 91(6):468–476, 2013.

[44] V. A. Eremeyev, A. Skrzat, and F. Stachowicz. On computational evaluation of stress concentration using micropolar elasticity. In *Lecture Notes in Electrical Engineering*, pages 199–205. Springer International Publishing, jul 2017.

[45] A. Eringen. *Microcontinuum Field Theories : I. Foundations and Solids*. Springer New York, New York, NY, 1999.

[46] A. C. Eringen. Linear theory of micropolar elasticity. *J. Math. Mech.*, 15(6):909–923, 1966.

[47] A. C. Eringen. Theory of micropolar plates. *ZAMP - J. Appl. Math. Phys.*, 18(1):12–30, 1967.

[48] A. C. Eringen. Mechanics of micromorphic continua. In *Mechanics of Generalized Continua*, pages 18–35. Springer Berlin Heidelberg, 1968.

[49] A. C. Eringen. Theory of micropolar elasticity. In *Microcontinuum Field Theories*, pages 101–248. Springer New York, 1999.

[50] A.Cemal Eringen and D.G.B. Edelen. On nonlocal elasticity. *Int. J. Eng. Sci.*, 10(3):233–248, mar 1972.

[51] Jan Fikar, Roman Gröger, and Robin Schäublin. Effect of orientation of prismatic dislocation loops on interaction with free surfaces in BCC iron. *J. Nucl. Mater.*, 497:161–165, dec 2017.

[52] S. Y. Long G. Q. Xie. Elastic vibration behaviors of carbon nanotubes based on micropolar mechanics. *Computers, Materials & Continua*, 4(1):11–20, 2006.

[53] X.-L. Gao and G. Y. Zhang. A microstructure- and surface energy-dependent third-order shear deformation beam model. *ZAMP - Zeitschrift für angewandte Mathematik und Physik*, 66(4):1871–1894, sep 2014.

[54] R. D. Gauthier and W. E. Jahsman. A quest for micropolar elastic constants. *J. Appl. Mech.*, 42(2):369–374, 1975.

[55] A. Gharahi, M. Dai, G. F. Wang, and P. Schiavone. Interaction of a screw dislocation with a bi-material interface in anti-plane couple stress elasticity. *Math. Mech. Solids*, 23(4):651–666, jan 2017.

[56] A. Gharahi and P. Schiavone. Effective elastic properties of plane micropolar nanocomposites with interface flexural effects. *Int. J. Mech. Sci.*, 149:84–92, 2018.

[57] A. Gharahi and P. Schiavone. Plane micropolar elasticity with surface flexural resistance. *Continuum Mech. Thermodyn.*, 30(3):675–688, 2018.

[58] A. Gharahi and P. Schiavone. Edge dislocation with surface flexural resistance in micropolar materials. *Acta Mech.*, 230(5):1513–1527, May 2019.

[59] A. Gharahi and P. Schiavone. Uniqueness of solution for plane deformations of a micropolar elastic solid with surface effects. *Continuum Mech. Thermodyn.*, Apr 2019.

[60] A. Gharahi and P. Schiavone. Existence and integral representation of solutions for plane deformations of a micropolar elastic solid with surface elasticity. *ZAMM - Journal of Applied Mathematics and Mechanics / Zeitschrift für Angewandte Mathematik und Mechanik*, jan 2020.

[61] J. D. Goddard. From granular matter to generalized continuum. In *Mathematical Models of Granular Matter*, pages 1–22. Springer Berlin Heidelberg, 2008.

[62] R. J. Good. Surface free energy of solids and liquids: Thermodynamics, molecular forces, and structure. *J. Colloid Interface Sci.*, 59(3):398–419, may 1977.

[63] J. G. Guo and Y. P. Zhao. The size-dependent bending elastic properties of nanobeams with surface effects. *Nanotechnology*, 18(295701):1–6, 2007.

[64] M. E Gurtin and A. I. Murdoch. A continuum theory of elastic material surfaces. *Arch. Ration. Mech. Anal.*, 57:291–323, 1975.

[65] M. E. Gurtin and A. I. Murdoch. Surface stress in solids. *Int. J. Solids Struct.*, 14(6):431–440, 1978.

[66] J. Hadamard. Sur les problèmes aux dérivées partielles et leur signification physique. *Princeton University Bulletin*, pages 49–52, 1902.

[67] Z. Han, S. G. Mogilevskaya, and D. Schillinger. Local fields and overall transverse properties of unidirectional composite materials with multiple nanofibers and Steigmann–Ogden interfaces. *Int. J. Solids Struct.*, 147:166–182, aug 2018.

[68] Soroosh Hassanpour and Glenn R. Heppler. Micropolar elasticity theory: a survey of linear isotropic equations, representative notations, and experimental investigations. *Math. Mech. Solids*, 22(2):224–242, aug 2016.

[69] L. H. He and Z. R. Li. Impact of surface stress on stress concentration. *Int. J. Solids Struct.*, 43(20):6208–6219, oct 2006.

[70] D. Hull and D. J. Bacon. *Introduction to Dislocations*. Elsevier, 2011.

[71] D. Ieşan. Existence theorems in the theory of micropolar elasticity. *Int. J. Eng. Sci.*, 8(9):777 – 791, 1970.

[72] D. Ieşan. Torsion of micropolar elastic beams. *Int. J. Eng. Sci.*, 9(11):1047–1060, nov 1971.

[73] P. Intarit, T. Senjuntichai, and R. K. N. D. Rajapakse. Dislocations and internal loading in a semi-infinite elastic medium with surface stresses. *Eng. Fract. Mech.*, 77(18):3592 – 3603, 2010. Computational Mechanics in Fracture and Damage: A Special Issue in Honor of Prof. Gross.

[74] R. S. Isahanov. On a class of singular integro-differential equations. *Sov. Math. Dokl*, 1:529–532, 1960.

[75] E. A. Ivanova, A. M. Krivtsov, N. F. Morozov, and A. D. Firsova. Description of crystal packing of particles with torque interaction. *Mech. Solids*, 2003.

[76] E. A. Ivanova, A. M. Krivtsov, N. F. Morozov, and A. D. Firsova. Inclusion of the moment interaction in the calculation of the flexural rigidity of nanostructures. *Doklady Physics*, 48(8):455–458, aug 2003.

[77] G. Y. Jing, H. L. Duan, X. M. Sun, Z. S. Zhang, J. Xu, Y. D. Li, J. X. Wang, and D. P. Yu. Surface effects on elastic properties of silver nanowires: Contact atomic-force microscopy. *Phys. Rev. B*, 73(235409):1–6, 2006.

[78] P. N. Kaloni and T. Ariman. Stress concentration effects in micropolar elasticity. *Acta Mech.*, 4(3):216–229, 1967.

[79] T. C. Kennedy and J. B. Kim. Dynamic analysis of cracks in micropolar elastic materials. *Eng. Fract. Mech.*, 44(2):207–216, jan 1993.

[80] C. I. Kim, C. Q. Ru, and P. Schiavone. A clarification of the role of crack-tip conditions in linear elasticity with surface effects. *Math. Mech. Solids*, 18(1):59–66, feb 2012.

[81] C. I. Kim, P. Schiavone, and C. Q. Ru. Analysis of plane-strain crack problems (mode-I & mode-II) in the presence of surface elasticity. *J. Elast.*, 104(1):397–420, 2011.

[82] C. I. Kim, P. Schiavone, and C. Q. Ru. Effect of surface elasticity on an interface crack in plane deformations. *Proceedings of the Royal Society A: Mathematical, Physical and Engineering Sciences*, 467(2136):3530–3549, jul 2011.

[83] R. Kress. *Linear Integral Equations*. Springer New York, 2014.

[84] E. Kröner and B. K. Datta. Nichtlokale elastostatik: Ableitung aus der gittertheorie. *Zeitschrift für Physik*, 196(3):203–211, jun 1966.

[85] V. D. Kupradze. *Three-dimensional problems of the mathematical theory of elasticity and thermoelasticity*. North-Holland Pub. Co. Sole distributors for the U.S.A. and Canada Elsevier/North-Holland, Amsterdam New York New York, 1979.

[86] R. A. Lakes. Physical meaning of elastic constants in cosserat, void, and microstretch elasticity. *J. Mech. Mater. Struct.*, 11(3):217–229, 2016.

[87] R. S. Lakes. Dynamical study of couple stress effects in human compact bone. *J. Biomech. Eng.*, 104(1):6–11, feb 1982.

[88] R. S. Lakes. Experimental microelasticity of two porous solids. *Int. J. Solids Struct.*, 22(1):55–63, 1986.

[89] R. S. Lakes, D. Gorman, and W. Bonfield. Holographic screening method for microelastic solids. *J. Mater. Sci.*, 20(8):2882–2888, aug 1985.

[90] R. S. Lakes, S. Nakamura, J. C. Behiri, and W. Bonfield. Fracture mechanics of bone with short cracks. *J. Biomech.*, 23(10):967–975, jan 1990.

[91] Markus Lazar. Dislocations in generalized continuum mechanics. In *Advances in Mechanics and Mathematics*, pages 235–244. Springer New York, 2010.

[92] Markus Lazar, Gérard A. Maugin, and Elias C. Aifantis. Dislocations in second strain gradient elasticity. *Int. J. Solids Struct.*, 43(6):1787–1817, mar 2006.

[93] S. Li and G. Wang. *Introduction to Micromechanics and Nanomechanics*. World Scientific, 2008.

[94] X. Li and C. Mi. Nanoindentation hardness of a Steigmann–Ogden surface bounding an elastic half-space. *Math. Mech. Solids*, page 1081286518799795, 2018.

[95] C. Liebold and W. H. Muller. *Generalized Continua as Models for Classical and Advanced Materials. Advanced Structured Materials*, volume 42, chapter Applications of higher-order continua to size effects in bending: theory and recent experimental results. Springer, Cham, 2016.

[96] X. Liu and G. Hu. A continuum micromechanical theory of overall plasticity for particulate composites including particle size effect. *Int. J. Plast.*, 21(4):777–799, 2005.

[97] I. Jasiuk M. Ostoja-Starzewski. Stress invariance in planar Cosserat elasticity. *Proc. R. Soc. London, Ser. A*, 451(1942):453–470, 1995.

[98] G. A. Maugin and A. V. Metrikine. *Mechanics of Generalized Continua*. Springer, 2010.

[99] Gérard A. Maugin. *Generalized Continuum Mechanics: What Do We Mean by That?*, pages 3–13. Springer New York, New York, NY, 2010.

[100] M. A. Meyers and K. K. Chawla. *Mechanical Behavior of Materials*. Cambridge University Press, 2008.

[101] R. E. Miller and V. B. Shenoy. Size-dependent elastic properties of nanosized structural elements. *Nanotechnology*, 11:139–147, 2000.

[102] R. D. Mindlin. Influence of couple-stresses on stress concentrations. *Exp. Mech.*, 3(1):1–7, 1963.

[103] R. D. Mindlin and N. N. Eshel. On first strain-gradient theories in linear elasticity. *Int. J. Solids Struct.*, 4(1):109–124, jan 1968.

[104] R. D. Mindlin and H. F. Tiersten. Effects of couple-stresses in linear elasticity. *Arch. Ration. Mech. Anal.*, 11(1):415–448, 1962.

[105] P. Moon and D. E. Spencer. *Field Theory Handbook*. Springer Berlin Heidelberg, 1971.

[106] R. Mora and A. M. Waas. Measurement of the Cosserat constant of circular-cell polycarbonate honeycomb. *Philosophical Magazine A*, 80(7):1699–1713, jul 2000.

[107] K. Mori, M. Shiomi, and K. Osakada. Inclusion of microscopic rotation of powder particles during compaction in finite element method using Cosserat continuum theory. *Int. J. Numer. Methods Eng.*, 42(5):847–856, jul 1998.

[108] T. Mori and K. Tanaka. Average stress in matrix and average elastic energy of materials with misfitting inclusions. *Acta Metall.*, 21(5):571–574, 1973.

[109] N. I. Muskhelishvili. *Singular Integral Equations*. Wolters-Noordhoff, Groningen, 1972.

[110] F. Noether. Über eine klasse singulärer integralgleichungen. *Mathematische Annalen*, 82:42–63, 1921.

[111] J. P. Nowacki. The theory of dislocations in the Cosserat elastic continuum, I. *Bull. Acad. Polon. Sci., Ser. Sci. Tech.*, 21(11):585, 1973.

[112] W. Nowacki. *Theory of Asymmetric Elasticity*. Pergamon Press, 1986.

[113] Xia-Hui Pan, Shou-Wen Yu, and Xi-Qiao Feng. Oriented thermomechanics for isothermal planar elastic surfaces under small deformation. In *IUTAM Symposium on Surface Effects in the Mechanics of Nanomaterials and Heterostructures*, pages 1–13. Springer Netherlands, jul 2012.

[114] A. Pau and P. Trovalusci. Block masonry as equivalent micropolar continua: the role of relative rotations. *Acta Mechanica*, 223(7):1455–1471, may 2012.

[115] R. W. Perkins and D. Thompson. Experimental evidence of a couple-stress effect. *AIAA Journal*, 11(7):1053–1055, jul 1973.

[116] S. Ramezani, R. Naghdabadi, and S. Sohrabpour. Analysis of micropolar elastic beams. *Eur. J. Mech. A. Solids*, 28(2):202–208, mar 2009.

[117] W.T. Read. *Dislocations in Crystals*. International series in pure and applied physics. McGraw-Hill, 1953.

[118] C. Q. Ru. Simple geometrical explanation of gurtin-murdoch model of surface elasticity with clarification of its related versions. *Science China Physics, Mechanics and Astronomy*, 53(3):536–544, mar 2010.

[119] Z. Rueger and R. S. Lakes. Experimental Cosserat elasticity in open-cell polymer foam. *Philosophical Magazine*, 96(2):93–111, jan 2016.

[120] H. Sadeghian, C. K. Yang, J. F. L. Goosen, E. van der Drift, A. Bossche, P. J. French, and F. van Keulen. Characterizing size-dependent effective elastic modulus of silicon nanocantilevers using electrostatic pull-in instability. *Applied Physics Letters*, 94(22):221903, 2009.

[121] S. H. Salehi and M. Salehi. Numerical investigation of nanoindentation size effect using micropolar theory. *Acta Mechanica*, 225(12):3365–3376, apr 2014.

[122] S. H. Sargsyan. General theory of micropolar elastic thin shells. *Phys. Mesomech.*, 15:69–72, 2012.

[123] P. Schiavone. Integral equation methods in plane asymmetric elasticity. *J. Elast.*, 43(1):31–43, 1996.

[124] P. Schiavone. Integral solutions of mixed problems in a theory of plane strain elasticity with microstructure. *Int. J. Eng. Sci.*, 39(10):1091 – 1100, 2001.

[125] P. Schiavone and C. Q. Ru. On the exterior mixed problem in plane elasticity. *Math. Mech. Solids*, 1(3):335–342, 1996.

[126] P. Schiavone and C. Q. Ru. The traction problem in a theory of plane strain elasticity with boundary reinforcement. *Math. and Mech. Solids*, 5(1):101–115, 2000.

[127] J. Schijve. Note on couple stresses. *J. Mech. Phys. Solids*, 14(2):113–120, mar 1966.

[128] M. Shaat, F. F. Mahmoud, X. L. Gao, and A. F. Faheem. Size-dependent bending analysis of kirchhoff nano-plates based on a modified couple-stress theory including surface effects. *Int. J. Mech. Sci.*, 79:31–37, feb 2014.

[129] P. Sharma, S. Ganti, and N. Bhate. Effect of surfaces on the size-dependent elastic state of nano-inhomogeneities. *Appl. Phys. Lett.*, 82:535–537, 2003.

[130] E. Shmoylova, S. Potapenko, and L. Rothenburg. Boundary element analysis of stress distribution around a crack in plane micropolar elasticity. *Int. J. Eng. Sci.*, 45(2-8):199–209, feb 2007.

[131] T. Sigaeva and P. Schiavone. Surface effects in anti-plane deformations of a micropolar elastic solid: integral equation methods. *Continuum Mech. Thermodyn.*, 28(1):105–118, 2016.

[132] Taisiya Sigaeva. *An examination of the design of mathematical models incorporating both microstructural and surface effects in anti-plane deformations.* PhD thesis, 2015.

[133] I.Y. Smolin, P.V. Makarov, D.V. Shmick, and I.V. Savlevich. A micropolar model of plastic deformation of polycrystals at the mesolevel. *Comput. Mater. Sci.*, 19(1-4):133–142, dec 2000.

[134] V. P. Smyshlyaev and N. A. Fleck. Bounds and estimates for linear composites with strain gradient effects. *J. Mech. Phys. Solids*, 42(12):1851–1882, 1994.

[135] Siegfried Prössdorf Solomon G. Mikhlin. *Singular Integral Operators*. Springer-Verlag GmbH, 1987.

[136] D. J. Steigmann and R. W. Ogden. Plane deformations of elastic solids with intrinsic boundary elasticity. *Proc. Royal Soc. A*, 453(1959):853–877, 1997.

[137] D. J. Steigmann and R. W. Ogden. Elastic surface-substrate interactions. *Proc. Royal Soc. A*, 455(1982):437–474, 1999.

[138] Roman Teisseyre. Asymmetric continuum: Standard theory. In *Physics of Asymmetric Continuum: Extreme and Fracture Processes*, pages 95–109. Springer Berlin Heidelberg.

[139] L. Tian and R. K. N. D. Rajapakse. Analytical solution for size-dependent elastic field of a nanoscale circular inhomogeneity. *J. Appl. Mech.*, 74(3):568–574, 2007.

[140] L. Tian and R. K. N. D. Rajapakse. Elastic field of an isotropic matrix with a nanoscale elliptical inhomogeneity. *Int. J. Solids Struct.*, 44(24):7988 – 8005, 2007.

[141] R. A. Toupin. Elastic materials with couple-stresses. *Arch. Ration. Mech. Anal.*, 11(1):385–414, 1962.

[142] R. A. Toupin. Theories of elasticity with couple-stress. *Arch. Ration. Mech. Anal.*, 17(2):85–112, jan 1964.

[143] C. Truesdell and W. Noll. The Non-Linear Field Theories of Mechanics. In *The Non-Linear Field Theories of Mechanics*, pages 1–579. Springer Berlin Heidelberg, 2004.

[144] N. P. Vekua. *Systems of Singular Integral Equations*. Noordhoff, Groningen, 1967.

[145] S. D. C. Walsh and A. Tordesillas. Finite element methods for micropolar models of granular materials. *Appl. Math. Modell.*, 30(10):1043–1055, oct 2006.

[146] Gang-Feng Wang and Xi-Qiao Feng. Effects of surface elasticity and residual surface tension on the natural frequency of microbeams. *Appl. Phys. Lett.*, 90(23):231904, jun 2007.

[147] X. Wang and P. Schiavone. Two circular inclusions with arbitrarily varied surface effects. *Acta Mechanica*, 226(5):1471–1486, nov 2014.

[148] Xu Wang and Hui Fan. Interaction between a nanocrack with surface elasticity and a screw dislocation. *Math. Mech. Solids*, 22(2):131–143, aug 2016.

[149] A. Waseem, A. J. Beveridge, M. A. Wheel, and D. H. Nash. The influence of void size on the micropolar constitutive properties of model heterogeneous materials. *Eur. J. Mech. A. Solids*, 40:148–157, jul 2013.

[150] F. Xun, G. Hu, and Z. Huang. Effective in plane moduli of composites with a micropolar matrix and coated fibers. *Int. J. Solids Struct.*, 41:247–265, 2004.

[151] F. Yang. Size-dependent effective modulus of elastic composite materials: Spherical nanocavities at dilute concentrations. *J. Appl. Phys.*, 95(7):3516–3520, apr 2004.

[152] J. F. C. Yang and R. S. Lakes. Experimental study of micropolar and couple stress elasticity in compact bone in bending. *J. Biomech.*, 15(2):91 – 98, 1982.

[153] H. Yao, G. Yun, N. Bai, and J. Li. Surface elasticity effect on the size-dependent elastic property of nanowires. *J. Appl. Phys.*, 111(8):083506, 2012.

[154] A. Yavari, S. Sarkani, and E. T. Moyer. On fractal cracks in micropolar elastic solids. *J. Appl. Mech.*, 69(1):45–54, jan 2001.

[155] X. Yuan and Y. Tomita. Effective properties of Cosserat composites with periodic microstructure. *Mech. Res. Commun.*, 28(3):265–270, 2001.

[156] A. Y. Zemlyanova. A straight mixed mode fracture with the Steigmann-Ogden boundary condition. *Q. J. Mech. Appl. Math.*, 70(1):65–86, 2017.

[157] A. Y. Zemlyanova. An adhesive contact problem for a semi-plane with a surface elasticity in the steigmann-ogden form. *J. Elast.*, 136(1):103–121, sep 2018.

[158] A. Y. Zemlyanova and S. G. Mogilevskaya. Circular inhomogeneity with Steigmann-Ogden interface: Local fields, neutrality, and Maxwell's type approximation formula. *Int. J. Solids Struct.*, 135:85–98, 2018.

[159] A. Y. Zemlyanova and S. G. Mogilevskaya. On spherical inhomogeneity with Steigmann–Ogden interface. *J. Appl. Mech.*, 85(12), 2018.

[160] H. W. Zhang, H. Wang, P. Wriggers, and B. A. Schrefler. A finite element model for contact analysis of multiple Cosserat bodies. *Comput. Mech.*, 36(6):444–458, apr 2005.

[161] X. Zhang and P. Sharma. Size dependency of strain in arbitrary shaped anisotropic embedded quantum dots due to nonlocal dispersive effects. *Phys. Rev. B*, 72(19), nov 2005.